Development of Clinical Biomarkers of DNA Double Strand Breaks for Cancer Care

A thesis submitted for the degree of

Doctor of Philosophy at the University of Oxford

Ketan Shah

Green Templeton College

Trinity Term, 2012

Development of Clinical Biomarkers of DNA Double Strand Breaks for Cancer Care

A thesis submitted for the degree of

Doctor of Philosophy at the University of Oxford

Ketan Shah

Gray Institute for Radiation Oncology and Biology

& Green Templeton College

Trinity Term, 2012

Abstract

Development of Clinical Biomarkers of DNA Double Strand Breaks for Cancer Care

Ketan Shah, Green Templeton College

Submitted for the degree of Doctor of Philosophy

at the University of Oxford, Trinity Term 2012

Many anticancer therapies, including radiotherapy, act by damaging the deoxyribosenucleic acid (DNA) that is fundamental to cell function and proliferation. H2AX is a histone protein associated with DNA that is phosphorylated to produce γH2AX in response to DNA double strand breaks (DSBs), the most lethal lesions caused in cancer cells. This thesis examines the translation of γH2AX detection assays to clinical situations in order to provide biomarkers of response that might help to guide the treatment of cancer patients.

γH2AX immunohistochemistry was developed in preclinical xenograft models, and validated over a range of radiation doses and over time after irradiation. The method was prepared for translation to archived clinical biopsy and surgical specimens.

The DSB Biomarkers Pilot Study was established in order to develop a method for γH2AX quantification in direct tumour cell specimens obtained using the clinical technique of fine needle aspiration (FNA) cytology. Eleven patients undergoing anticancer therapy were recruited to the study, and the method evaluated. The coefficient of variation of the measure was 49%.

Non-invasive imaging for γH2AX would allow DNA damage to be quantified in all tumour sites, and on multiple occasions. An antibody-based nuclear medicine imaging agent was re-engineered using Fab fragments of the antibody. The novel agent demonstrated improved pharmacokinetics when compared to the whole antibody agent, but reduced target specificity.

The findings further develop the potential to exploit DNA damage biomarker measurements in clinical oncology.

Acknowledgements

I am indebted to my supervisor, Professor Kate Vallis, for her unstinting support, guidance and encouragement over the years that went into this thesis. I am also grateful to the other members of my thesis committee, Professor Gillies McKenna and Dr Tim Humphrey, for their giving me some of their much-sought-after time.

Bart Cornelissen has been there to explain mysteries, to draw complex diagrams on the Benchkote, and to lend a hand until the *fingerspitzengefühl* came through.

The Vallis group and Gray Institute staff, evolving through the years, have provided countless useful tips. I am especially grateful to Sarah Able, Paul Barber, Veerle Kersemans, Kate Sleeth, Carol Target, Sam Terry, and Sabira Yameen. Kamila Hussein and Neel Patel probably provided more distraction than tips, but I needed that all the same! Thanks to Geoff Higgins who proved it could be done.

In the hospital, my namesake Ketan A. Shah in Cellular Pathology taught me patiently. Colin Clelland, Amanda Salisbury and Mark Middleton were ready with friendly advice at key points.

My Gray Clinical Research Fellowship was funded by Cancer Research UK, the Oxford Biomedical Research Centre and the Oxford Cancer Imaging Centre. The Gray Institute receives core funding from CRUK and the Medical Research Council.

There would have been no way through without my friends and family. I am always grateful to my parents, and to my children Apsara, Amrita and Nibodh. The greatest thanks must go to my wife Maheshi. We've supported one another through synchronous D Phils in Oxford; I think we can probably do anything, as long as we're together.

Table of Contents

Abstract……4

Acknowledgements……5

Table of Contents……6

Table of Figures……11

Table of Tables……15

List of Abbreviations……16

Chapter 1: Introduction ……20

1.1. Measuring the response to anticancer therapies ……20

1.1.1. Anticancer treatment strategy is planned at diagnosis ……20

1.1.2. Clinical measurement is governed by biology and logistics……22

1.1.3. The range of clinical responses to anticancer treatments is poorly understood……23

1.1.4. Biomarkers of response would be clinically and scientific useful ……26

1.2. DNA Damage and Cancer ……27

1.2.1. Anticancer treatments damage DNA ……27

1.2.2. Double strand breaks (DSBs) ……30

1.2.3. DNA DSBs are quantified using direct and indirect assays ……30

1.3. γH2AX is a candidate biomarker of response to clinical radiation therapy ..

……31

1.3.1. γH2AX is part of the early response to DNA DSBs ……31

1.3.2. γH2AX interacts with other DNA repair components, especially MDC1 ……33

1.3.3. In vitro assays have been developed for γH2AX……36

1.3.4. γH2AX is implicated in processes other than treatment-induced DSB formation ……38

1.3.5. Interpreting the presence of γH2AX in dynamic DNA damage and repair ……42

1.3.6. γH2AX remains an attractive biomarker for DSBs 48
1.3.7. Clinical γH2AX assays answer questions in oncology 50
1.4. Clinical biomarker development 61

1.4.1. Biomarker can be classified by their clinical application 61
1.4.2. Biomarker development is a multi-stage process 62
1.4.3. Potential tumour response assays 65
1.5. Conclusion 66

1.6. Aim of the thesis 67

Chapter 2: Development of a solid tumour tissue immunohistochemistry method to demonstrate γH2AX 69
2.1. Introduction 69

2.1.1. γH2AX in solid tumours 69
2.1.2. Immunohistochemistry 69
2.1.3. Dose response and kinetics 70
2.1.4. Chapter outline 71
2.2. Materials and Methods 72

2.2.1. Cell culture 72
2.2.2. Establishment of xenografts 72
2.2.3. Irradiation of xenografts 73
2.2.4. Xenograft harvesting and fixation 73
2.2.5. Paraffin embedded tumours 74
2.2.6. Frozen tumours 74
2.2.7. Heat induced epitope retrieval 74
2.2.8. γH2AX immunohistochemistry 75
2.2.9. Microscopy 76
2.2.10. Image analysis 76
2.3. Results 76

2.3.1. Immunohistochemistry method development 76
2.3.2. Validation over a dose range 79
2.3.3. Kinetics study 81
2.4. Discussion 83

2.4.1. Importance of tissue fixation....83
2.4.2. Automated quantification....84
2.4.3. Dose response and kinetics....84
2.4.4. Conclusion....85

Chapter 3: Clinical Development of Fine Needle Aspiration Cytology to Demonstrate γH2AX in Tumours....87
3.1. Introduction....87

3.1.1. Fine Needle Aspiration....87
3.1.2. The DSB Biomarkers Pilot Study....88
3.2. Materials and Methods....91

3.2.1. Human blood samples....91
3.2.2. Separation of peripheral blood mononuclear cells (PBMCs)....91
3.2.3. *Ex vivo* irradiation of PBMCs....91
3.2.4. DSB Biomarkers Pilot Study....92
3.2.5. Fine needle aspiration (FNA)....92
3.2.6. Immunocytochemistry....94
3.2.7. Confocal microscopy....95
3.2.8. Cell identification quality control....95
3.2.9. Image processing and recognition software....95
3.2.10. Quantification and statistical analysis....96
3.3. Results....96

3.3.1. Validation of antibody in human PBMCs irradiated *ex vivo*....96
3.3.2. Study conduct....98
3.3.3. Liquid based cytology method development....99
3.3.4. Direct smear cytology....100
3.3.5. Application of method before and after treatment....102
3.3.6. Co-staining for γH2AX and 53BP1....105
3.3.7. FNA up to 1 week after radiotherapy....107
3.3.8. Analysis....109
3.4. Discussion....110

3.4.1. Development of the FNA Assay....110
3.4.2. Comparisons with published data....113

3.4.3. Late residual foci 115
3.4.4. Conclusion 115

Chapter 4: Development of a SPECT imaging probe from Fab fragments of anti-γH2AX antibodies 118
4.1. Introduction 118

4.1.1. Clinical SPECT Imaging 118
4.1.2. Antibodies for imaging applications 119
4.1.3. Intracellular imaging targets 120
4.1.4. Chapter Outline 121
4.2. Materials and Methods 123

4.2.1. Generation of antibody Fab fragments 123
4.2.2. Measurement of protein concentration 124
4.2.3. Sodium dodecyl sulphate polyacrylamide gel electrophoresis 124
4.2.4. Labelling of proteins with ^{123}iodine (Iodogen method) 125
4.2.5. Size exclusion chromatography (SEC) 125
4.2.6. Carbodiimide peptide coupling of Tat peptide to antibody Fab fragments 126
4.2.7. Conjugation of p-isothiocyanate benzyl DTPA by thiourea linkage 126
4.2.8. Conjugation of cyclic DTPA anhydride 127
4.2.9. SEC Quantification and Statistics 128
4.2.10. Cell culture 128
4.2.11. Immunocytochemistry 129
4.2.12. Internalisation assay 129
4.2.13. Mice 130
4.2.14. Establishment of xenografts 130
4.2.15. *In vivo* irradiation and SPECT imaging experiments 131
4.2.16. Irradiation of xenografts 131
4.2.17. Preparation of Radiopharmaceutical 132
4.2.18. Administration of Radiopharmaceutical 132
4.2.19. Computed Tomography/ Single Photon Emission Computed Tomography (CT/SPECT), Image Reconstruction and Region of Interest (ROI) Analysis 132
4.2.20. Biodistribution studies 134
4.3. Results 134

4.3.1. Papain digestion of anti-γH2AX antibody 134
4.3.2. Conjugation of Tat peptide to Fab fragments using carbodiimide coupling 135
4.3.3. Conjugation of DTPA 139
4.3.4. ^{111}Indium radiolabelling of Anti-γH2AX Fab-Tat-DTPA 142
4.3.5. Anti-γH2AX Fab-Tat-DTPA binds γH2AX in cells *in vitro* 143
4.3.6. Anti-γH2AX Fab-Tat internalises into H2N cells 145
4.3.7. SPECT imaging using Anti-γH2AX Fab-Tat-DTPA and control probes – blood clearance and normal tissues 147
4.3.8. SPECT imaging using anti-γH2AX Fab-Tat-DTPA and control probes – tumour and irradiated muscle 152
4.4. Discussion 157
4.4.1. Synthesis of probes 157
4.4.2. *In vivo* SPECT imaging 159
4.4.3. Conclusion 163

Chapter5:Discussion 165
5.1. γH2AX is a candidate clinical biomarker 165
5.2. γH2AX immunohistochemistry in tumour tissue 165
5.3. A novel FNA assay for yH2AX 167
5.4. In vivo imaging of γH2AX 169
5.5. Taking γH2AX assays into the clinic 170

Bibliography 172

Appendix - DSB Biomarkers Pilot Study Protocol 192

Table of Figures

Figure 1.1 Simplified process diagram for clinical decisions in oncology……..21

Figure 1.2 Progression-free survival by the Kaplan Meier method in the EORTC 22845 trial of early radiotherapy vs. no early radiotherapy in low-grade glioma.25

Figure 1.3 The role of biomarkers in the clinical process in oncology.....27

Figure 1.4 DNA damage lesions and repair processes in relation to cancer treatments.....29

Figure 1.5 Heirarchical recruitment of DNA repair machinery to sites of γH2AX to form irradiation induced foci. 35

Figure 1.6 The relationship between γH2AX and its assays and clinical anticancer therapy 43

Figure 1.7 Cancer Research UK Pharmacological Biomarker Roadmap.....64

Figure 2.1 Chapter 2 outline 71

Figure 2.2 Immunoblot assay of lysates from irradiated (10 Gy) and unirradiated H2N cells using mouse anti-γH2AX antibody.....77

Figure 2.3 Epifluorescence microscopy demonstrating immunohistochemistry of H2N xenograft tissue sections prepared used different tissue handling methods during development. 78

Figure 2.4 Automated quantification of foci per cell section (normalised for nuclear area) in H2N xenografts harvested one hour after irradiation with 300kV Xrays.. 79

Figure 2.5 Confocal imaging of immunohistochemistry of H2N xenografts harvested one hour after irradiation with 300 kV Xrays (0-10 Gy) 80

Figure 2.6 γH2AX foci quantification in MDA-MB-231/H2N xenografts sacrificed at stated times after 10 Gy photon irradiation.. 81

Figure 2.7 Immunohistochemistry for yH2AX after 10Gy photon irradiation.....82

Figure 3.1 Chapter 3 outline 90

Figure 3.2 Validation of γH2AX and 53BP1 antibodies used for immunohistochemistry in human peripheral blood mononuclear cells irradiated *ex vivo* to 2Gy.....97

Figure 3.3 Immunocytochemistry of fine needle aspiration tumour specimens from squamous cell carcinoma cervical lymph node from participant DSB01.....99

Figure 3.4 Immunocytochemistry of fine needle aspiration tumour specimens from squamous cell carcinoma cervical lymph node from participant DSB03..... 100

Figure 3.5 Immunocytochemistry of fine needle aspiration tumour specimens from metastatic melanoma from participant DSB04 102

Figure 3.6 Immunocytochemistry of fine needle aspiration tumour specimens from participant DSB07..... 103

Figure 3.7 Example of automated image recognition by TRI2 sofware in participant DSB07. 104

Figure 3.8 Mean foci number normalised for nuclear area in individual FNAs from participant DSB07..... 104

Figure 3.9 Immunocytochemistry of fine needle aspiration tumour specimens of non-Hodgkins lymphoma deposits from participant DSB09 106

Figure 3.10 Mean γH2AX foci normalised for nuclear area in individual FNAs from participant DSB09..... 107

Figure 3.11 Immunocytochemistry of fine needle aspiration tumour specimens from participant DSB10..... 108

Figure 3.12 Mean γH2AX foci normalised for nuclear area..... 109

Figure 4.1 Schematic diagram of an antibody molecule. 120

Figure 4.2 Chapter 4 outline 122

Figure 4.3 Example coronal SPECT-CT reconstruction for definition of regions of interest (ROIs). 133

Figure 4.4 SDS PAGE of rabbit antibody before digestion, after papain digestion, and after affinity purification. 135

Figure 4.5 Polyacrylamide P2 size exclusion radiochromatography demonstrating larger, early eluting iodinated ^{123}I-Tat peptide molecules generated using Iodogen and smaller, later eluting free ^{123}I control 136

Figure 4.6 Sephadex G25 size exclusion radiochromatography after ^{123}I-Tat conjugation to rabbit IgG and anti-γH2AX Fab fragments 138

Figure 4.7 SDS PAGE of early-eluting phase from size exclusion chromatography after rabbit IgG Fab conjugation with Tat under non-reducing (NR) and reducing (R) conditions. 138

Figure 4.8 Sephadex G25 size exclusion radiochromatography of purified rabbit IgG Fab-Tat-DTPA and anti-γH2AX Fab-Tat-DTPA after conjugation with ^{111}Indium. 142

Figure 4.9 Immunocytochemistry demonstrating accumulation of anti-γH2AX Fab-Tat-DTPA at foci in irradiated (6Gy) but not unirradiated H2N cells. 144

Figure 4.10 Immunocytochemistry demonstrating co-localisation of anti-γH2AX Fab-Tat-DTPA with a monoclonal mouse anti-γH2AX antibody. 145

Figure 4.11 Radioassay demonstrating internalisation of ^{123}I-labelled Tat- and non Tat-conjugated probes into live H2N cells 146

Figure 4.12 Summary data from the same experiments as shown in Figure 4.10 divided by Tat conjugation of probe and irradiation of cells. 146

Figure 4.13 Blood pharmacokinetics of ^{111}In labelled anti-yH2AX Fab-Tat-DTPA and control SPECT probes calculated by quantification of heart regions of interest on serial SPECT scans.. 148

Figure 4.14 Normal tissue pharmacokinetics of anti-γH2AX Fab-Tat-DTPA and control SPECT probes calculated by quantification of regions of interest on serial SPECT scans..... 150

Figure 4.15 Biodistribution of imaging probes by dissection at 24 hours post-injection (organs comparable to SPECT signal intensity data).. 151

Figure 4.16 Biodistribution of imaging probes by dissection at 24 hours post-injection (for organs not shown in Figure 4.14).. 152

Figure 4.17 Maximal intensity projection SPECT images obtained at 1,6 and 24 hours after tail vein injection anti–γH2AX Fab-Tat-DTPA (5 μg and 2 μg), whole antibody anti-γH2AX-Tat-DTPA (5 μg) and rabbit IgG Fab-Tat-DTPA (5 μg).. 153

Figure 4.18 Relative SPECT intensity in tumour regions of interest at 1, 6 and 24h post injection in mice either unirradiated, irradiated 1h pre-injection or irradiated 4h pre injection.. 155

Figure 4.19 Excised tumour xenograft activity at 24h expressed as %injected dose per gram..... 156

Figure 4.20 Relative SPECT intensity in muscle at 1, 4, 6 and 24h post injection and biodistribution at 24h of 5μg anti-γH2AX Fab-Tat-DTPA in mice.. 157

Table of Tables

Table 1.1 Selected clinical studies employing γH2AX as a biodosimeter of radiation exposure 52

Table 1.2 Clinical studies employing γH2AX as a marker of normal tissue radiosensitivity or chemosensitivity. 54

Table 1.3 Studies employing γH2AX for clinical cancer diagnosis or prognosis. 56

Table 1.4 Clinical studies employing γH2AX measurements of tumour cells during chemotherapy or radiotherapy treatment 59

Table 3.1 Recruitment to DNA DSB Biomarkers Pilot Study 98

Table 3.2 Coefficient of variation from repeated quantification of γH2AX foci 110

Table 4.1 Optimisation of carbodiimide conjugation of ^{123}I-Tat peptide to antibody Fab fragments. 136

Table 4.2 Optimisation of DTPA conjugation. 140

List of Abbreviations

γH2AX	Phosphorylated histone H2A subtype X
53BP1	p53 binding protein 1
ATs	Alkyltransferases
ATM	Ataxia telangiectasia mutated
ATR	Ataxia telangectasia and Rad3-related
BER	Base excision repair
BRCA1	Breast cancer protein 1
CT	Computed tomography
CTC	Circulating tumour cell
CV	Coefficient of variation
DMSO	Dimethylsulfoxide
DNA	Deoxyribose nucleic acid
DNA-PK	(DNA)-protein kinase
DSB	(DNA) double strand break
DTPA	Diethylenetriaminepentaacetic acid
EDC	1-Ethyl-3-(3-dimethylaminopropyl) carbodiimide
EGF	Epidermal growth factor
ENDO	Endonuclease mediated repair
EORTC	European Organisation for Research and Treatment in Cancer
EXP1	EXPAND 1 protein
FA	Fanconi anaemia repair pathway
Fab	Fragment: antigen binding
FACS	Fluorescence activated cell sorting
FDG	Fluorodeoxyglucose
FFPE	Formalin fixed paraffin embedded
Gy	Gray (unit of absorbed radiation energy)
H2AFX	Gene encoding histone H2A subtype X
H2AX	Histone H2A subtype X
H2N	MDA-MB-231/H2N cell line

HR	Homologous recombination
IRIF	Irradiation-induced foci
kDa	Kilodaltons
MDC1	Mediator of DNA damage checkpoint 1
MES	Morpholinoethanesulfonic acid
MRI	Magnetic resonance imaging
NBS	Nijmegen break syndrome
NER	Nucleotide excision repair
NHEJ	Non-homologous end joining
O2G	DNA dioxygenases
p53	p53 protein
PARP	Poly (ADP) ribose polymerase
PET	Positron emission tomography
PFGE	Pulsed field gel electrophoresis
PTIP	Pax interaction with transcription-activation domain protein
Rad18	Radiation protein 18
Rad50	Radiation protein 50
Rad51	Radiation protein 51
RT	Radiotherapy
sNHS	Sulfo N-hydroxysuccinimide
SPECT	Single positron emission computed tomography
SSB	DNA single strand break
SSBR	DNA single strand break repair
TLS	Translesion synthesis
WIP1	Wild type p53-induced phosphatase.

Chapter 1

Introduction

Chapter 1: Introduction

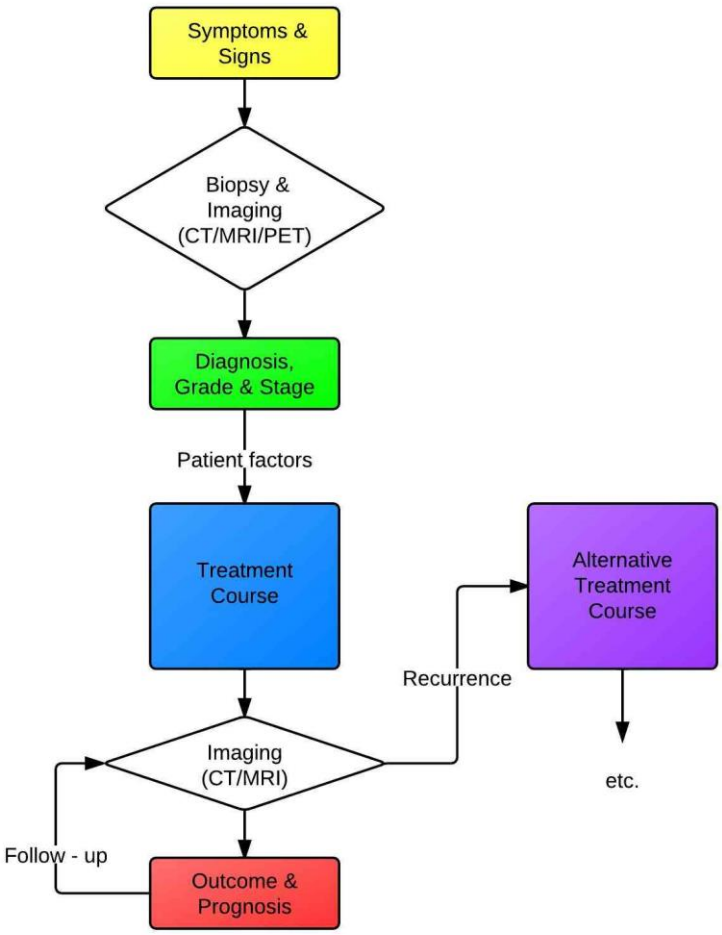
1.1. Measuring the response to anticancer therapies

1.1.1. Anticancer treatment strategy is planned at diagnosis

There were 12.7 million cancer cases registered worldwide in 2008 and 7.6 million deaths [1] so that cancer treatment is acknowledged as a global priority. [2] In the developed world, there are three basic categories of anticancer strategy – surgery, radiotherapy and drug therapy (broadly termed chemotherapy), which can be applied either individually or in combination.[3]

A traditional cancer care pathway is illustrated in simplified form in Figure .1. It illustrates the gathering of as much information as possible about tumour characteristics and behaviour at the outset in order to make as complete a diagnosis as possible. For most solid tumours this would include at least the cell type, histological *grade*, a measure of the cancer's aggressiveness based on cell morphology, and *stage*, a description of the extent of local invasion and distant spread of the cancer.[4]

Figure 1.1 Simplified process diagram for clinical decisions in oncology



Information obtained about the tumour is considered alongside information about the patient, including their level of physical fitness, other medical conditions and personal preferences, and a treatment strategy is formulated. In general the aim is to complete this planned treatment course in as short a time as possible, especially in the case of radiotherapy[5] although this is limited by the patient's tolerance of often complex and toxic treatments.

Further assessment of the effectiveness of treatment is sometimes undertaken at the end of the course, typically several weeks after the therapy was delivered. This

reassessment may be repeated periodically or in response to new symptoms in an attempt to detect recurrence of the cancer.

1.1.2. Clinical measurement is governed by biology and logistics

The rationale for the process outlined above is both practical and scientific. Initiating and completing a treatment course in as short a time as possible is important both to meet the (typical) desire of patients diagnosed with cancer to be treated quickly, and because of clear evidence that delay and prolongation of therapy lead to poorer outcomes, including a smaller chance of survival.[6-8]

Time is invested to provide information to guide an appropriate treatment choice. Direct tumour sampling by biopsy is usually required before treatment, to establish the histological cancer type and grade and to ensure that potentially toxic treatments are not given to patients without cancer. Non-invasive imaging modalities, especially computed tomography (CT) and magnetic resonance imaging (MRI), and more recently ^{18}Fluorodeoxyglucose positron emission tomography (FDG-PET) are used to assess the cancer's size and stage of spread.

Once chosen, treatments are then completed in as timely a manner as possible, essentially without interruption in the cases of surgery and radiotherapy.[6] Chemotherapy regimens delivered in courses, consisting of treatment days followed by a few weeks for recovery, can allow for interim assessments of response.

Assessments of response to interventions tend to rely on imaging, usually with CT or MRI, which can compare images taken at diagnosis to those taken after treatment. These comparisons are based on the size of tumour lesions visualised

by the imaging modality, which can be measured in 1, 2 or 3 dimensions. International collaboration has been required to standardise the technical method for size comparison, which has been essential for research and useful for clinical applications.[9, 10]

The timing of size-based assessment relies on the biology and geometry of tumour response. Consider an archetypal spherical tumour lesion (for example axillary lymph node metastasis from breast adenocarcinoma) whose linear measurement reduced from 12mm on a CT scan at diagnosis to 10mm on a CT scan taken after a course of treatment. To achieve this change, which is at the limits of detection, the volume of the lesion would need to reduce by 42%, and around $7x10^8$ cells would need to die and be resorbed (assuming 10^9 cells per cubic centimetre^3). These changes in size take time, so that size based assessments cannot be used too frequently (e.g. at least every 6-8 weeks for CT), or too soon after a treatment (e.g. at least 4-6 weeks after radiotherapy).

Patients wish to have information in a timely manner, but cancer diagnosis and treatment can be a complex and daunting series of hospital attendances and invasive procedures. The patient experience is an important concern in choosing clinical measurement schedules and modalities.

1.1.3. The range of clinical responses to anticancer treatments is poorly understood

Following the simplified schema of Figure 1.1, treatment response may be defined as the difference between an assessment made at diagnosis and one made after treatment. This difference will depend on many factors, including the biology of

the cancer, whether the treatment could be fully delivered and the uncertainty in the measurement, as well as the effectiveness of the treatment.

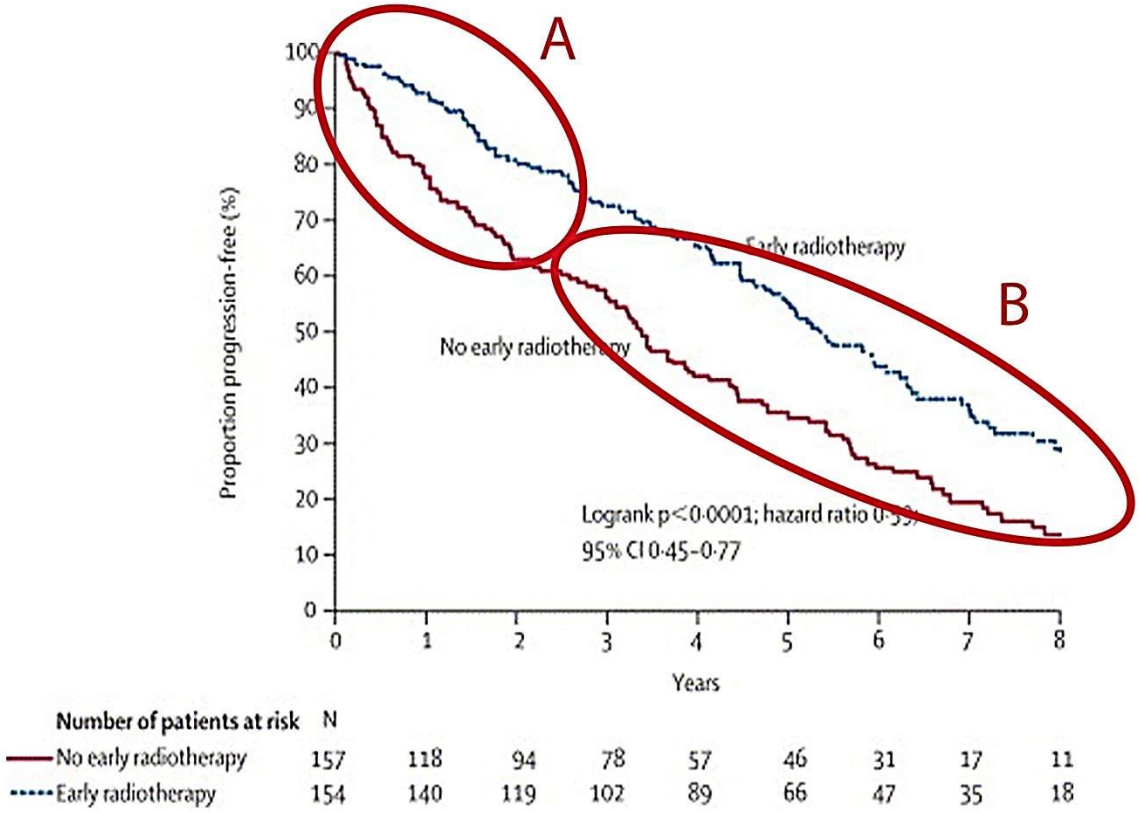
Clinical trials represent a systematic attempt to resolve these factors. Typically information regarding tumour type, grade and stage, along with patient age and comorbidity are collected and controlled for in the design of the study (e.g. by stratification within randomisation groups[11]). Measurement is standardised as far as possible, and its accuracy may be measured.

Despite all of these efforts, the variability in responses to interventions in clinical trials is striking. It should be noted that documenting this variability is not the focus of most randomised clinical trials. Rather, the comparison between the groups informs the primary outcome measure, and this variability within groups is merely an inconvenience that for reasons of statistics necessitates the large number of patients recruited to such studies.

This thesis focuses largely on measuring responses to radiotherapy alone. Few trials with modern methodology have randomised cancer patients between radiotherapy and no treatment, since there is seldom clinical equipoise regarding the benefits of radiotherapy. The EORTC 22845 trial however randomised patients with slow-growing brain tumours, termed low grade gliomas, between immediate radiotherapy and radiotherapy delayed until progression on CT scan (i.e. no upfront treatment).[12] Patients had undergone biopsy or incomplete surgery. Figure 1.2 illustrates progression-free survival measured in the two groups. The data can be used to illustrate two messages that are relevant to this argument. Firstly, within each group there is an enormous diversity in outcome, with some

patients progressing almost immediately, and others only after many years. There is however no final plateau of the curve that might indicate long term cure.

Figure 1.2 Progression-free survival by the Kaplan Meier method in the EORTC 22845 trial of early radiotherapy (blue line) vs. no early radiotherapy (red line) in low-grade glioma. "A" denotes early separation of curves, "B" denotes parallel curves (see text). Adapted from The Lancet with permission from Elsevier.[12]



Secondly, while radiotherapy can make a difference in a clinically important outcome, this is only in a subset of those treated. Over the first two years of the study (highlighted as "A" in Figure 1.2), the curves diverge so that in the early radiotherapy group around 20% of patients have shown progression, compared to 35% in the group that did not receive radiotherapy. After this ("B") the curves become parallel, such that around 10% of patients' tumours progress each year, regardless of previous treatment.

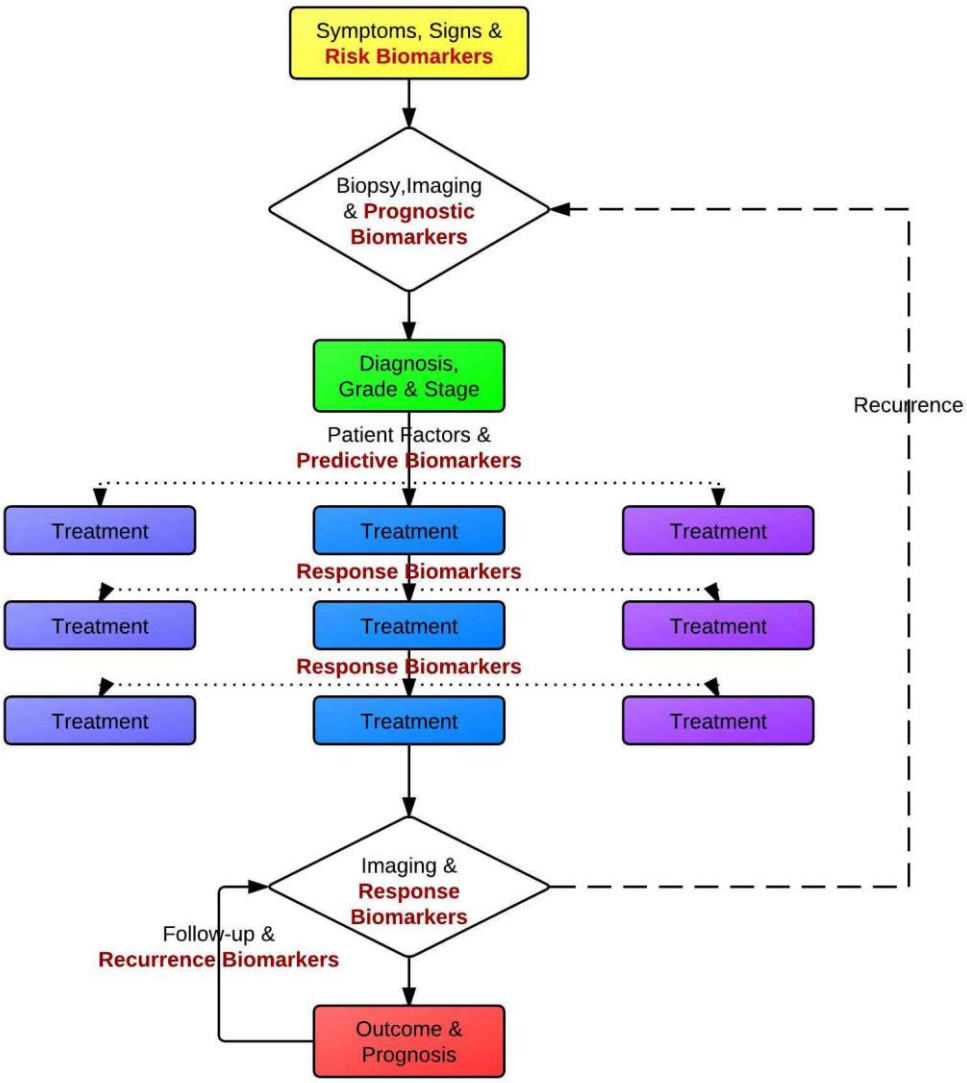
To complete the clinical picture in this trial, most of those who progressed then had radiotherapy, and overall survival between the groups was the same, but this is less relevant to the current discussion.

The point here is that there are those who undergo toxic anticancer treatments including radiotherapy, but will not benefit from them. If it were possible to identify these patients earlier, perhaps during treatment, then further unnecessary treatment and side effects could be avoided.

1.1.4. Biomarkers of response would be clinically and scientific useful

Figure 1.1 was a simplified illustration of therapeutic decision-making in oncology. In fact, translational cancer research continues to provide multiple treatment options, but also increasing "biomarker" information on which to base decisions between those options. Biomarkers are measurements of biological processes[13], and the term "clinical biomarker" could be applied to traditional measures such as blood pressure just as it is applied to novel tests. Figure 1.3 illustrates some of the potential roles for biomarkers in the clinical process in oncology. Biomarker development is considered in detail in Section 1.4, but particular attention is now drawn to the way in which response biomarkers might not only improve the information for clinical decisions, but might actually change the treatment paradigm by allowing an adaptive treatment course to evolve in response to ongoing new information. The development and application of biomarkers forms part of the future for oncology.[14]

Figure 1.3 The role of biomarkers in the clinical process in oncology



1.2. DNA Damage and Cancer

1.2.1. Anticancer treatments damage DNA

All cells are subject to physiological damage to the double stranded DNA molecule, arising from endogenous and exogenous physical, chemical and biological processes. These result in a variety of molecular lesions, ranging from minor

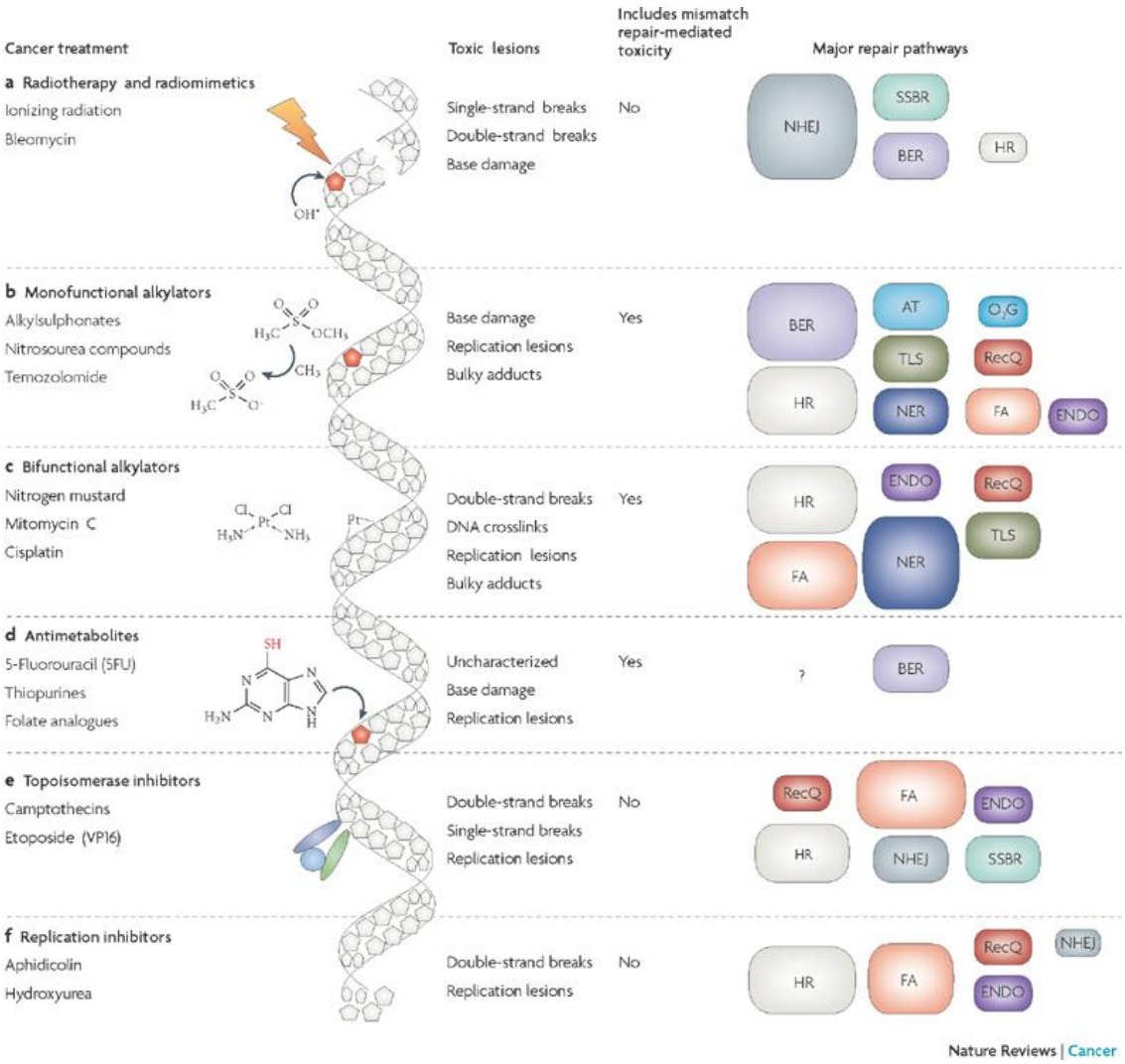
modifications of single bases to single strand breaks (SSBs) and complete, double strand, breaks (DSB).[15]

The integrity of DNA is crucial to cell survival and division and to the stability of the cell's genetic information. It is protected by an array of repair processes that mirror the chemical nature of the damage that DNA can undergo (see Figure 1.4). In addition there are mechanisms to ensure that damaged DNA is not replicated, and that irreparable damage results in cell death or senescence.[15, 16]

Among the many effects of radiotherapy on cells, the chemical damage mediated by reactive oxygen species generated in close proximity to DNA is the most deleterious to the cell.[5] Cytotoxic anticancer drugs have a variety of modes of action, but many target DNA. Cisplatin for example, forms covalent adducts along and between DNA strands, while etoposide prevents the topoisomerase II enzyme from rejoining DNA breaks that it has formed for physiological reasons.[3]

Figure 1.4 DNA damage lesions and repair processes in relation to cancer treatments (adapted by permission from Macmillan Publishing Group: Nature Reviews Cancer©2008)[15] See pages 16-17 for abbreviations.

.



Cancers also need to maintain cellular function, but genomic instability can actually help them to develop and evolve through mutation, and is described as an enabling hallmark of cancer.[17] Genomic homeostasis mechanisms are often therefore altered in cancer cells, particularly through mutations of p53, the prime orchestrator of cell cycle and apoptosis decisions.[18]

The extent of DNA damage incurred and the cell's response to it are therefore critical to the outcome for that cell. It may be hypothesised that measurements of DNA damage and repair within the cancer are potential biomarkers of clinical outcome.

1.2.2. Double strand breaks (DSBs)

Arguably the most difficult to repair and hence lethal lesion is the DSB.[19, 20] There are several reasons for this; in contrast to repair of SSBs and base damage the complementary DNA strand cannot be used as a template; broken ends of DNA may be able to move apart from one another requiring physical realignment for religation; free DNA ends can be vulnerable to degradation by nucleases; and the repair process occurs in the context of chromatin, which is also disrupted by the DSB.[21] As well as being difficult to repair, DSBs can potentially lead to mutagenic chromosome translocations.

Ionising radiation causes many different DNA lesions, but cell death correlates most closely with DSBs.[22] For every Gray (Gy) of radiation energy absorbed by the cell, it has been estimated that around 40 DSBs are generated (compared to up to 1000 SSBs). The cell's repair mechanisms are crucial, as even a single unrepaired DSB can be lethal to the cell.[23]

1.2.3. DNA DSBs are quantified using direct and indirect assays

Several assays for DSBs have been developed. Direct methods visualise DNA itself, and utilise changes in its physical behaviour as a result of breaks in the molecule. Gradient sedimentation and filter elution detect extensive DNA fragmentation. Pulsed field gel electrophoresis requires large numbers of cells but can detect damage from doses as low as a few Gray, although some sources claim sensitivity

as low as 0.5Gy.[5, 24] The principle of electrophoresis has been powerfully extended to single cells in the so called comet assay,[25] in which cells are embedded in agarose under neutral or alkaline conditions, subjected to a weak electrophoretic field, and DNA migration visualised using fluorescent dyes such as acridine orange. DSBs can be detected above 4Gy using this technique, and conditions can be varied to allow the detection of DNA single strand breaks and interstrand crosslinks.[26] The method has been applied clinically, including in fine needle aspirate biopsies.[27]

More indirect methods visualise aspects of the cellular response to DNA damage, such as the formation of micronuclei[28] or the accumulation of DNA damage-sensing and repair-mediating proteins including γH2AX (phosphorylated histone subtype H2AX), 53BP1 (p53 binding protein 1) and where DSBs are repaired by homologous recombination, Rad51.[29, 30] These methods have the advantage of exquisite sensitivity, but represent only circumstantial evidence of the presence of a physical DNA double strand break.

Since anticancer therapies, and in particular radiotherapy cause DSBs, and DSBs relate to clinical outcomes, DSB assays provide potential biomarkers of therapeutic response.

1.3. γH2AX is a candidate biomarker of response to clinical radiation therapy

1.3.1. γH2AX is part of the early response to DNA DSBs

In 1998, Rogakou *et al.* described the identification of a novel species isolated from two-dimensional histone gels of nuclear extracts from irradiated SF268 glioblastoma cells.[31] The species, initially termed simply "γ", ran close on the gel to

the H2AX subtype of histone H2A. It was subsequently demonstrated to consist primarily of histone H2AX phosphorylated on the serine residue 139, close to the C-terminal end of the 143 residue protein. This "γH2AX" formed in conditions known to induce primarily DNA double strand breaks, as opposed to other forms of DNA damage. The potential importance of the finding was underlined by the ability to detect γH2AX in cells fixed as little as 20 seconds after irradiation, and (at low doses) the proportional relationship between irradiation dose and the amount of γH2AX detected.[31]

Later studies have further characterised γH2AX. [32-35] Human chromatin arranges DNA into nucleosomes, each of which consists of a 147 base pair length of DNA molecule wrapped around octameric histone cores. These histone cores contain two H2A proteins, most of which belong to one of the highly genetically conserved subtypes H2A1, H2A2, H2AX or H2AZ. [36] It is estimated that between 2% and 25% of human cell H2A protein consists of the H2AX subtype, depending on cell type.[33] In response to DNA double strand breaks, there is activation of the kinases ATM (ataxia telangiectasia mutated), ATR (ataxia telangiectasia and Rad3-related) and DNA-PK (DNA-protein kinase). All of these phosphoinositol-3-kinase-like kinases can independently phosphorylate H2AX at serine 139 *in vitro* to form γH2AX, although on the basis of genetic knockout cell line studies ATM activity is thought to predominate in the response to DSBs *in vivo*.[35, 37-39] ATR in particular is important in the generation of γH2AX in other contexts (see Section 1.3.4). Phosphorylation at serine 139 can be accompanied by dephosphorylation at tyrosine 142, a site otherwise constitutively phosphorylated in undamaged chromatin.[40] γH2AX is generated in a region of roughly 2 megabase pairs around a

DNA DSB[36] and chromatin immunoprecipitation experiments have shown that γH2AX density is highest close to the break[41, 42] and that the constitution of foci is different in euchromatin (where most foci occur) and heterochromatin.[43]

1.3.2. γH2AX interacts with other DNA repair components, especially MDC1

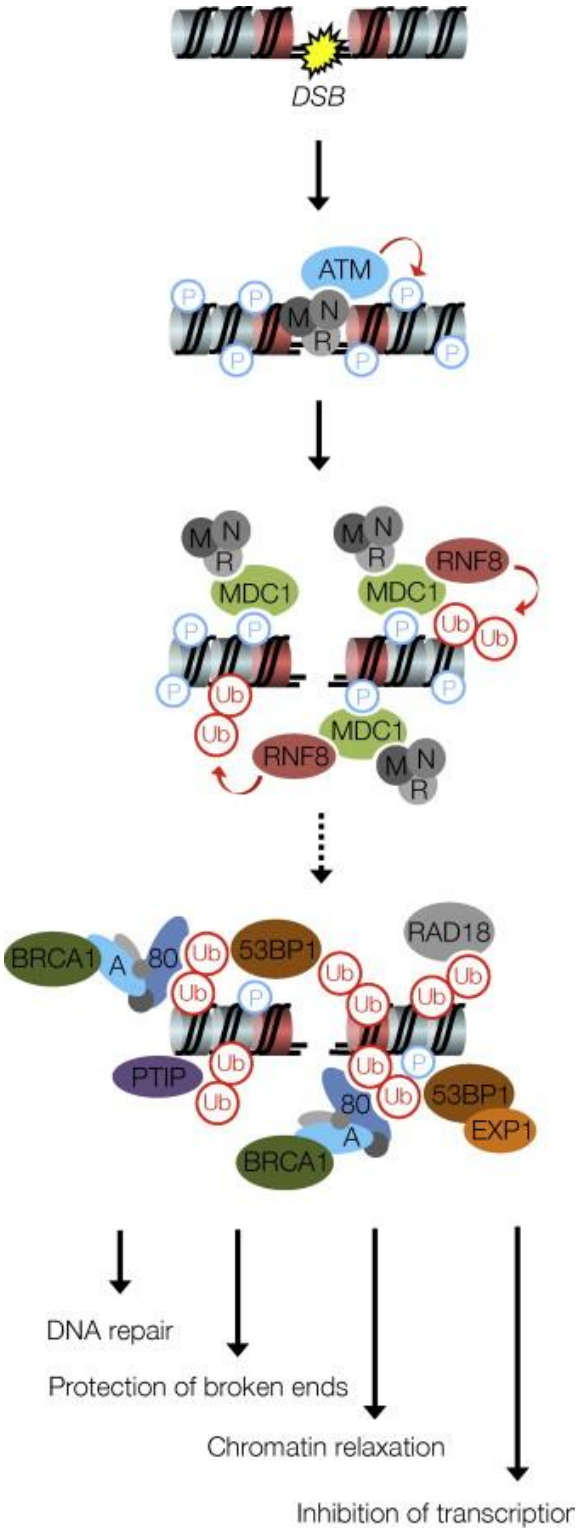
The function of γH2AX has been investigated with biochemical studies of its molecular interactions and by gene knockout in whole mice and in cell lines. Mice bred with no functional H2AX (*H2AFX* gene -/-) were viable but retarded in growth, sensitive to whole body irradiation, and showed male infertility. Immunoglobulin class switching, but not V(D)J recombination was impaired.[44] *H2AFX* -/- mouse embryonic fibroblasts were able to divide, and to activate cell cycle checkpoints in response to irradiation. However, the recruitment of Rad51, BRCA1 (Breast Cancer Protein 1) and NBS1 (Nijmegen Break Syndrome 1) to form irradiation induced foci (IRIF) was impaired.[45] Interestingly NBS1 was still able to localise to sites of DNA replication, indicating a mechanism independent of H2AX.[46] Loss of even one allele of the H2AX gene increases tumourigenesis on a p53 mutated background.[45]

The most important direct interaction of γH2AX appears to be with MDC1 (mediator of DNA damage checkpoint 1) – see Figure 1.5.[47-50] Formation of the species at high density close to a DSB is dependent on the presence of MDC1, which probably serves to anchor ATM close to the break, allowing it to phosphorylate neighbouring H2AX histones. Lower density γH2AX distant to the break is however independent of MDC1.[38, 41, 51] MDC1 recruits several components of downstream DSB signalling and repair including the MRN complex (MRE11 Meiotic Recombination Protein 11, NBS1 and Rad50), RNF8 (Ring Finger Protein

8), 53BP1 (p53 Binding Protein 1) and BRCA1. Extensive chromatin remodelling occurs around the break, consisting of both the localisation of nuclear proteins to the immediate environment and post-translational modification of histones.[51, 52] Although most of the downstream effects of γH2AX are mediated by MDC1, microcephalin (also known as MCPH1 or BRIT1) is an independent sensor of γH2AX that also remodels chromatin.[53]

The cell is under continuous physical and chemical stress and so DNA damage lesions occur continuously. To avoid the accumulation of DNA damage signalling and repair complexes, this recruitment cascade must be terminated. The termination of this repair initiation cascade is distinct from resolution of the process of repair itself. While several γH2AX phosphatases have been identified, including protein phosphatases PP2A, PP2Cγ, PP4, PP6 and WIP1, the coordination of γH2AX dephosphorylation is not well characterised. Interestingly the most recently identified of these enzymes, WIP1,[54] is induced by p53, which itself is induced by genotoxic stress.[55]

Figure 1.5 Heirarchical recruitment of DNA repair machinery to sites of γH2AX to form irradiation induced foci (adapted from Bekker-Jensen et al. 2010 with permission from Elsevier.)[52] M, MRE11; R, Rad 50; N, NBS; P, Phosphorylated H2AX; Ub, Ubiquitin. For other abbreviations see pp16-17.



1.3.3. In vitro assays have been developed for γH2AX

The means of detection and measurement of γH2AX are relevant both to the investigation of its roles and to its implementation as a biomarker. Part of the attraction of the marker is that while the H2AX histone is constitutively present, its modification by phosphorylation at serine 139 and dephosphorylation at threonine 142 is a rapid, in situ event that results in a new protein moiety. Antibodies have been raised to this modified carboxyl tail[56] and applied to develop several assays.

Immunocytochemical assays for γH2AX demonstrated multiple intranuclear foci thought to represent individual DSBs.[57, 58] The extent to which this inference is justified is considered below in relation to the quantity and dynamics of foci and DSBs (see Section 1.3.5). Discrimination of individual foci requires immunofluorescent techniques with high power microscopy, and depends on the quality of the antibody and staining technique. At low levels of damage, and hence low numbers of DSBs, individual foci can be distinguished and characterised. Manual counting of visualised γH2AX foci can then be applied as a sensitive assay requiring very few cells. The quality of the staining, and different patterns of staining are also apparent.[59] Higher levels of damage can result in foci coalescing, and this may represent either a true reflection of adjacent areas of altered chromatin colliding,[60] an artefact of the accumulation of fluorescent antibody around its target, or the optical limitations of visualisation (which can be improved by confocal and newer microscopy techniques[61]).

In vitro applications typically draw statistically stronger conclusions by increasing the number of cells assayed, but the manual counting method then becomes

laborious. Attempts have been made to automate the recognition and counting process using high-throughput microscopy and digital image analysis techniques. [62-66]

Absolute numbers of intranuclear γH2AX foci may be reported, but it is generally not possible to draw comparisons between these numbers in different studies, as they will be influenced by both immunocytochemical and microscopic methodology.

The major alternative to microscopy for γH2AX assays is fluorescence-activated cell sorting (FACS). [67] This technology has the advantage of measuring populations of thousands of cells at one time, and also easily integrates information about cellular DNA content. Position in the cell cycle can be relevant to the susceptibility of tumour cells to treatments.[68] It is not as sensitive as microscopic foci counting when DSB numbers are low, and unusual expression patterns are not easily recognised. The FACS method measures the total γH2AX signal (by immunofluorescent intensity) on a cell by cell basis. Relating this to the number of DNA DSBs usually requires the mathematical assumption that the amount of γH2AX per DSB is constant. However the phosphorylation of H2AX histones takes time to propagate around a DSB[36] and the process of dephosphorylation and/or substitution of γH2AX histones will affect the amount of γH2AX in a single focus, seriously challenging this assumption.[54, 69]

High throughout automation to measure "total γH2AX" in lysates from cultured cells has also been reported with electrochemiluminescence. This method appears to improve the dynamic range of the assay at high levels of damage when

compared to foci counting, at the expense of some sensitivity at low levels of damage.[70]

Foci counting and cell sorting approaches are combined in laser scanning cytometry. This method has the potential to combine sensitivity with high throughput and cell cycle information but its applicability and optimisation has yet to be fully explored.[71, 72]

As they are developed, different γH2AX assays are cross-validated to one another,[56, 70, 73] and occasionally to independent measures of DSBs such as the neutral comet assay.[74] Cross-validation studies between methods have focussed on the extent to which they are concordant, rather than the nature and importance of discordance. The choice of technology for a particular application depends on the nature of the specimen (for example the number of cells available) and the expected range of measurement, as well as being governed by practical availability.

1.3.4. γH2AX is implicated in processes other than treatment-induced DSB formation

As discussed, the presence of γH2AX at sites of irradiation induced DNA DSBs has been observed across tissue and species types (primarily mouse, human and yeast) including normal and tumour cells. These observations are necessary but not sufficient in order to designate γH2AX as a biomarker of irradiation induced DSBs. This section addresses whether γH2AX is present in other contexts, and the next considers the relationship of the presence of γH2AX to the underlying presence of treatment-induced DSBs.

The nature of the DNA double strand break has been described above. Investigative attention has focussed on DSBs that are induced by external insults, in part because these are relevant to anticancer treatments and radiation incidents, and in part as they can be readily manipulated experimentally. There are physiological situations however in which DNA fragmentation occurs, such as replication stress, the S phase of the cell cycle, spermatogenetic meiosis and apoptosis. Investigations of these processes have clarified the role of H2AX and its phosphorylated counterpart, as well as the functional mechanics of the molecular response in those contexts. However they are considered here only as far as they impact on the application of γH2AX as a biomarker for treatment response.

1.3.4.1. Replication Stress and S phase

Agents such as hydroxyurea and ultraviolet light are recognised to disrupt DNA replication during cellular S phase, resulting in so called replication stress, and the collapse of DNA replication forks.[75] γH2AX is also generated in this situation, and co-localises with the proliferating cell nuclear antigen (PCNA), BRCA1 and 53BP1. γH2AX in this context appears to be generated predominantly by ATR rather than ATM.[76] The pattern of intense pan-nuclear staining produced in early S phase can be recognised in immunofluorescent microscopy and integrated into image recognition algorithms. It may also be apparent from FACS data, where the DNA content can be used to identify cells in S phase.

A separate but equally distinctive pattern of γH2AX phosphorylation throughout a subset of micronuclei in several cell lines was recently described in response to agents known to induce replication stress during S phase.[77] The presence of micronuclei indicates genomic instability, and some micronuclei may contain

fragmented DNA and hence γH2AX. The presence of this pattern was apparently independent of apoptosis.

1.3.4.2. Apoptosis

DNA fragmentation occurs during the latter stages of apoptosis, and this is accompanied by a nucleus-wide phosphorylation of H2AX. This event may follow on from replication stress in S phase, with the cell diverting down a cell death pathway to avoid mitosis in a stressed state. There is conflicting evidence about the dominant PI3-like kinase involved in this process, with knockout experiments that favour DNA-PK[78] but evidence of a maintained role for ATM[79] and other kinases.[80, 81] While knockout experiments can illustrate redundancy in pathways, they are not conclusive evidence for the importance of the remaining functional components to the native situation. Nevertheless it is clear that γH2AX is generated during apoptosis,[81-83] and more recent evidence suggests that it is involved in caspase-independent programmed cell necrosis. [84]

1.3.4.3. Hypoxia

Despite previous evidence that DNA damage *per se* was caused by hypoxia,[85] an ATR-dependent widespread phosphorylation of H2AX has been described in around 25% of cells from transformed cancer cell lines (RKO and H1299) at oxygen concentrations of <0.02%.[86] This could confound the use of γH2AX as a biomarker of treatment-induced DNA DSBs. However this effect was not observed in a fibroblast hypoxia model nor in cancer cell lines HCT116 and 22RV1. Hypoxic cells incur fewer DSBs than normoxic cells in response to radiation (measured both by γH2AX foci and the neutral comet assay), but after 24 hours of repair under ongoing hypoxia there are more residual DSBs,[87] indicating that repair is

modulated by the oxygen context. The relevance of hypoxia to the use of γH2AX as a DNA damage biomarker is therefore complex – the underlying background of γH2AX is increased, the number of DSBs decreased and their repair impaired. Since the aim of this thesis is to measure the actual behaviour of all tumour cells, hypoxic or otherwise, the successful measurement of γH2AX (*in vitro* at least)[88] is encouraging for this choice of biomarker.[89]

1.3.4.4. Spermatogenesis

Early in the characterisation of γH2AX, it was noted that testicular expression of H2AX, as well as its phosphorylated form was high. γH2AX is present at several stages of spermatogenesis, including those that do not indicate underlying DNA DSBs[90, 91] and disappears at synapsis, the homologous chromosome pairing event that precedes cell division in meiosis. Clearly the generation of γH2AX during spermatogenesis is relevant only in the testis, although a whole body imaging approach to γH2AX measurement might have to make allowance for this (notwithstanding the blood-testis barrier that might limit the availability of target to a circulating imaging agent).

1.3.4.5. Carcinogenesis

As first reported by both Bartkova and Gorgoulis in 2005 [92, 93] pre-neoplastic tissues exhibit increased replication stress which can lead to upregulation of DDR pathways. Increased expression of γH2AX compared to normal tissue was shown in pre-neoplastic and neoplastic lesions in the skin, lung, breast and kidney [93-97], γH2AX assays may therefore develop a clinical role in detecting the process of carcinogenesis. The role of γH2AX in these situations is not yet clear, but it may

represent genomic instability in the presence of intact DNA damage repair machinery.

1.3.4.6. Other situations

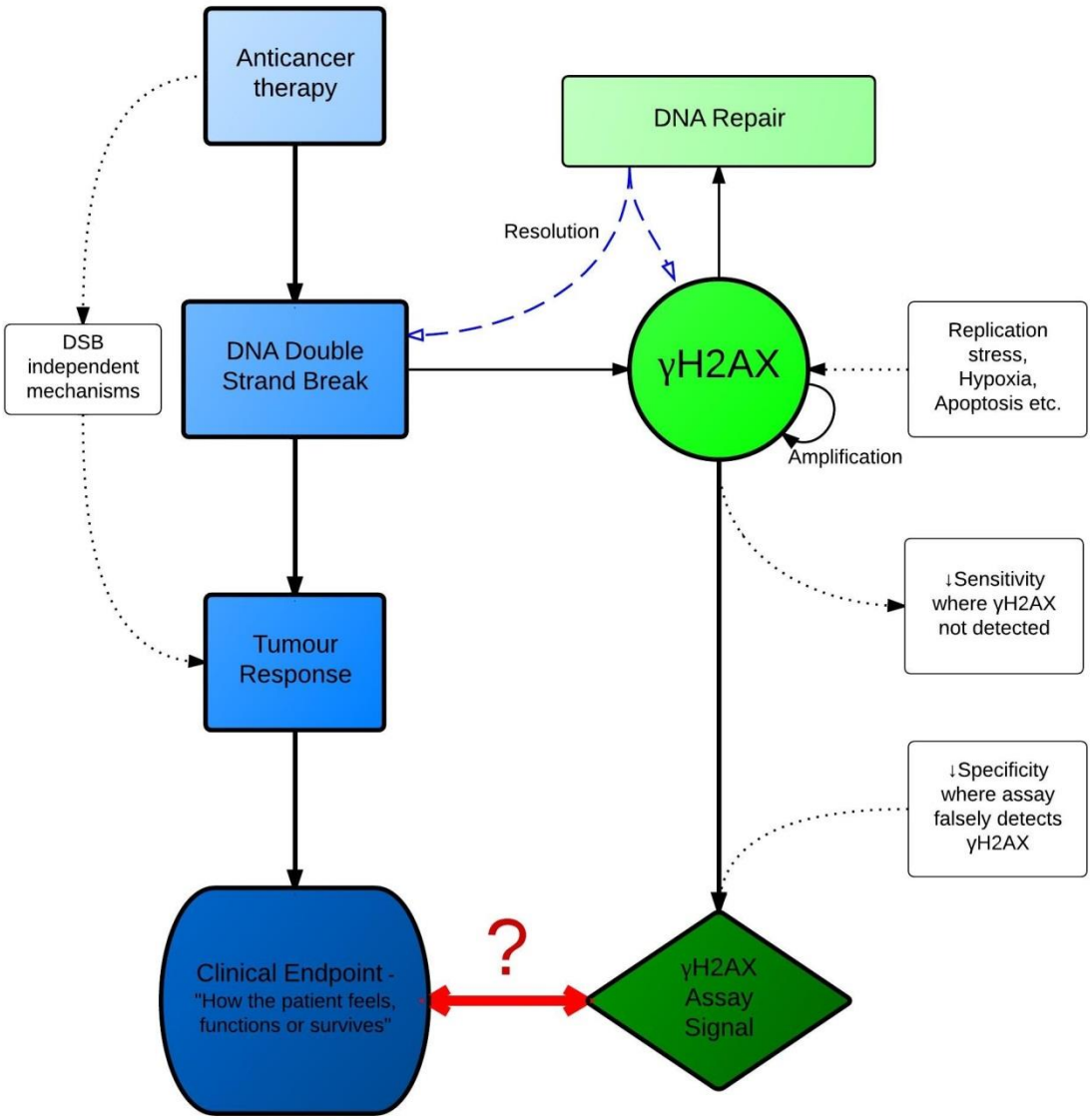
Several other *in vitro* perturbations of the cellular environment that induce γH2AX formation have been described. Changes in osmolality can activate γH2AX in the absence of DSBs through chromatin remodelling [98, 99] while sodium butyrate-induced p21 causes cell senescence accompanied by γH2AX foci in the absence of DNA breaks.[100] γH2AX foci are formed during retroviral post-integration repair, which involves the transient creation of DSBs, although knockout of *H2AFX* does not protect cells from retroviruses.[101] Epidermal growth factor (EGF) induces γH2AX independent of DNA damage in some cell lines in a mechanism dependent on DNA-PK as well as ribosomal S6 kinase 2 (RSK2). [102] Applications outside oncology have included neurodegenerative disease [103] and aging. [104, 105]

1.3.5. Interpreting the presence of γH2AX in dynamic DNA damage and repair

In order to consider rationally the utility of γH2AX measurements as clinical biomarkers of treatment response, some pitfalls in interpreting the presence of γH2AX must be acknowledged. As discussed in Section 1.2, the amount of DNA damage, specifically DSBs, caused by treatments is a plausible proxy for their clinical effectiveness. Section 1.3.4 addressed situations other than DNA DSBs in which γH2AX is known to be generated. But even where γH2AX is generated in the context of treatment-induced DSBs, it is too simplistic to assume that the γH2AX signal at the moment of measurement is a direct report of the number of DNA DSBs at that moment.[46, 106]

Rather, DSB creation and repair are dynamic processes, and γH2AX generation and disappearance are distinct but related dynamic processes. In addition, the assays of γH2AX discussed above (in Section 1.3.3) and considered in this thesis have limitations that complicate the relationship of the assay signal to the actual amount and distribution of γH2AX (see Figure 1.6).

Figure 1.6 The relationship between γH2AX and its assays and clinical anticancer therapy



Cell cycle position also affects γH2AX. Its generation during S phase is considered in Section 1.3.4.1 above. Total DNA content also determines the potential amount of the target, with twice as much being available in G2 phase (after replication) when compared to G1.

To add a further level of complexity, cellular origin and phenotype, including relationships to the microenvironment, will be expected to affect the response to DNA damage. Several studies have addressed these interrelationships, although no comprehensive synthesis has emerged.

1.3.5.1. γH2AX is produced in proportion to the induction of DNA DSBs

The experiments reviewed above (Section 1.3.1) that first identified γH2AX as a component of the cellular response to DSBs employed agents including ionising radiation[57], topoisomerase inhibitors[58] and the DNA cleaving-antibiotic calicheamycin[73].

The extent and kinetics of the induction of breaks depends on the cellular context as well as the DNA damaging agent used. Concentrating on cervical cancer cell lines and ionising radiation, Banath *et al.* compared clonogenic survival to total γH2AX measurement by FACS in six cervical cancer cell lines. Both γH2AX signal and mean tail moment in the comet assay (see Section 1.2.3) were directly proportional to ionising radiation dose in the range 0-10Gy for all cell lines. However the ratio of γH2AX signal at 10Gy to that in unirradiated cells varied from 5 (HeLa cell line) to 13 (SiHa cell line).[107] Maximal γH2AX visualisation occurs 20-60 minutes after ionising radiation depending on cell type and assay.[108]

The correlation between γH2AX signal and clonogenic cell survival was closest when considering p53 wild type and mutant lines separately.[107, 109, 110] This approach appears to be valid since p53 is involved in the cell cycle and apoptosis decisions relevant to cell survival that occur downstream of γH2AX formation in response to DNA damage. The overriding importance of p53 status may explain other groups' failure to find such correlations between γH2AX and clonogenic cell survival across a range of cell lines, albeit using digital analysis of immunocytochemical foci.[111, 112] Interference with γH2AX phosphorylation, for example using synthetic carboxyl terminal peptides or inhibition of PI3 kinases, has been shown to affect cell survival in proportion to its effect on γH2AX formation.[113, 114]

Cytological γH2AX induction analyses have been extended to normal human peripheral blood mononuclear cells irradiated *ex vivo*. Studies have indicated a wide inter-individual variation in both the background γH2AX signal and the extent of γH2AX induction in response to radiation.[115, 116] However, γH2AX induction remains maximal at one hour post-irradiation, directly proportional to dose, and is best demonstrated using immunocytochemistry in the dose range 0-1Gy and FACS in the dose range 2-8Gy.[117]

The kinetics of γH2AX induction in solid normal tissues have been described from 10 minutes after *in vivo* irradiation. Fewer foci appear to be generated per Gray when compared to *in vitro* data, but this may represent an artefact of tissue preparation for microscopy.[118, 119]

Very few data are available from solid tumours. Kinders *et al.* reported the preclinical validation of a tissue biopsy method for γH2AX foci counting to apply in

early phase clinical trials of topoisomerase I and PARP inhibitors.[120] Only initial qualitative data have been reported from clinical trials employing this method.[121, 122] The clinical studies from the Olive group during chemoradiotherapy for cervical cancer[123, 124] represent a proof of principle that γH2AX is induced in human tumours, with a suggestion of dose response at clinically relevant doses.

Thus the use of γH2AX measurements (as a ratio to baseline measures) to quantify the induction of DNA damage is accepted even by authors who are critical of the marker.[46, 69, 106]

1.3.5.2. The kinetics of γH2AX disappearance depend on assay and cell context

The nature of the resolution of γH2AX foci has implications both for the behaviour of the cell and for the interpretation of γH2AX assays, a distinction that is not always apparent in discussions in the literature.[106]

It is assumed that while a DNA DSB persists, the tendency for ATM-mediated phosphorylation of γH2AX will remain. Once the DSB is repaired and this impetus is removed, the balance will shift towards dephosphorylation by the protein phosphatases discussed above (Section 1.3.2) and also histone exchange (the *in situ* substitution of H2AX for γH2AX).[69] Note that histone exchange may dissipate a γH2AX focus so that it may no longer be demonstrated by immunocytochemistry, but that if the free histone protein remains phosphorylated, its presence may contribute to the intensity signal detected by FACS.[73]

The question of whether a γH2AX signal disappears before, with or after repair of the DNA DSB that prompted its generation is primarily important for interpreting

an assay that uses γH2AX as a marker for extant DSBs. Thus unfavourable comparisons have been made with more direct physical assays of DSB such as comet assays (single cell gel electrophoresis) and pulsed field gel electrophoresis (PFGE),[125] notwithstanding the inability of such methods to detect low levels of damage.

The physical methods of DSB demonstration have identified a fast and a slow phase of DSB repair.[126] γH2AX foci have been shown to disappear with similar bi-exponential kinetics, albeit with delayed timing when compared to physical PFGE and comet analyses.[106, 107]

Repair kinetics are dependent on cell type, with transformed and cancer cell lines showing altered repair when compared to primary cultures[127] as well as increased background γH2AX consistent with genomic instability. Cell cycle phase is also important, since cells can invoke homologous recombination (HR) during S phase, and DNA content increases during S phase until G2. Cells in G0/G1 phase which have lost DNA ligase IV, which is necessary for non-homologous end-joining (NHEJ) start to show decreased clearance of foci as early as 15 minutes from ionising radiation [128] and persistent foci up to 7 days after treatment.

In human PBMCs irradiated *ex vivo*, and maintained in culture, the disappearance of γH2AX foci or reduction in intensity can also be fitted to a bi-exponential decay model, the fast and slow components of which have half-lives of approximately 1.5 hours and around 36 hours respectively. For doses above 0.5Gy, irradiated cells continue to have significantly greater γH2AX signals than unirradiated cells some 96 hours after irradiation.[117]

For intact normal tissues irradiated *in vivo*, remarkably similar data have been obtained from immunofluorescence in the lung, heart, intestine, brain and kidney[119] despite differences in biochemical assays between organs.[129] Focus loss is once again consistent with bi-exponential decay, but the half-lives of fast and slow components are shorter, at around 0.8 and 6.5 hours. These kinetics are altered in genetic backgrounds that affect DNA repair, including ATM truncation mutations and severe combined immunodeficiency (SCID) which affects DNA-PK.[130] There is evidence from knockout mice that DNA-PK does play a role in phosphorylation and elimination of γH2AX in normal tissues *in vivo*.[129, 131] Indeed DNA-PK may have a role when DSBs persist in the elaboration of foci.[132]

A common theme among descriptions of the kinetics of γH2AX measurement has been the persistence of an altered signal, sometimes for several days after an insult. The timing is clearest when ionising radiation is considered, since circulating DNA damaging drugs may themselves persist *in vivo*.

Immunocytochemical methods are more sensitive than FACS in identifying these small amounts of γH2AX remaining 1, 4 or 7 days after radiation, and hence the concept of "late residual foci" has emerged, albeit without a uniform definition.[117, 133, 134] This is consistent with the idea that even small numbers of unrepaired DSBs will force the cell towards death.

1.3.6. γH2AX remains an attractive biomarker for DSBs

It is clear from the discussion above (in particular Sections 1.3.4 and 1.3.5) that γH2AX does not simply represent a cellular reaction to exogenous DNA DSBs. A global appreciation of the role or roles of γH2AX[46, 51, 125, 135] is distinct from its

consideration as a biomarker for clinical translation [136-138] that forms the subject of this thesis.

The choice of assay and its clinical context will help determine the effect of other roles of γH2AX on the specificity of the biomarker signal for treatment induced DSB-related outcomes. The inclusion of pre-treatment pharmacodynamic assay measurements could identify the "background" γH2AX signal to be considered in interpreting measurements taken after the treatment under investigation. The importance of this background measure would depend on it magnitude, variability over time and the accuracy with which it could be determined.

The pervasive γH2AX effects throughout spermatogenesis for example would limit biomarker application, albeit only in the testis. Apoptosis and S phase replication stress, where γH2AX indicates endogenous DNA breaks, may well correlate with the same outcomes as exogenous DNA DSBs. [77, 139, 140] Some assays are able to distinguish the pan-nuclear staining pattern of apoptosis or late S phase from the widespread nuclear focal pattern of exogenous DNA DSBs.[46, 141]

Confounding by hypoxia is more difficult to integrate. Considering radiation treatment, hypoxia famously protects cells from radiation-induced cell damage[142] so that where γH2AX reflects a very low oxygen concentration, it would indicate radioresistance rather than deleterious DNA damage. Nevertheless, γH2AX has not been reported to be a universal accompaniment to hypoxia [87] and where is does coincide, this is in a minority of cells.[86] *In vivo*, a circulating imaging agent for example might not perfuse into hypoxic areas in order to return a confounding signal.

Questions of the absolute level of γH2AX assayed, and in particular the kinetics of its induction and resolution are critical to its application. It is biologically plausible that the peak amount of damage, the integral of the time-damage curve, the remaining unrepaired damage at time X, the physical distribution of damage or any of countless time-space-damage metrics could correlate best with the outcome for a tissue or cell population.[106] Clinical investigations need to establish what an assay measures, how its application relates to DNA damage and repair metrics, and apply this empirically to clinical questions.

In conclusion while there is reason to be cautious about the simplistic interpretation of γH2AX as a marker of treatment induced DNA DSBs, there is no *ab initio* case against pursuing its investigation as a clinical biomarker.

1.3.7. Clinical γH2AX assays answer questions in oncology

1.3.7.1. Whole body dosimetry after radiation exposure

The use of γH2AX induction as a sensitive marker of general radiation exposure is not considered comprehensively here since it is related only tangentially to its application as a response biomarker to treatment in oncology. Applications outside oncology are not considered here, but have included neurodegenerative disease[103] and aging.[104]

Almost all biodosimetry investigations have used peripheral blood mononuclear cells (PBMCs) since they can be assumed to be distributed throughout the body during exposure, and can be collected with ease using separation of whole blood by density gradient centrifugation. Table 1.1 illustrates a selection of studies of exposures relevant to oncology, both simulated using *ex vivo* γ- irradiation of PBMCs and actual clinical exposures during diagnostic and therapeutic

procedures. While some earlier studies neglected individual variability in the γH2AX response, later ones have tended to calibrate that response using *ex vivo* irradiation and dose and timing studies. It is not clear however, whether *ex vivo* simulations mimic either the immediate environment of cells *in vivo* or radiation parameters such as dose rate and quality.[117]

Table 1.1 Selected clinical studies employing γH2AX as a biodosimeter of radiation exposure

Clinical setting	Treatment	Tissue sampled	γH2AX assay	Result/Comment	Reference
Diagnostic X-ray exposure	Clinical CT scan	PBMC	Manual IF foci	Pre vs. post difference	Labrich *et al.* 2005[143]
Diagnostic X-ray exposure	Clinical CT scan	PBMC	Manual IF foci	Pre vs. post difference	Rothkamm *et al.* 2007[144]
Simulated accidental radiation exposure	*Ex vivo* IR + caliceamicin	PBMC	FACS	Unifixed cell method	Ismail *et al.* 2007[145]
Incidental exposure during radiotherapy	Clinical EBRT	PBMC	Manual IF foci	Complex relation to simulated dose	Sak *et al.* 2007[146]
Paediatric X-ray exposure	Clinical cardiac catheterisation	PBMC	Manual IF foci	Dose estimates	Beels *et al.* 2009[147]
Incidental exposure during radioisotope therapy	Clinical radioiodine treatment	PBMC	Manual IF foci	Costained for 53BP1	Lassmann et al. 2010[148]
Incidental exposure during radiotherapy	Clinical low dose localised EBRT	PBMC	Manual IF foci	No significant difference. Background varied with steroid use	Lindholm *et al.* 2011[149]
Simulated accidental radiation exposure	*Ex vivo* IR 0.5, 1, 4Gy	PBMC	Manual IF foci +FACS	Foci better at later timepoints	Horn *et al.* 2011[117]
Incidental exposure during radiotherapy	Clinical EBRT techniques	PBMC	Manual IF foci		Zwicker *et al.* 2011[150]

PBMC= peripheral blood mononuclear cell; EBRT= external beam radiotherapy; IR= ionising radiation; 53BP1= p53 binding protein 1; IF= immunofluorescence; FACS= fluorescence activated cell sorting

1.3.7.2. Normal tissue radiosensitivity and chemosensitivity

As discussed above individual variation in γH2AX responses can confound the use of the biomarker as a measure of dose. Some studies have concentrated on this variation in an attempt to relate it to normal tissue radiosensitivity,[30, 151] usually manifest as normal tissue toxicity from external beam radiotherapy (alone or in combination with chemotherapy).[152] As shown in Table 1.2, the availability of PBMCs makes them an attractive source of nucleated cells. PBMCs are however not generally implicated in the pathogenesis of normal tissue reactions.[5] A distinction must also be drawn between early and late normal tissue toxicity. These reactions are thought to arise from different cell types, and relate both to the extent of initial DNA damage and the capacity for repair. A closer correlation to clinical outcome might be found by examining the extent and kinetics of repair (as evidenced by disappearance of γH2AX foci/signal)[153, 154] rather than merely the dose-dependence of γH2AX induction. However, all of these parameters may well differ across cell types, and the use of easily accessible PBMCs as a proxy for a variety of normal tissue cell types that are already known to react differently to genotoxic insults may be flawed. Two reports from the Turesson group have investigated skin as an accessible normal tissue that is the directly affected by radiation and results in toxicity.[155, 156] 53BP1 foci have also been investigated in this context.[157] An extension of this approach in larger patient numbers, explicitly addressing the cellular pathogenesis of early and late toxicity is warranted.

Table 1.2 Clinical studies employing γH2AX as a marker of normal tissue radiosensitivity or chemosensitivity53BP1, p53 binding protein 1; EBRT, external beam radiotherapy; FACS, fluorescence activated cell sorting; H&N, head and neck; IF, immunofluorescence; IR, ionising radiation; PBMC, peripheral blood mononuclear cells.

Clinical setting	Treatment	Tissue sampled	γH2AX assay	Result/Comment	Reference
Relation to dose from clinical simulation for EBRT	Clinical EBRT	Normal skin	Manual IF foci	Descriptive result over 0-1 Gy, n=5 Digitally enhanced images	Qvarnstrom *et al.* 2004[155]
Relation to clinical diode dosimetry	Clinical EBRT	Normal skin	Automated IF foci	Descriptive result during fractionated therapy	Simonsson *et al.* 2008[156]
Late normal tissue effects in prostate brachytherapy	*Ex vivo* IR	PBMC	FACS	Case control study. No correlation of γH2AX foci to late toxicity	Olive *et al.* 2008[158]
Ataxia Telangectasia (AT) diagnosis assay development	*Ex vivo* IR	PBMC	FACS	Identified 4/4 AT cases, excluded 15/15 non-AT suspected cases	Porcedda *et al.* 2008[159]
Cisplatin-containing chemo RT for lung/H&N/pelvic tumours	Clinical chemo/EBRT+	PBMC	Manual IF foci	Costained Rad51, neutral comet. Counted only 50-70 nuclei/patient	Sak *et al.* 2009[152]
Phase 1 trial of Poly (ADP-Ribose) Polymerase inhibitor	Olaparib	Eyebrow hairs	Manual IF foci	Pharmacodynamic marker of collapsed replication forks	Fong *et al.* 2009[160]
Oral mucositis from adjuvant EBRT for H&N cancers	*Ex vivo* IR dose+ kinetics	PBMC	Manual IF foci	No clear relation to mucositis severity	Fleckenstein *et al.* 2010[154]
Normal tissue toxicity from EBRT for breast, prostate	*Ex vivo*/ cultured IR	Cell lines	Automated IF foci	Limited scope as a predictive assay for toxicity	Vasireddy *et al.* 2010[116]
Normal tissue toxicity from EBRT for pelvic cancers	*Ex vivo* IR	T cells	Manual IF foci	Limited relation to toxicity	Werbrouck *et al.* 2010[161]
Oral mucosa radiation toxicity	*Ex vivo* IR	Buccal scrapings	Manual IF foci	Changes with irradiation described in range 0-4 Gy.	Gonzalez *et al.* 2010[162]
Normal tissue toxicity from EBRT for breast cancers	*Ex vivo* IR dose + kinetics	PBMC	FACS	Descriptive correlation to toxicity	Bourton *et al.* 2011[153]

1.3.7.3. Tumour diagnosis/stratification

Genomic instability is associated with the development of malignancy.[163] DNA damage, and in particular DNA double strand breaks, can contribute to that instability.[164] Markers of DSBs could then be potential markers of carcinogenesis.[93] γH2AX has therefore been investigated as a marker for malignancy (see Table 1.3) but most of these studies have used a horseradish peroxidase-diaminobenzidine immunohistochemical methodology with light microscopy. Such technology lacks the sensitivity of immunofluorescent methods resulting in less quantitative results that may fail to correlate with the subtle and gradual increase in genomic instability that accompanies carcinogenesis. Mechanisms of genomic instability have been related to prognosis and chemosensitivity,[165] a paradigm exemplified by the case of microsatellite instability and chromosomal instability in colon cancer.[166]

Table 1.3 Studies employing γH2AX for clinical cancer diagnosis or prognosis.

CIN=cervical intraepithelial neoplasia; DAB=diaminobenzidine; FFPE= Formalin fixed paraffin embedded FNA= fine needle aspiration

Clinical setting	Tissue sampled	γH2AX assay	Result/Comment	Reference
Diagnosis of renal cell cancer	Kidney FNA	Manual DAB intensity	Positive stain in majority of malignant cases	Wasco *et al.* 2008[167]
Diagnosis of malignancy in melanocytic skin lesions	Archived FFPE skin biopsies	Manual DAB intensity	Poor correlation to malignancy as most lesions express γH2AX. DAB method less quantitative	Wasco *et al.* 2008[168]
Endometrial cancer prognosis	Archived FFPE endometrial biopsies	Manual DAB intensity	No relation to prognosis in multivariate analysis Co stained with p53	Brunner *et al.* 2010[169]
Diagnosis of malignancy in cervical cancerous and pre-cancerous lesions	Archived FFPE cervical biopsies	Manual DAB intensity	Co-stained with EGFR	Brustmann *et al.* 2010[170] Abstract only
Bladder cancer risk of recurrence	Archived FFPE bladder biopsies	Manual DAB intensity	No significant relationship	Cheung 2010[171]

1.3.7.4. Tumour cell pharmacodynamics or "radiodynamics"

Malignant transformation[17] and the tumour microenvironment[142] affect the cellular response to drugs and radiation. So the question of tumour response to anticancer treatments is distinct from that of normal tissue toxicity, and requires a tailored translational research strategy[137, 138, 172] (see Table 1.4). In leukaemias, circulating malignant cells can be collected and isolated, allowing pre-treatment *ex vivo* testing of drug treatments.[173, 174] Radiosensitivity could also be measured on such *ex vivo* samples, although as a local treatment radiotherapy plays little part in the acute treatment of systemic leukaemia.[175, 176]

Circulating cells from solid tumours (CTCs) represent a potential source of tumour cells accessible for multiple sampling.[177] A method has been developed using normal blood samples spiked with cultured tumour cells,[178] and applied in small subsets of patients within phase I trials of poly(ADP) ribose polymerase inhibitors. [121, 122] The assay can demonstrate an interaction of the trial drug with tumour cells, however in applications to date the quantification of this interaction is hindered by the low and changing number of CTCs, which ranged from 0 to 119 in 7.5ml of blood in the validation study.[178] In addition the relationship between the cells that circulate and those in the tumour bulk has yet to be established, so that any inductions regarding overall tumour behaviour based upon the characterisation of CTCs would require further validation. Similar arguments arise when considering cells from central nervous system tumours isolated from cerebrospinal fluid. [179]

Cell sampling from solid tumours during anticancer therapy would give the most direct information about its effects. Obtaining such samples can present a logistical challenge, however, since patients undergoing such treatments already have to

contend with the inconvenience and toxicity of treatment. The burden on patients is compounded where repeated sampling is attempted. The Olive group in Vancouver, Canada, have published data from biopsies obtained from patients before and during combined radiotherapy and chemotherapy treatment for squamous cell cancers of the uterine cervix. [123, 124] This approach explored the feasibility of γH2AX immunohistochemistry in clinical samples taken during treatment, and the principle that differences could be seen between pre-treatment baseline measurements and those taken after treatments known to damage DNA. By staining some tumour sections for carbonic anhydrase IX and pimonidazole, the authors have also attempted to relate baseline γH2AX expression with hypoxia (see Section 1.3.4.3). No data are presented at this early stage of assay development regarding the reproducibility of the γH2AX measurements, however, or differences between archived and fresh samples.

Table 1.4 Clinical studies employing γH2AX measurements of tumour cells during chemotherapy or radiotherapy treatment

ALL, acute lymphoblastic leukaemia; CSF, cerebrospinal fluid; CTC, circulating tumour cells; DAB, diaminobenzidine; EBRT, external beam radiotherapy; EC, epirubicin + cyclophosphamide; FACS, fluorescence activated cell sorting; FFPE, fresh frozen paraffin embedded; IF, immunofluorescence; PARP, poly (ADP ribose) polymerase; PBMC, peripheral blood mononuclear cells

Clinical setting	Treatment	Tissue sampled	γH2AX assay	Result/Comment	Reference
Phase 1 trial in relapsed acute lymphoblastic leukaemia (ALL)	Cyclophosphamide +/- clofarabine	Relapsed ALL blasts	FACS	Pre and post treatment assay combination chemo versus cyclophosphamide alone n=13	Karp *et al.* 2007[174]
Combined chemo+EBRT for cervical cancer	Cisplatin + EBRT	Fresh FFPE cervical biopsies	Manual IF foci + FACS	Feasability of measurement in biopsies. Pre and during chemo/EBRT. Costained with caspase, carbonic anhydrase IX; n=8	Banuelos *et al.* 2009[123]
Phase 1 trial of intrastrand crosslinking agent (SJG-136)	SJG-136	PBMC + tumour cells (?which)	Manual IF foci	Increase in foci in PBMC (n=16) Tumour cell pharmocodynamics not yet fully reported; n=2	Hochhauser *et al.* 2009[180]
Phase 1 trial in acute myeloid leukaemia (AML)	Tipifarnib	AML blasts	FACS	Related γH2AX to DNA content and response; n=33	Karp *et al.* 2009[173]
Preoperative chemotherapy for breast cancer	EC chemotherapy	Core biopsies of breast ca	Manual DAB	Costained with Rad51, ubiquitin, BRCA1; n=60	Asakawa *et al.* 2010[181]

Table 1.4 (continued)

Clinical setting	**Treatment**	**Tissue sampled**	**γH2AX assay**	**Result/Comment**	**Reference**
Combined chemo+EBRT for cervical cancer	Cisplatin + EBRT	Archived + fresh FFPE cervical biopsies	Manual IF foci	Pre and post treatment pharmacodynamics. Co-stained carbonic anhydrase IX, hypoxia discussion	Olive *et al.* 2010[124]
Various cancers	Various chemotherapy agents	CTC	FACS	Pre vs post treatment pharmacodynamics. Measured %cells positive	Wang *et al.* 2010[178]
Anaplastic astrocytoma	Brain EBRT	Archived + fresh CSF	Manual DAB intensity	Pre vs. post EBRT evaluation	Abe *et al.* 2011[179]
Phase I study of PARP inhibitor ABT-888 in advanced solid tumours	ABT-888	PBMC + tumour biopsy + CTC	CTC:FACS Biopsy/ PBMC: Automated IF	γH2AX responses: Biopsies 0/2, CTC 3/4, PBMCs 5/10 (Total 24 trial patients)	Kummar *et al.* 2011[121]
Phase I study of PARP inhibitor velaparib + cyclophosphamide in advanced solid tumours	Velaparib + cyclophosphamide	PBMC + CTC	FACS	γH2AX responses: PBMCs 2/17, CTC 7/9. Caution as low CTC numbers.	Kummar *et al.* 2012[122]

1.4. Clinical biomarker development

1.4.1. Biomarker can be classified by their clinical application

Biomarkers are defined as "objective measurements evaluated as indicators of normal biological processes, pathogenic processes, or pharmacologic responses to a therapeutic intervention."[13] The term "pharmacologic" betrays the elaboration of the biomarker concept in the context of drug development, but this work is readily translated to radiation treatment.[182] The utility of a biomarker can only be judged by relating it to a clinical endpoint, defined as a reflection of how a patient feels, functions or survives.[13, 183]

As discussed above, (Section 1.1.4, Figure 1.3), biomarkers can inform all stages of the clinical process in oncology.[184] *Prognostic* biomarkers indicate the likelihood of a clinically relevant outcome, such as survival without cancer recurrence, in a particular tumour and treatment context. However they do not give direct evidence to guide the choice between different treatments.[185]

Predictive biomarkers provide information to guide the choice between treatments. For example epigenetic silencing of the gene for DNA repair protein methylguanine methyltransferase (MGMT) identifies patients who gain a survival advantage from the addition of temozolamide chemotherapy to radiotherapy for the aggressive brain malignancy glioblastoma multiforme. This biomarker was established as a result of a large randomised trial.[186, 187]

The effect of a drug therapy on the body or disease is measured by a *pharmacodynamic* biomarker. By extending this concept to include radiotherapy, but focussing on tumour effects, this thesis considers γH2AX as a "radiodynamic" or *response* biomarker.

1.4.2. Biomarker development is a multi-stage process

While biological indicators of some sort have always been used in medicine, advances in molecular biology have led to a proliferation of potential biomarkers. Their translation into useful clinical tools depends on questions of assay and application that are individual to that marker, but some general principles of biomarker development have been described. [184, 188, 189]

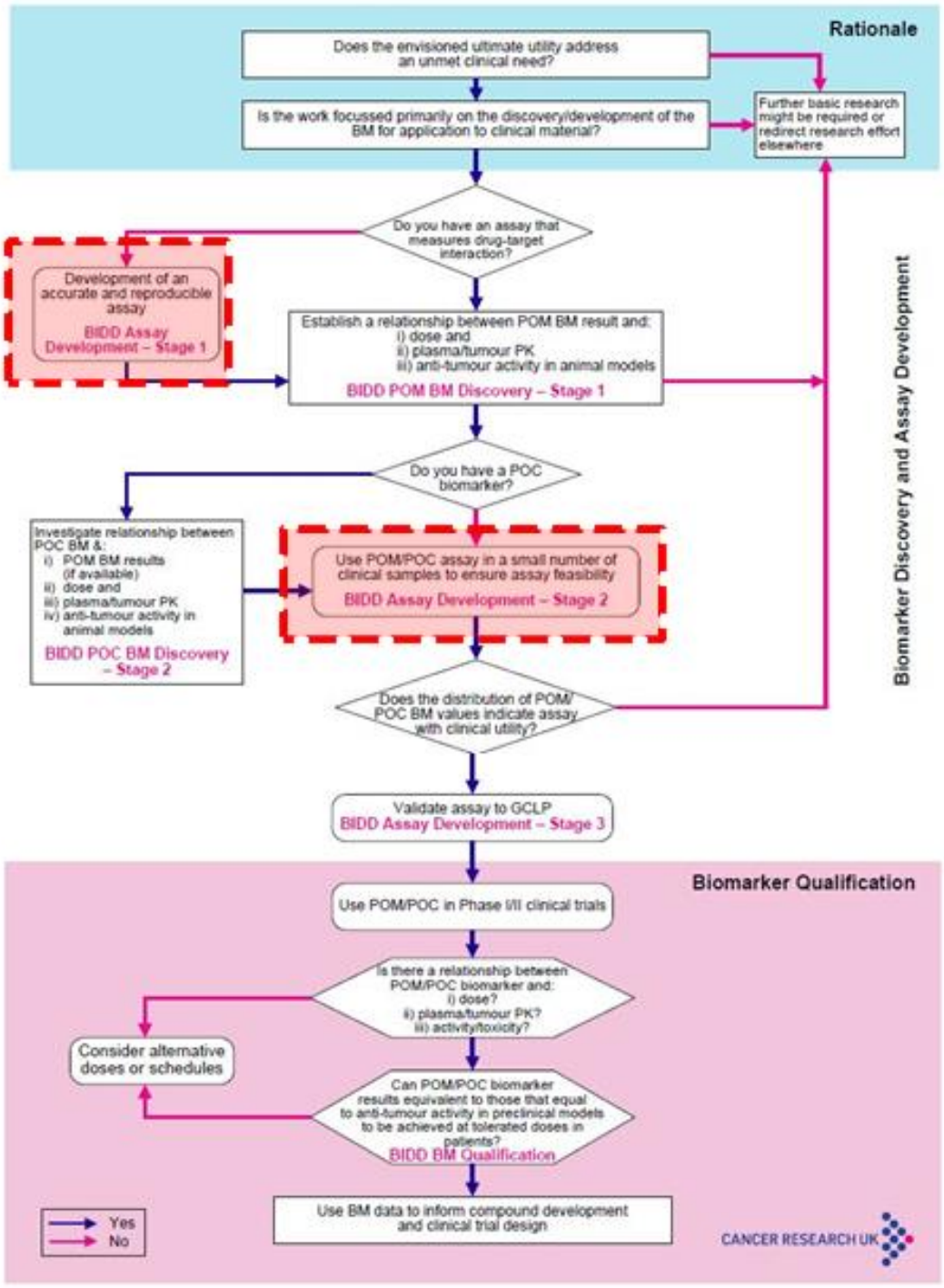
Three major conceptual stages of development are described (see for example Figure 1.7). After considering the theoretical rationale for applying a biomarker, the analytical performance of the assay must be examined. At this stage the precision or reliability of the assay is most pertinent. Variations in repeat measurements may arise from biological variation in the patient, but also from measurement methods and intra-observer error. [190] Pre-analytical factors of specimen handling and storage must also be considered to reduce error.[191]

The second stage is termed qualification, and is concerned with the association between the biomarker and the true disease state, or response. This validity may in simple cases be described by specificity and sensitivity (the ability of the test to correctly identify negative and positive states respectively). It should be noted however that this negative and positive dichotomy may oversimplify disease or response characterisation. The endpoint to which the test is validated should be relevant – truly clinical endpoints are defined as "[reflections of] how the patient feels, functions or survives".[13]

In the utilisation stage analysis is based on the specific use proposed. Clinical trials can be useful to test the feasibility of the assay, and biomarkers can ideally accompany both early and later phase trials of novel therapies. Complications may

arise when the primary endpoint is replaced by surrogates however,[192, 193] since even a statistically strong correlation between assay results and clinical endpoints can be misleading.[194] A priority for translational research is to improve the characterisation of its biomarkers and comparisons made between them.[195-197] Translation from clinical trials to everyday clinical practice may entail further challenges.[198-200]

Figure 1.7 Cancer Research UK Pharmacological Biomarker Roadmap (reproduced with permission) highlighting development areas addressed in this thesis



1.4.3. Potential tumour response assays

As discussed above (Section 1.1.2) direct tumour biopsies are usually carried out only at cancer diagnosis. The response biomarker paradigm, employing γH2AX in this thesis, however requires ongoing information about changes in the tumour.

The most direct approach is to repeat the biopsy procedure during treatment. Biopsies that remove a solid core of tumour tissue are generally invasive, and may be unacceptable to patients during a course of toxic anticancer therapy. The less invasive but still direct tumour sampling technique of fine needle aspiration (FNA) cytology is explored in this thesis as a potential modality for a γH2AX assay in accessible tumours. FNA involves directly drawing cells from the tumour through a fine bore needle, typically 22G (0.7mm diameter) compared to 14G (2.1mm) for a core biopsy needle (see Chapter 3.)

It may be possible to measure blood-borne biomarkers secreted by the tumour, either as whole cells,[122, 201] or as humoral factors,[3] including microRNA,[202] and circulating cell-free DNA.[203]

Molecular imaging with emerging technologies including positron emission tomography (PET), single photon emission computed tomography (SPECT), magnetic resonance imaging and spectroscopy (MRI/MRS) extends the concept of a biomarker. It has the advantage of being non-invasive, and the potential to provide information about multiple sites within a tumour and multiple tumour deposits with a single procedure. The geometrical nature of the information is particularly attractive in radiotherapy, where increasing sophistication in delivery technology might allow the targeting of less responsive tumour areas.

The quality of the imaging information depends on the modality and (if employed) the molecular imaging probe. The precision and accuracy of imaging outputs are important considerations, but their evaluation may be impeded by the complexity of signal quantification.

As discussed in section 1.1.2 treatment response is often currently assessed using non-invasive imaging (with CT and MRI).[9] It is a natural progression to elaborate these size-based criteria to include functional information.[204] Some clinical implementation of ^{18}FDG-PET for this purpose has been explored, and there are interesting preclinical approaches to the measurement of normal tissue toxicity,[205] cell death[206, 207] and indeed γH2AX.[208, 209]

1.5. Conclusion

There is a clinical advantage to be gained in assessing response to anticancer treatments earlier. For treatments, including radiotherapy, that act through DNA damage and in particular DNA double strand breaks (DSBs), measurements of these lesions could help to guide treatment. The generation of γH2AX in the histone core of chromatin is a highly conserved, rapid, measureable event that occurs in response to DSBs. This thesis explores the development of clinical assays of γH2AX as biomarkers for cancer care.

1.6. Aim of the thesis

The thesis aims to explore the clinical translation of γH2AX as a biomarker of the response to anticancer therapy. Its objectives are therefore:

1. To extend the characterisation of yH2AX by immunohistochemistry in solid tumours towards clinical application;
2. To develop a method for measuring γH2AX by immunocytochemistry in clinical tumour fine needle aspirate (FNA) samples;
3. To develop antibody-based molecular imaging of the DNA damage response using Fab fragments of an anti-γH2AX antibody.

Chapter 2

Development of a solid tumour tissue immunohistochemistry method to demonstrate γH2AX

Chapter 2: Development of a solid tumour tissue immunohistochemistry method to demonstrate γH2AX

2.1. Introduction

2.1.1. γH2AX in solid tumours

This chapter describes the development and application of tumour immunohistochemistry for γH2AX. The clinical translation of γH2AX assays for measurement of tumour response to therapy and DNA damage repair is built upon the preclinical application of those assays.

Almost all experimental investigations of the formation and cellular role of γH2AX have been performed on cells in culture (see Chapter 1). Solid tumours behave differently to cells in culture, however, since the cellular microenvironment is different. Many of these microenvironmental factors are relevant to tumour radiosensitivity[142] and DNA repair[210] and these include tumour oxygenation, the immune response to tumours, and tumour signalling.

2.1.2. Immunohistochemistry

Immunohistochemistry employs antibodies to demonstrate specifically the presence of defined epitopes in tissue sections. It can be used to correlate morphological information with evidence about the chemical constituents of cells and tissues, providing an indication of the functional anatomy of a tissue. As such it has proved to be a useful clinical tool in oncology (particularly diagnosis)[3] as well as other areas of medicine. There are established clinical pathways involving immunohistochemical analyses, and corresponding technical and clinical experience. An immunohistochemical biomarker, such as a γH2AX assay to

indicate the extent of therapy related tumour DNA damage and repair, would therefore be readily applicable to cancer care.

Since sections that preserve tissue architecture can be produced, γH2AX immunohistochemistry could provide information on the extent of DNA double strand break (DSB) damage and its subsequent repair in different parts of the tumour, at single cell resolution. While γH2AX immunohistochemistry methods have been published, both for sections from freshly frozen tissues[211] and for clinical formalin fixed paraffin embedded tumours[123], these methods had not been widely applied, even by the groups that published them, at the time that the work described in this chapter was carried out.

2.1.3. Dose response and kinetics

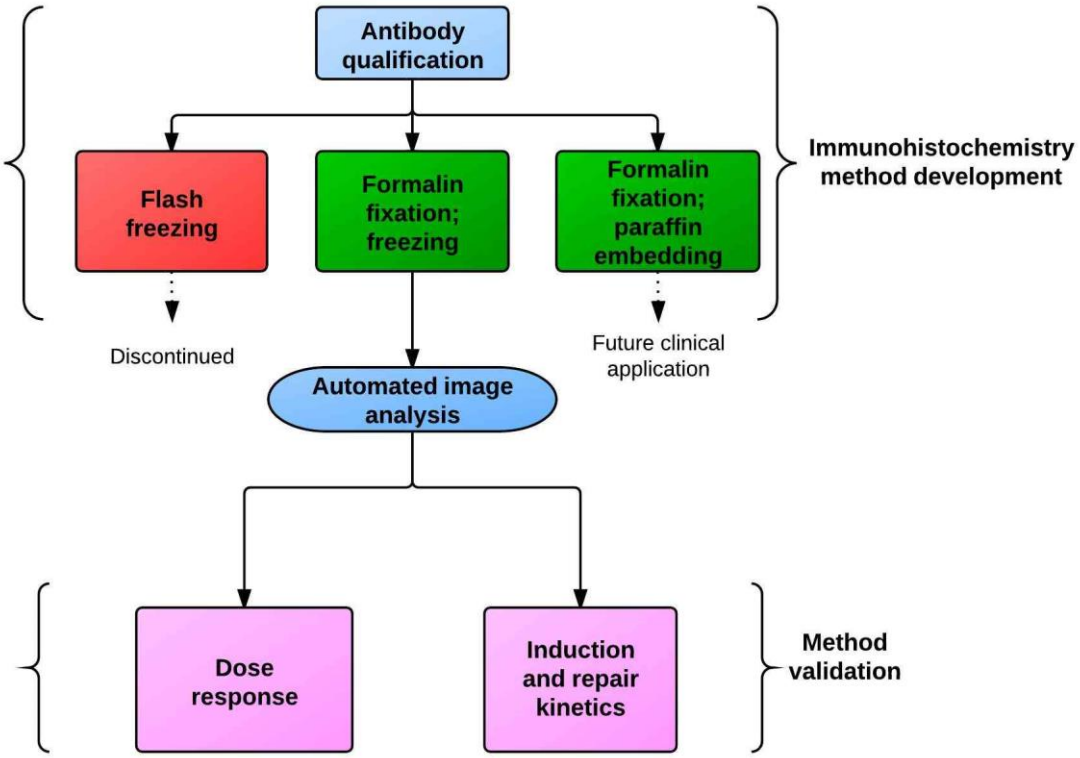
Early direct applications of whole tissue immunohistochemistry for γH2AX include confirmation that the visualised target increases in a situation where the number of double strand breaks is expected to increase. This is most simply achieved using increasing doses of external beam irradiation to a tumour xenograft.

The kinetics of double strand break induction and repair, and their correlation to γH2AX measurements using a number of assay modalities, have been discussed above (Section 1.3.5.2). In particular, these kinetics have been investigated in several normal tissues *in vivo*.[119, 129] Further validation of the immunohistochemistry method can therefore be provided by following the quantification of the target over time after a DNA damage event such as external photon beam irradiation.

2.1.4. Chapter outline

The chapter starts with quality control of the main antibody employed, before moving on to method development for various tissue preparations. Immunohistochemistry and microscopy protocols were optimised for automated image analysis for foci recognition and quantification. The method was applied to increasing doses of ionising radiation, as well as a time course after an irradiation event.

Figure 2.1 Chapter 2 outline



2.2. Materials and Methods

2.2.1. Cell culture

The cell lines used for this project were the breast cancer lines MDA-MB-468 (obtained from the American Type Culture Collection, LGC Distributors, Middlesex, UK) and MDA-MB-231/H2N ("H2N", obtained from MDA-MB-231 cells stably

transfected with HER2 courtesy of Dr Robert Kerbel, Sunnybrook Cell Research Centre, Toronto, Canada). Cultures were grown in plastic tissue culture flasks (Sarstedt, VWR International) in Dulbecco's Modified Eagle's Medium (DMEM, Sigma-Alrich, Dorset, UK) supplemented with 10% Fetal Bovine Serum(Gibco, Invitrogen, Paisley,UK) and 0.1% penicillin/streptomycin/glutamate mixture (PSG, Sigma-Aldrich, Dorset, UK). Cultures were passaged to new flasks on reaching 75-100% confluence, generally twice per week. Cultures were not propagated beyond 20 weeks or 30 passages.

2.2.2. Establishment of xenografts

H2N cells were harvested from culture (half a confluent T175 flask per xenograft, i.e. 3-5 million cells), washed, resuspended in DMEM (100 uL per xenograft) and placed on ice. Immediately before injection, the cell suspension was mixed with 100 µL of basement membrane (BD Matrigel, BD Biosciences, Bedford, MA, USA) and drawn up into a 0.5 mL B.Braun Omnican insulin syringe. The cell and basement membrane suspension was injected subcutaneously into the flank of the mouse under brief isofluorane anaesthesia. Mice were observed for the development of subcutaneous tumours which generally first appeared within one week and allowed to grow until the experiment, up to five weeks later. Under the

terms of the Home Office project licence, tumours were not allowed to grow to more than 12mm in any dimension.

2.2.3. Irradiation of xenografts

Mice were sedated with an intraperitoneal injection of 30 uL of a 1:1:10 mixture of Hypnorm (fentanyl citrate 0.315 mg/mL + fluanisone 10mg/mL, Vetapharma, Leeds, UK) : Hypnovel (midazolam hydrochloride 5mg/mL, Roche, Welwyn Garden City, UK): Water (water for injections Ph Eur, BM Browne, Reading, UK). Mice were introduced into a brass tube custom made at the Gray Institute for this purpose. A slit in the tube allowed the left hindlimb and hind flank of the mouse, including the xenograft, to protrude. The brass tube device (which could hold up to 4 mice) was placed into a Gulmay 320 irradiator cabinet. X-rays were delivered at 300kV, 10mA, and the time of irradiation adjusted to deliver the planned dose, based on dosimetry measurements performed by Dr Mark Hill of the Gray Institute.

2.2.4. Xenograft harvesting and fixation

At times described in the results section below, mice were sacrificed by cervical dislocation and tumour xenografts immediately dissected. During method development, several tissue handling methods were employed. Xenografts were initially placed in empty Perspex counting tubes (VWR International, Lutterworth, UK) and stored at room temperature for up to 30 minutes before transfer to a freezer at -80°C or immediately immersed in optimal cutting temperature compound (OCT, Tissue-Tek, Qiagen Ltd. Crawley, UK) and frozen on dry ice. Later, dissected xenografts were placed immediately in tubes containing 10 mL 10% neutral buffered formalin (NBF, Sigma-Aldrich, Dorset, UK) at room temperature for 24 hours before transfer to 70% ethanol at room temperature for paraffin

embedding (see below) or to 20% sucrose solution (Sigma-Aldrich, Dorset, UK) at 4°C for 3-5 days before immersion in OCT and placement in a freezer at -80°C.

2.2.5. Paraffin embedded tumours

Samples fixed in formalin and ethanol, as described above, were embedded in paraffin using an automated tissue processor within 2 weeks of harvest by the Clinical Pathology department of the John Radcliffe Hospital in Oxford and 5μm sections were cut and mounted on positively charged glass slides (VWR International, Lutterworth, UK). Slides were stored at room temperature. Immediately before immunohistochemical processing the slides were dewaxed using sequential incubations in xylene (3 minutes x2), xylene 1:1 with 100% ethanol (3 minutes), 100% ethanol (3 minutes x2), 95% ethanol (3 minutes), 70% ethanol (3 minutes) and 50% ethanol (3 minutes; all reagents Sigma-Aldrich, Dorset, UK).

2.2.6. Frozen tumours

Samples frozen as described above were kept at -20°C overnight, then sectioned at 8 μm using a cryostat (Bright, Huntingdon, UK) and placed on positively charged slides (VWR International, Lutterworth, UK). During method development, slides were dried overnight at 37°, at 4°C, or immediately refrozen at -20°C. Samples that had not been formalin-fixed immediately were fixed in 10% NBF (Sigma-Aldrich, Dorset, UK) for 10 minutes at room temperature immediately before immunohistochemical processing.

2.2.7. Heat induced epitope retrieval

Tumours that had been fixed in formalin for 24 hours were incubated in 10 mM sodium citrate solution pH6.0 (Sigma-Aldrich, Dorset, UK) maintained at 98°C

using a domestic microwave oven (Panasonic, UK) for 20 minutes to expose epitopes immediately before immunohistochemical processing.

2.2.8. γH2AX immunohistochemistry

Slide sections prepared as described above were rehydrated in phosphate buffered saline (PBS, 10 mM phosphate buffer, 2.7 mM potassium chloride and 137 mM sodium chloride, pH 7.4, Sigma Aldrich, Dorset, UK) for 5 minutes, and cell walls were lysed by incubation in 1% Triton-X100 solution (Sigma-Aldrich, Dorset, UK) in PBS for 10 minutes, then PBS alone for 5 minutes. 0.05% Triton-X100 was added to all subsequent incubations except for final mounting.

During method development, protein binding was blocked for 30 minutes to 16 hours at room temperature, 4°C or 37°C using combinations of: Strepavidin, Biotin and MOM (mouse on mouse) blocking solutions (Vector Laboratories, Peterborough, UK); 10% normal goat serum in PBS and 2% bovine serum albumin in PBS (Sigma-Aldrich, Dorset, UK). Multiple blocking incubations were separated by 5 minute incubation in PBS, but no such incubation followed the final block. The primary mouse monoclonal anti-γH2AX antibody (Clone JBW301, Merck Millipore, Watford, UK) was diluted between 1:50 and 1:3000 in the final blocking solution. Incubation in primary antibody lasted 1-16 hours at room temperature, 4°C or 37°C, followed by three, 5 minute incubations in PBS at room temperature, and 30-60 minutes in 1:100 to 1:3000 AlexaFluor-488 or AlexaFluor-594 conjugated goat anti-mouse secondary antibody in the final blocking solution. Sections were then washed by incubation in PBS, thrice for 5 minutes, and mounted in using Vectorshield mounting medium (Vector Laboratories, Peterborough, UK) containing 4',6-diamidino-2-phenylindole (DAPI).

2.2.9. Microscopy

Images were obtained using a Zeiss Confocal Microscope (Carl Zeiss Ltd., Welwyn Garden City, UK) controlled using Zen 2008 and Zen 2010 software. Confocal 0.5 μm planes were imaged using consecutive acquisition channels through a 63x/1.40 oil immersion Plan-Apochromat lens (DAPI: illumination 405 nm power 8.0, detection 415-493 nm detector gain 702 amplifier gain 1.0; Alexa Fluor 488: illumination 488 nm power 8.0, detection 493-630 nm detector gain 905 amplifier gain 1.0).

2.2.10. Image analysis

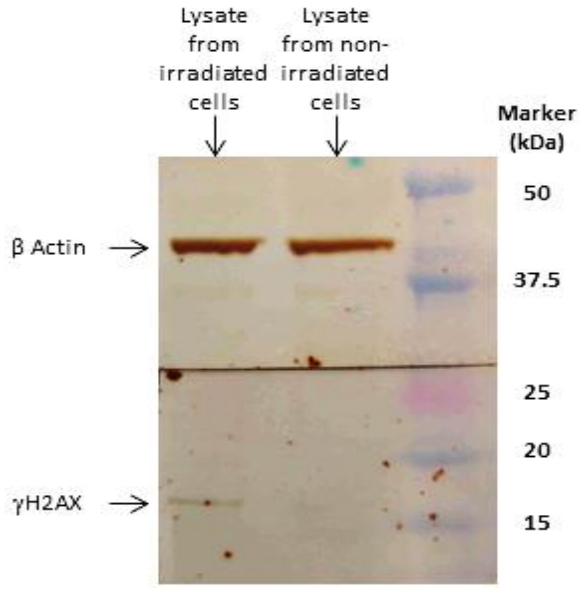
Image files were processed using ImageJ (US National Institutes of Health, Bethesda, USA, http://imagej.nih.gov/ij) with LSM Toolbox plugin (Patrick Pirotte) and IrfanView (Irfan Skiljan, Vienna, Austria, www.irfanview.com). Image recognition was carried out using TRI2 (Paul Barber, Gray Institute, Oxford, UK) optimised using images obtained during the study. Processed images showing recognised outlines (see far right panel of Figure 3.7 for example) were all inspected manually for quality control.

2.3. Results

2.3.1. Immunohistochemistry method development

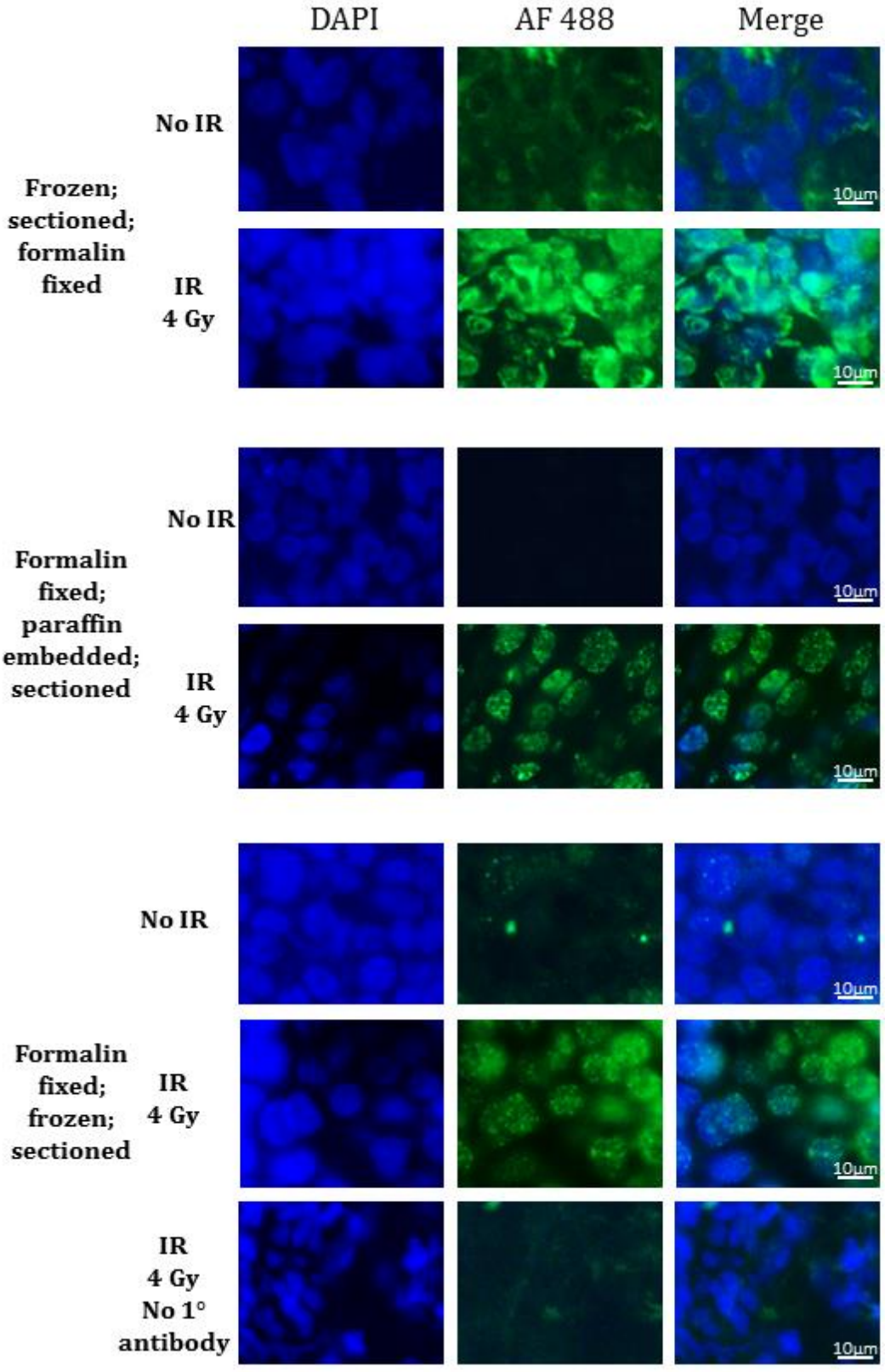
An immunoblot assay confirmed that the mouse anti-γH2AX antibody used in all the staining procedures described in this chapter bound to a single band at 15 kDa, in lysates from irradiated but not unirradiated cells (see Figure 2.2)

Figure 2.2 Immunoblot assay of lysates obtained 1 hour after irradiation (10 Gy) and from unirradiated H2N cells using mouse anti-γH2AX antibody, demonstrated with anti-mouse horseradish peroxidase conjugated secondary antibody. Beta actin loading control also shown. Experiment conducted with Sarah Able.



An immunohistochemistry method was developed to demonstrate radiation induced γH2AX foci in the tumour xenograft models used in this thesis. The method of fixation and the sequence of tissue preparation steps proved to be important factors in obtaining optimal staining. As illustrated in Figure 2.3, a difference in nuclear γH2AX signal was demonstrated between irradiated and unirradiated H2N tumour xenografts frozen at dissection and fixed after sectioning. However, individual foci could not be discriminated. A formalin fixed paraffin embedded (FFPE) tissue handling protocol was applied with the help of a clinical pathology department, resulting in focal staining in the expected pattern in irradiated tumours only. This tissue handling protocol was then adapted for use with frozen tumours, for application using equipment available within the Gray Institute. Similar results were obtained (see Figure 2.3).

Figure2.3 Epifluorescence microscopy demonstrating immunohistochemistry of H2N xenograft tissue sections prepared used different tissue handling methods during development. Tumours were harvested one hour after 4 Gy irradiation (IR 4 Gy) or sham (No IR). AF 488= Alexa Fluor 488 conjugated secondary antibody.



2.3.2. Validation over a dose range

The tissue handling, immunohistochemical and automated image recognition and quantification methods were validated across a range of doses from 0 to 10 Gy. Figure 2.5 demonstrates increasing numbers of visually resolvable foci in immunohistochemical sections from tumours irradiated over this range. Numbers of foci, quantified using automated image analysis, increased linearly with dose over this range as shown in Figure 2.4. The linear regression was fitted to a line with the equation

$$Foci\ per\ cell\ section = 0.96 + 1.15\ (Dose\ in\ Gy)$$

Figure 2.4 Automated quantification of foci per cell section (normalised for nuclear area) in H2N xenografts harvested one hour after irradiation with 300kV Xrays. The mean number of foci per cell section (*i.e.* confocal imaging plane) normalised for nuclear area, ± standard error of mean from twenty sections, each with >100 cells, obtained in two separate experiments, are plotted. Linear regression is shown (solid line) with 95% confidence interval (interrupted curves; r2=0.9388, p<0.0001).

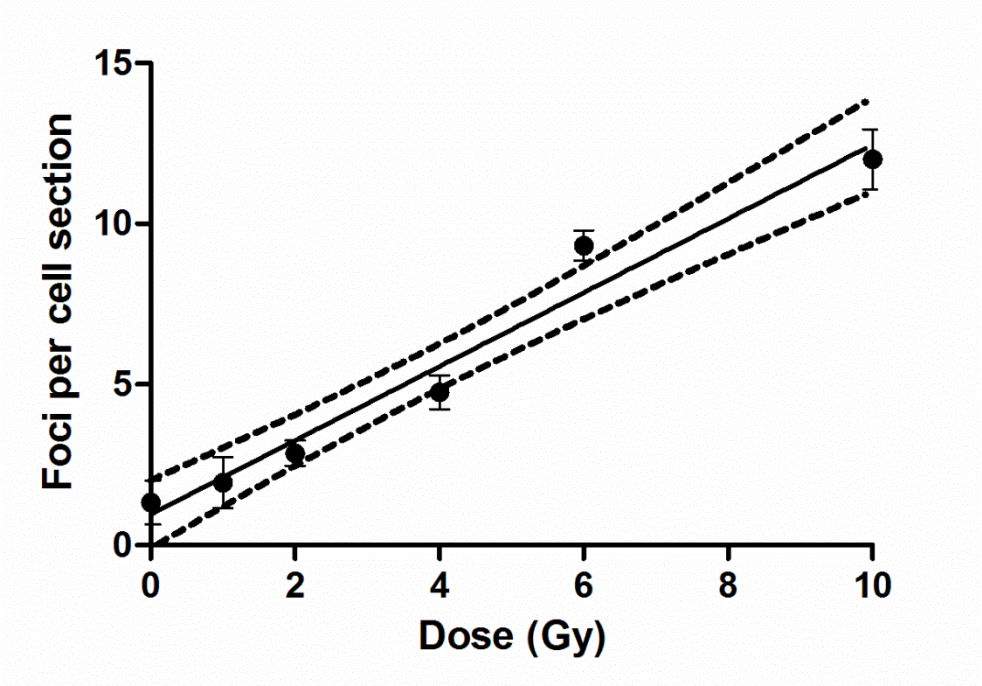
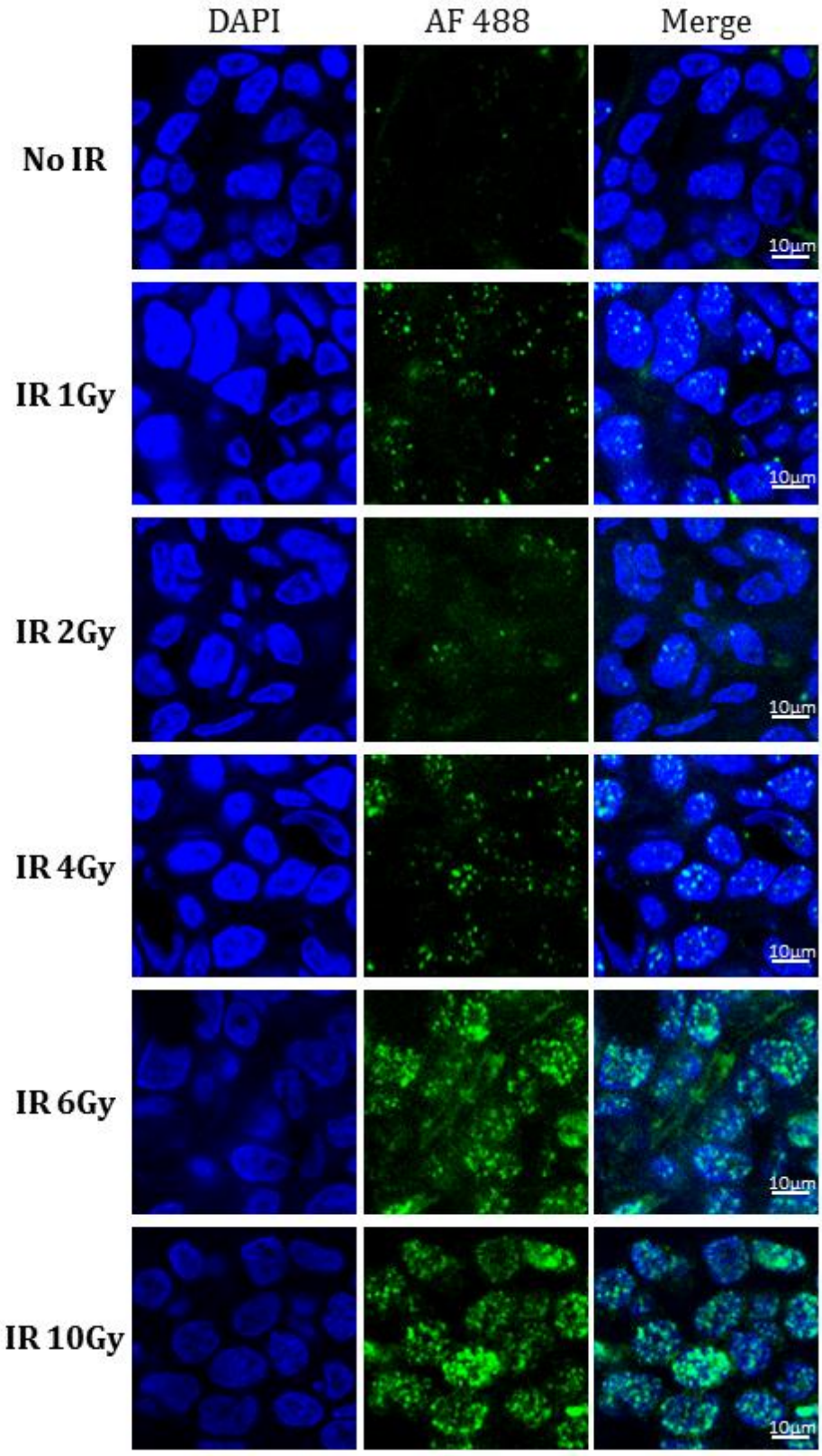


Figure 2.5 Confocal imaging of immunohistochemistry of H2N xenografts harvested one hour after irradiation with 300 kV Xrays (0-10 Gy)



2.3.3. Kinetics study

The method was also validated over a time series following 10 Gy irradiation of xenografts. Figure 2.6 shows that maximal foci induction occurs between 30 minutes and 2 hours after irradiation but that significant numbers of foci remain after 6 and 24 hours. Foci numbers returned to the pre-irradiation baseline by 96 hours, but are higher at 168 hours. Figure 2.7 shows representative immunohistochemical sections. Foci are subjectively brightest 2 hours following irradiation. Fewer, better defined foci survive at 6 and 24 hours, but most are gone by 96 hours. A smaller proportion of cells remaining at 168 hours have foci, but those that do have abundant numbers of them.

Figure 2.6 γH2AX foci quantification in MDA-MB-231/H2N xenografts sacrificed at stated times after 10 Gy photon irradiation. The mean number of foci per cell section (*i.e.* confocal imaging plane) normalised for nuclear area, ± standard error of mean from twenty sections, each with >100 cells, obtained in two separate experiments, are plotted..

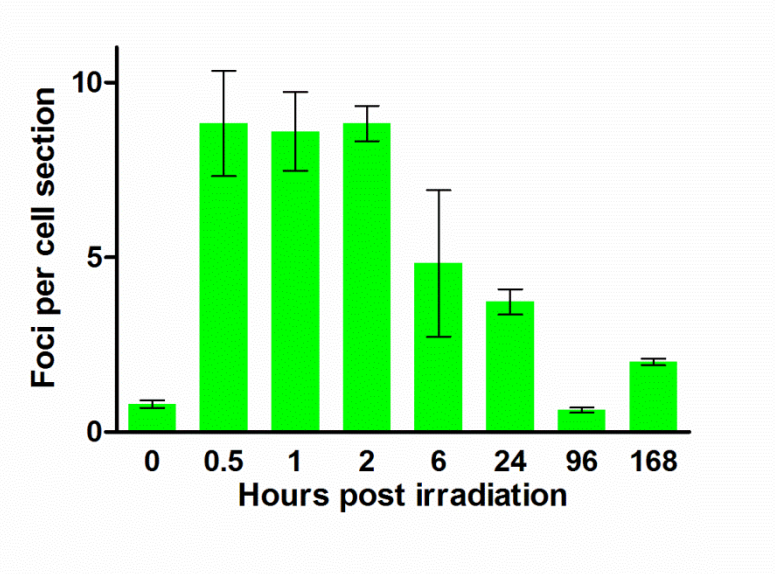
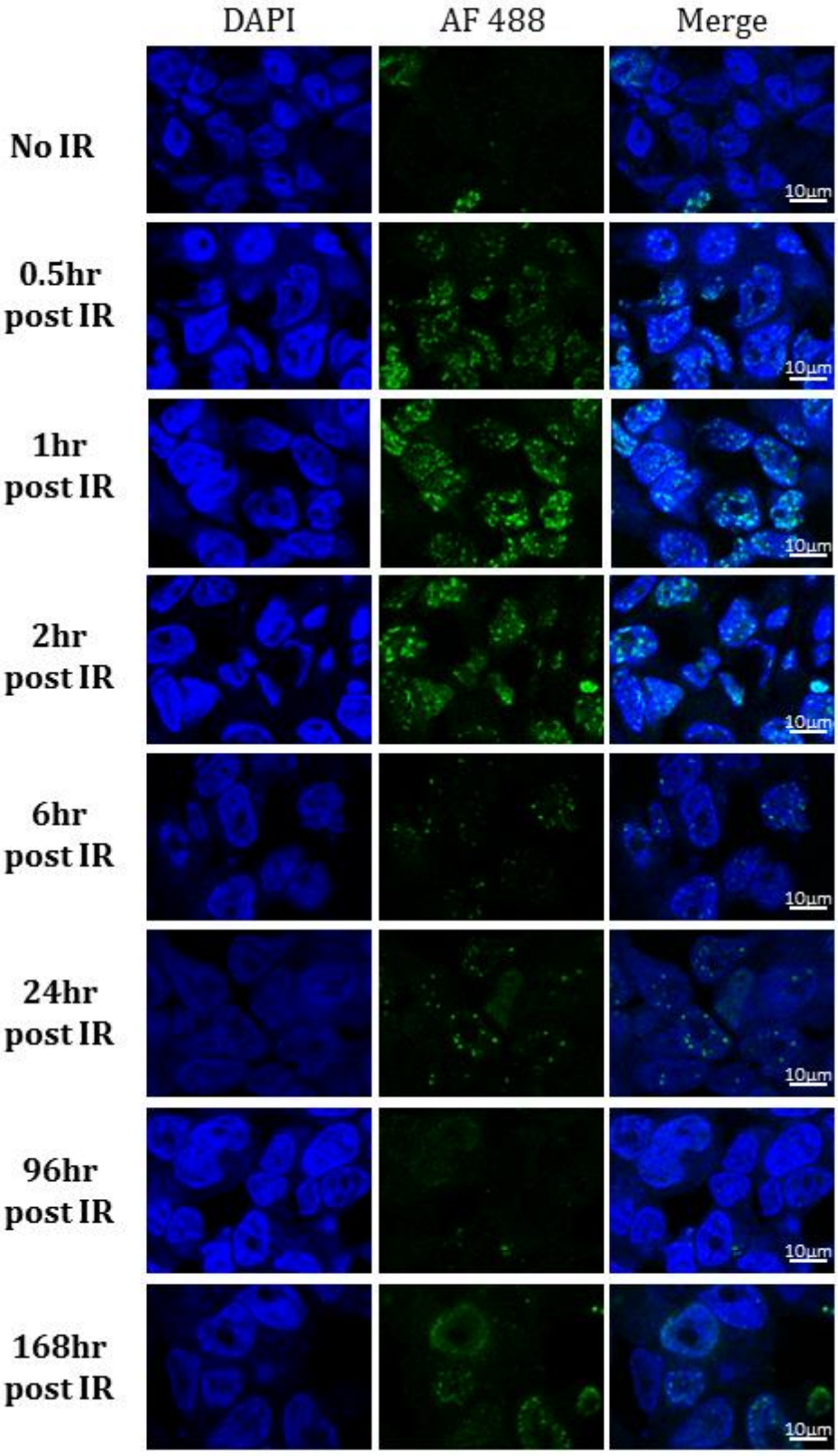


Figure 2.7 Immunohistochemistry for yH2AX after 10Gy photon irradiation



2.4. Discussion

2.4.1. Importance of tissue fixation

The development and optimisation of an immunohistochemistry method requires perturbation of the different stages of the staining process, including tissue harvest and initial processing, slide preparation, fixation, cell lysis, non-specific protein blocking, primary antibody binding and visualisation. The method development process outlined in this chapter suggested that for γH2AX, at least in this tumour xenograft model, the chemical fixation of tissue was critical. Individual intranuclear foci were demonstrated only using protocols that required the tissue to be fixed immediately after harvesting from the freshly euthanised animal.

There are two potential explanations for the importance of immediate fixation. Firstly the visualisation of in situ foci requires the molecular architecture of γH2AX within the chromatin to be maintained. Note that where fixation occurred later, such as after sections had been cut from frozen tumours, a diffuse intranuclear accumulation of anti-γH2AX antibody was observed. While the amount of this accumulated signal could have been quantified, this would be unlikely to produce as sensitive an assay as that based on foci counts. Secondly, γH2AX is necessarily recognised by its antibody at a phosphorylated epitope (phosphorylated serine 139, see Section 1.3.1), and such post-translational modifications are known to be labile and therefore difficult to detect by immunohistochemistry.[212] Immediate fixation therefore minimises the chance that the target is dephosphorylated.

Another group published a γH2AX immunohistochemistry method soon after the development work described herein was performed.[120] They came to very similar conclusions to those presented here regarding the importance of tissue fixation.

They also achieved success with flash-frozen samples fixed before embedding and sectioning. Their method has since been translated to early phase clinical trials.[121, 122]

2.4.2. Automated quantification

Automation of image analysis has several potential advantages when compared to manual analysis.[213] Focus recognition can be objectively standardised, and those standards can be optimised at the start of the analysis before application in the remainder. Larger numbers of cells can be analysed than is the case with laborious manual methods, minimising random error in quantification. Most recently published methods for the quantification of γH2AX foci use a segmentation algorithm to identify cell nuclei followed by recognition of individual foci based on size, regularity and intensity.[138, 214, 215] A generic image analysis method developed by Dr Paul Barber and colleagues at the Gray Institute[66] was applied in this thesis to γH2AX foci quantification.

2.4.3. Dose response and kinetics

The results presented above confirm that for tumour xenograft tissue, as for isolated cells in culture, γH2AX foci are present in small but finite numbers in unirradiated tumour cells. Additional foci are induced in proportion to the applied radiation dose.[216] The absorbed doses studied here lie within and beyond the range of clinically applicable doses.

The outcome for the tumour as well as the patient is dependent on the extent of repair of DNA double strand breaks (DSBs) as well as the extent of their induction.[74, 158, 217] DNA DSB repair is more likely than induction to relate to the

cell type and its microenvironment,[218] highlighting the importance of γH2AX measurements in whole tumour tissue.

The rise in foci numbers at the end of the timecourse experiment (Figure 2.6) may indicate that a separate process to the initial damage is causing γH2AX foci. These late foci may therefore not be truly "residual". They may be related to cell senescence, a state of maintained growth arrest without cell death.[219]

The methods described in this chapter might usefully be applied to situations where DSB repair is experimentally perturbed, such as tissue hypoxia,[88] pharmacological DSB repair inhibition,[220] or induced genetic defects of the function of DNA repair proteins. The latter approach has been reported for normal tissue γH2AX kinetics.[130]

2.4.4. Conclusion

The development of a method to visualise γH2AX foci using immunohistochemistry and to quantify those foci using automated image analysis facilitates the investigation of γH2AX in tumours *in vivo*. The technique could be applied to questions of DNA damage and repair and to guide the development of other *in vivo* assays of γH2AX including non-invasive imaging agents.

Chapter 3

Clinical Development of Fine Needle Aspiration Cytology to Demonstrate γH2AX in Tumours

Chapter 3: Clinical Development of Fine Needle Aspiration Cytology to Demonstrate γH2AX in Tumours

3.1. Introduction

This chapter describes the development of a novel immunocytochemical assay for γH2AX foci in clinical fine needle aspirate tumour specimens.

Where the level of a biomarker signal is expected to alter over time, as is the case for γH2AX, both the investigation of the biomarker and its application depend on being able to take repeated assay measurements over time. This represents a significant challenge to clinical translation of such an assay, since each repeat measure is a potential additional burden on the patient. Avoiding unnecessary morbidity and use of patient time are ethical considerations in both clinical research and practice.

3.1.1. Fine Needle Aspiration

There is a rationale therefore to explore techniques that gain meaningful information about the tumour but minimise the burden on the patient. Fine needle aspiration (FNA) cytology is just such a technique. It involves the direct placement of a fine-bore needle (25-20 gauge, 0.5–0.9mm) into a tumour mass, and aspiration of a cell sample. This causes less trauma to the tissue than a needle core biopsy (typically 18-14 gauge, 1.3-2.1mm). FNA is routinely used clinically in diagnosing thyroid, breast, lymph node, skin and other masses. FNA is performed percutaneously, sometimes with imaging guidance, or via endoscopy in the oesophagus or lung.[3] It is used mainly for diagnosis, often simply to distinguish

malignant from benign pathology, but its potential for application in complex assays and molecular profiling is recognised.[221, 222]

The limitations of FNA cytology are that it provides relatively few cells (typically 10^2-10^4) and can sample only one small part of a tumour. Information about tissue architecture must be lost for cells to travel along the fine needle shaft. It is a mildly invasive procedure, involving pain for the patient if the skin is punctured. There is a theoretical risk of tumour cell "seeding" along the needle tract.

Sample handling in clinical cytology aims to preserve and demonstrate optimal information about the tumour. The most widely used clinical cytological procedure is cervical cancer screening, and liquid based cytology (LBC) where cells are kept in a liquid medium throughout processing and analysis, has been established as the optimal sample handling technology.[223] Its application to FNA cytology is debated.[224]

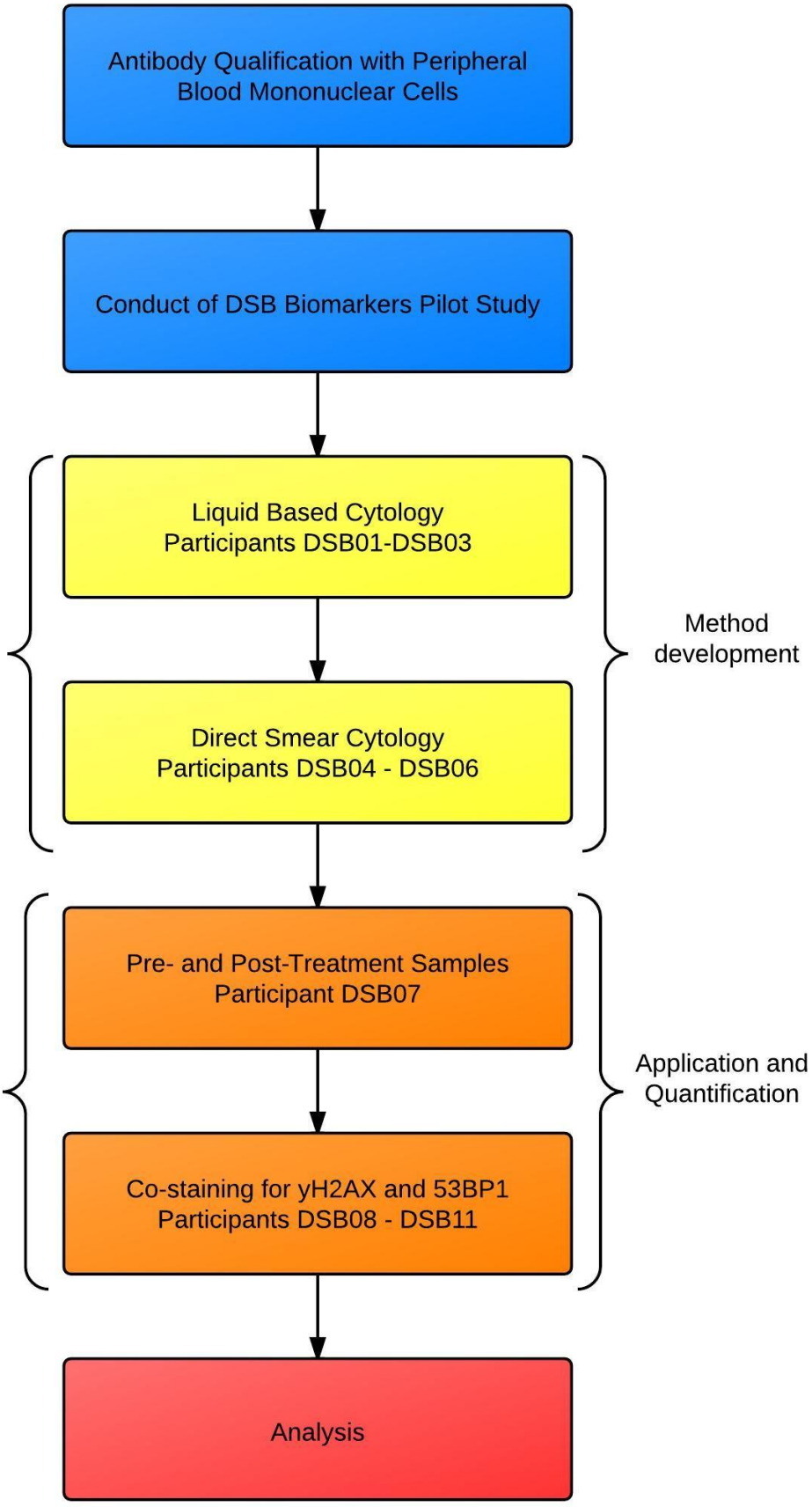
The biomarker assay signal will vary according to the biology of the marker, but also due to potential sources of error including differences between patients, between tumours within a patient, under different treatment conditions or times. Assay development involves an attempt to measure and minimise the effect of these factors, but this cannot occur without an appreciation of the inherent variation in the assay technique.

3.1.2. The DSB Biomarkers Pilot Study

The DSB Biomarkers Pilot Study was therefore set up under appropriate clinical research governance with a primary objective to establish a reliable method for the detection of DNA DSBs by immunocytochemistry in human tumour cells

obtained by fine needle aspiration. (See detailed methods below). Secondary objectives included: measuring the variability in quantitative measurement of DSB biomarkers between synchronous tumour samples; measuring the robustness in quantitative measurement of DSB biomarkers from the same tumour at different times; the use of peripheral blood mononuclear cells from participants in the study as a control; providing preliminary evidence that DSB biomarkers increase after treatment of the tumour.

Figure 3.1 Chapter 3 outline



3.2. Materials and Methods

3.2.1. Human blood samples

Whole blood samples were obtained from volunteers in accordance with University of Oxford policy. These samples were used to validate procedures and not to test a research hypothesis. Blood was collected using standard aseptic technique into heparin-containing vacuum collection tubes.

3.2.2. Separation of peripheral blood mononuclear cells (PBMCs)

Heparinised, whole blood was diluted 1:2 in RPMI-PSG (Roswell Park Memorial Institute medium with 1% penicllin/streptomycin/glutamine, Sigma, Dorset, UK) and gently layered on top of an equal volume of sucrose density gradient medium (Lymphoprep, Axis-Shield UK, Kimbolton, UK). The layered blood was centrifuged at 2200 rpm (approximately 800 x g) for 30 minutes with the brake off to prevent disruption of gradient. A sterile glass pasteur pipette was used to carefully remove the buffy coat layer immediately above the density medium, which was resuspended in RPMI-PSG. To wash the cells, the suspension was centrifuged at 2200 rpm for 20 minutes, supernatant removed, and cell pellet resuspended in RPMI-PSG.

Cells were counted on a haemocytometer using a 1:1:1 dilution of cell suspension : trypan blue : PBS (0.01 M phosphate buffer, 0.0027 M potassium chloride and 0.137 M sodium chloride, pH 7.4, Sigma Aldrich, Dorset, UK.)

3.2.3. *Ex vivo* irradiation of PBMCs

Cells were divided at 10^5 cells per well in 0.5 mL RPMI-PSG on to sterile glass coverslips (22 x 22 mm; VWR International, Lutterworth, UK) in 6 well polyurethane plates (BD Biosciences, Oxford, UK) and incubated for 1 hour at 37°C

to adhere cells to glass. Plates were then irradiated to 2 Gy using a ^{137}Cs irradiator (dose rate 2 Gy/minute calibrated by Dr Mark Hill, Gray Institute), or sham irradiated in the same room. PBMCs were fixed 1 hour after irradiation (or sham) by replacement of medium with 10% neutral buffered formalin (Sigma, Dorset, UK) for 10 minutes at room temperature.

3.2.4. DSB Biomarkers Pilot Study

A clinical research protocol was written (see Appendix) and underwent peer review by the Oxford Cancer Centre Trial Steering Committee in July 2009, and the University of Oxford Clinical Trials and Research Governance team, who agreed sponsorship of the study in August 2009. A Participant Information Leaflet (PIL) was piloted with patient volunteers, and all other study documentation completed. The protocol and study documents were considered by the Berkshire Research Ethics Committee in September 2009, and given a favourable ethical opinion in October 2009 (reference number 09/H0909/106). The study was approved by the Oxford Radcliffe Hospitals NHS Trust (ORH, later Oxford University Hospitals) Research and Development team in January 2010 (reference number 6018) and opened to recruitment. Initial Standard Operating Procedures (SOPs) were prepared, and developed throughout the study. The study was conducted in accordance with the International Committee on Harmonisation Good Clinical Practice (ICH-GCP) standard and the policies of the University of Oxford and ORH.

3.2.5. Fine needle aspiration (FNA)

After confirming the participant's identity and consent, the participant was placed in a comfortable (usually reclining) position. The sample area was agreed with the participant, cleaned with an alcohol swap and allowed to dry. A 23G hypodermic

needle (Terumo Europe, Leuven, Belgium) held by its hub was inserted into the tumour with a gentle in-and-out and simultaneous rotating motion until fluid was seen in the hub of the needle. If necessary, a 10 mL syringe was attached to the needle hub in order to apply gentle suction. A clean dry swab was held against the puncture site after the needle was withdrawn.

3.2.5.1. Liquid based cytology

The Thinprep 2000 (Hologic Inc., Crawley, UK) liquid based cytology system was used in accordance with the manufacturer's instructions and proprietary solutions and devices. Cells and fluid obtained during FNA were expressed into a 1.5 mL microcentrifuge tube (Sarstedt, Leicester, UK) containing 1 mL of Cytolyt fixative (Hologic Inc, Crawley, UK). This was centrifuged at 600 x g (g = 9.81 ms^{-2}) for 10 minutes. The supernatant was removed and cell pellet resuspended before addition to a vial containing PreservCyt fixative (Hologic Inc, Crawley, UK), for at least 15 minutes before processing on the Thinprep 2000 slide preparation device using Thinprep microscope slides (Cytyc, Crawley, UK).

3.2.5.2. Direct slide smear

Cells and fluid obtained during FNA were expressed directly onto a prelabelled positively-charged glass microscope slide (Superfrost Plus, VWR International, Leuven, Belgium) to form a single spot on the slide next to the label. An inverted clean slide was used to draw the expressed spot into a smear, and the sample slide placed immediately in a coplin jar containing 10% neutral buffered formalin (Sigma, Dorset, UK) for 10 minutes before transfer to a coplin jar containing phosphate buffered saline (PBS).

3.2.6. Immunocytochemistry

During immunocytochemistry, slides with fixed FNA cell preparations as described above were incubated using blebs (100-150 μL) of fluid enclosed using a hydrophobic marker (Pap liquid blocker, EM Sciences Inc, Hatfield, USA) and washed in glass coplin jars. PBMCs prepared on coverslips as described above were incubated after inversion onto a drop (50-75 μL) of fluid placed on the lid of the 6 well plate. They were washed within the wells of the plate. The precise protocol was adapted during method development, but the final protocol was as described here.

After washing with PBS, cells were lysed with 1% Triton X100 (Sigma, Dorset, UK) in PBS for 10 minutes. After 2 x 5 minute washes in PBS-T (0.05% Triton X100 in PBS), non-specific protein binding sites were blocked with 2% bovine serum albumin (BSA; Sigma, Dorset, UK) in PBS-T for 1-16 hours at room temperature or 37°C. This was followed by incubation with primary antibody/antibodies (mouse monoclonal anti-γH2AX, clone JBW301, Merck Millipore, Watford, UK and rabbit polyclonal anti-53BP1, Cell Signaling Technology, New England Biolabs, Hitchin, UK) diluted as described below in 2% BSA in PBS-T, overnight at 4°C, room temperature or 37°C. After 3 x 5minute washes in PBS-T, slides or coverslips were incubated with secondary antibody/antibodies (Alexa Fluor 488 conjugated goat anti-mouse and Alexa Fluor 594 conjugated goat anti-rabbit, Invitrogen, Paisley, UK) as described in the results below, diluted in 2%BSA in PBS-T as described below, for 30 minutes at room temperature.

FNA slides were mounted with sterile coverslips (22 x 50 mm, VWR International, Leuven, Belgium) and PBMC coverslips mounted onto clean slides (SuperFrost,

VWR International, Leuven, Belgium) using Vectorshield mounting medium (Vector Laboratories, Peterborough, UK) containing 4',6-diamidino-2-phenylindole (DAPI).

3.2.7. Confocal microscopy

Images were obtained using a Zeiss Confocal Microscope (Carl Zeiss Ltd., Welwyn Garden City, UK) controlled using Zen 2008 and Zen 2010 software. Confocal 0.5 μm planes through tumour cells or PBMCs were imaged using consecutive acquisition channels through a 63x/1.40 oil immersion Plan-Apochromat lens (DAPI: illumination 405 nm power 8.0, detection 415-493 nm detector gain 545 amplifier gain 1.0; Alexa Fluor 488: illumination 488 nm power 11.0, detection 493-630 nm detector gain 645 amplifier gain 1.0; Alexa Fluor 594: illumination 594 nm power 10.0, detection 602-728 nm detector gain 840 amplifier gain 1.0)

3.2.8. Cell identification quality control

Slides or images were examined by a Consultant Cytopathologist (Dr Ketan A. Shah, John Radcliffe Hospital, Oxford) who used qualitative morphological criteria to confirm that cells included in analyses and described below were likely to be of malignant origin consistent with the known tissue diagnosis of the participant.

3.2.9. Image processing and recognition software

Image files were processed using ImageJ (US National Institutes of Health, Bethesda, USA, http://imagej.nih.gov/ij) with the LSM Toolkit plugin (Philippe Pirotte) and IrfanView (Irfan Skiljan, Vienna, Austria, www.irfanview.com). Image recognition was carried out using TRI2 (Paul Barber, Gray Institute, Oxford, UK) optimised using images obtained during the study. Processed images showing

recognised outlines (see far right panel of Figure 3.7 for example) were all inspected manually for quality control.

3.2.10. Quantification and statistical analysis

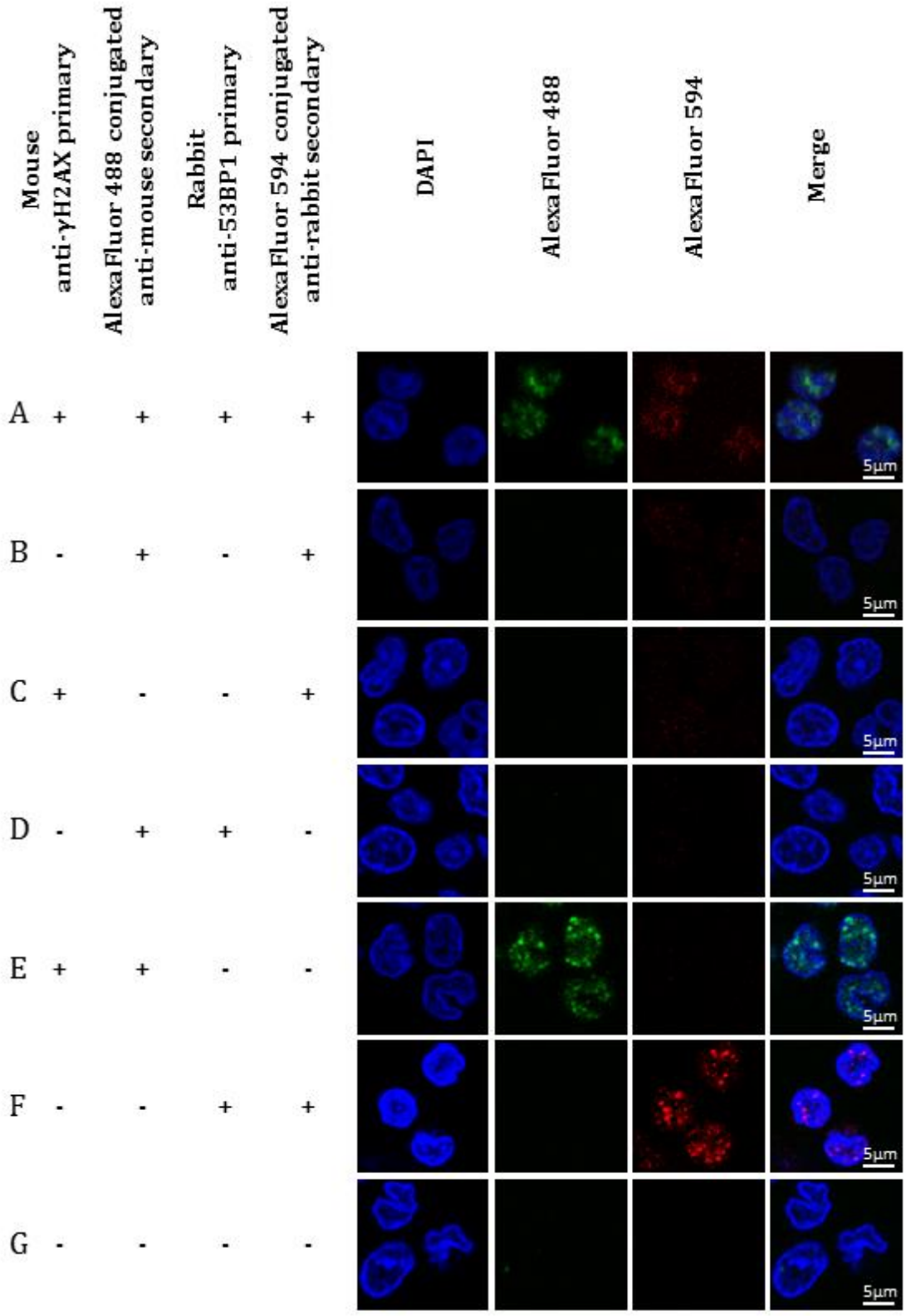
Images represented optical cross sections through the cell. To allow for variations in the volume of the nucleus within the plane of the image, foci numbers were normalised for nuclear area. Normalised foci numbers per slide or per condition are presented as an arithmetic means with the standard error of the mean. Statistical comparison between groups is by unpaired two-tailed t test (for two groups, using Welch's correction for unequal variance where necessary) or analysis of variance (more than two groups).

3.3. Results

3.3.1. Validation of antibody in human PBMCs irradiated *ex vivo*

The antibodies chosen for this study on the basis of preclinical experience within the research group were a mouse monoclonal anti-γH2AX antibody (paired with an Alexa Fluor 488 conjugated goat anti-mouse secondary antibody) and a rabbit polyclonal anti-53BP1 antibody (paired with an Alexa Fluor 594 conjugated goat anti-rabbit secondary antibody). Both antibodies demonstrated a focal intranuclear staining pattern in human peripheral blood mononuclear cells irradiated *ex vivo* (Figure 3.2A, E & F). There was no such pattern using the secondary antibodies alone (Figure 3.2B). There was no evidence of cross-reactivity between anti-rabbit secondary and the mouse anti-γH2AX primary (Figure 3.2C) or between anti-mouse secondary and rabbit anti-53BP1 primary (Figure 3.2D). There was no evidence of autofluorescence in the absence of secondary antibodies (Figure 3.2G).

Figure 3.2 Validation of γH2AX and 53BP1 antibodies used for immunohistochemistry in human peripheral blood mononuclear cells fixed 1 hour after irradiation *ex vivo* to 2Gy. Controls show lack of confounding patterns with secondary antibodies alone (B), lack of cross-reactivity between unpaired primary and secondary antibodies (C,D) and lack of autofluorescence (G)



3.3.2. Study conduct

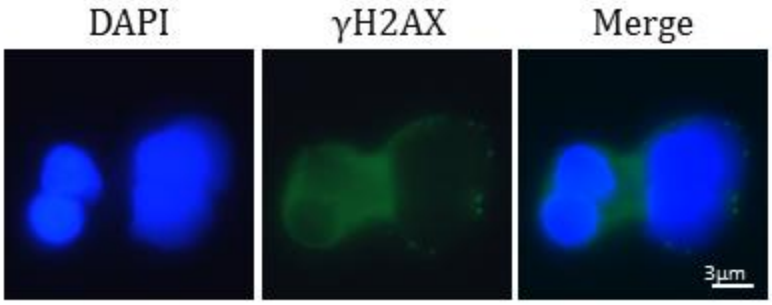
Table 3.1 Recruitment to DNA DSB Biomarkers Pilot Study

Study Code	Diagnosis	Date of Consent	Samples	Sample Site/ Comments
DSB01	Metastatic squamous cell carcinoma of left tonsil	17/2/10	17/2/10 3xFNA 1xblood	Left level IV neck node. Withdrew consent
DSB02	Metastatic squamous cell carcinoma of right tonsil	23/2/10	23/2/10 3xFNA 1xblood 26/2/10 2xFNA 30/2/10 2xFNA	Right level II neck node. Palliative radiotherapy 21/2 until 25/2
DSB03	T2N2 squamous cell carcinoma of left tonsil	13/4/10	13/4/10 3xFNA 1x blood	Left level IV eck node. Tumour resected 14/4/10
DSB04	Metastatic malignant melanoma	24/6/10	24/6/10 3xFNA 1x blood 1/7/10 3x FNA	Right thigh. Tumour resected 6/7/10
DSB05	Metastatic malignant melanoma	1/7/10	1/7/10 3x FNA 27/7/10 3xFNA 1xblood	Perianal. Declined third visit
DSB07	Metastatic squamous cell carcinoma of parapharyngeal space	24/8/10	24/8/10 Pre-RT:3xFNA 1xblood Post-RT:3xFNA 1xblood	Left Level III neck node. Discontinued RT after first fraction
DSB08	Metastatic non small cell lung cancer	1/12/10	1/12/10 Pre-RT:3xFNA Post-RT:3xFNA	Supraclavicular node. Inadequate samples.
DSB09	Low grade non Hodgkins lymphoma	19/1/11	19/1/11 Pre-RT:3xFNA 1xblood Post-RT:3xFNA 1xblood	Occipital node
DSB10	Metastatic non small cell lung cancer (adenocarcinoma)	7/2/11	7/2/11 Pre RT: 3xFNA Post RT: 3xFNA 14/2/11 3 xFNA 1 week post RT	Right upper arm cutaneous metastasis. RT 8.5Gy on 7/2/11
DSB11	Metastatic Breast cancer	7/9/11	7/9/11 3xFNA 1x blood 22/9/11 3 x FNA post chemo 27/9/11 3 x FNA 1 week post chemo	Anterior chest wall cutaneous metastasis.

3.3.3. Liquid based cytology method development

Participant DSB01 was diagnosed with metastatic squamous cell carcinoma of the left tonsil, and agreed to undergo one set of FNA samples from a cervical lymph node deposit. Scant cells were visible after slide processing and these showed apparent extranuclear staining with γH2AX primary antibody (see Figure 3.3). The participant opted to withdraw from the study before his planned radiotherapy treatment.

Figure 3.3 Immunocytochemistry of fine needle aspiration tumour specimens from squamous cell carcinoma cervical lymph node from participant DSB01 showing DNA (DAPI, blue) and γH2AX (green) with merged image

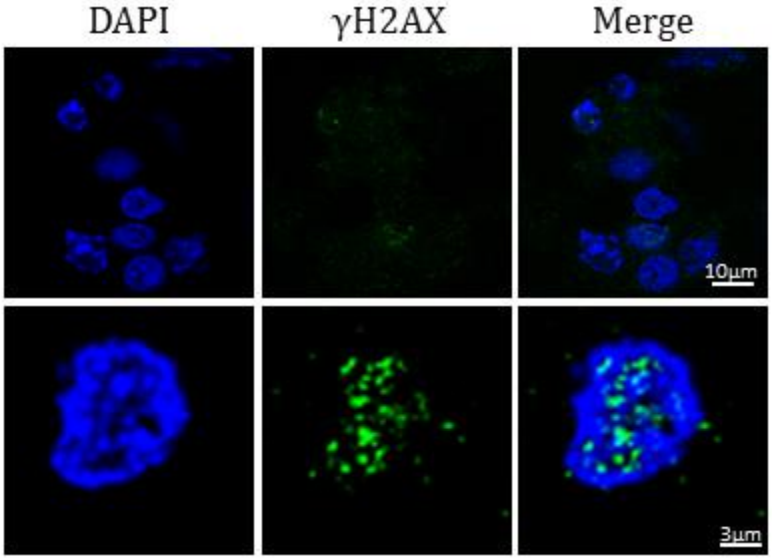


Participant DSB02 underwent 7 FNAs spread over 3 days during a course of palliative radiotherapy for recurrent metastatic squamous cell cancer of the tonsil. Despite visible fluid aspiration, no cells were visible on processed slides.

Participant DSB03 underwent one set of 3 FNAs immediately prior to neck dissection for metastatic squamous cell cancer of the tonsil. Despite the lack of any prior potentially DNA damaging therapy, some parts of the specimen displayed intranuclear anti-γH2AX staining in a focal pattern (see Figure 3.4). Cytoplasmic background staining was also visible, and the intranuclear deposits may have represented non-specific staining.

From the first three participants, few cells were visualised. Further method development particularly in regard to cell fixation was impeded by the warranty restrictions of the Thinprep 2000 slide processing system, as discussed below. Cell collection and processing was therefore altered.

Figure 3.4 Immunocytochemistry of fine needle aspiration tumour specimens from squamous cell carcinoma cervical lymph node from participant DSB03 showing DNA (DAPI, blue) and γH2AX (green) with merged image



3.3.4. Direct smear cytology

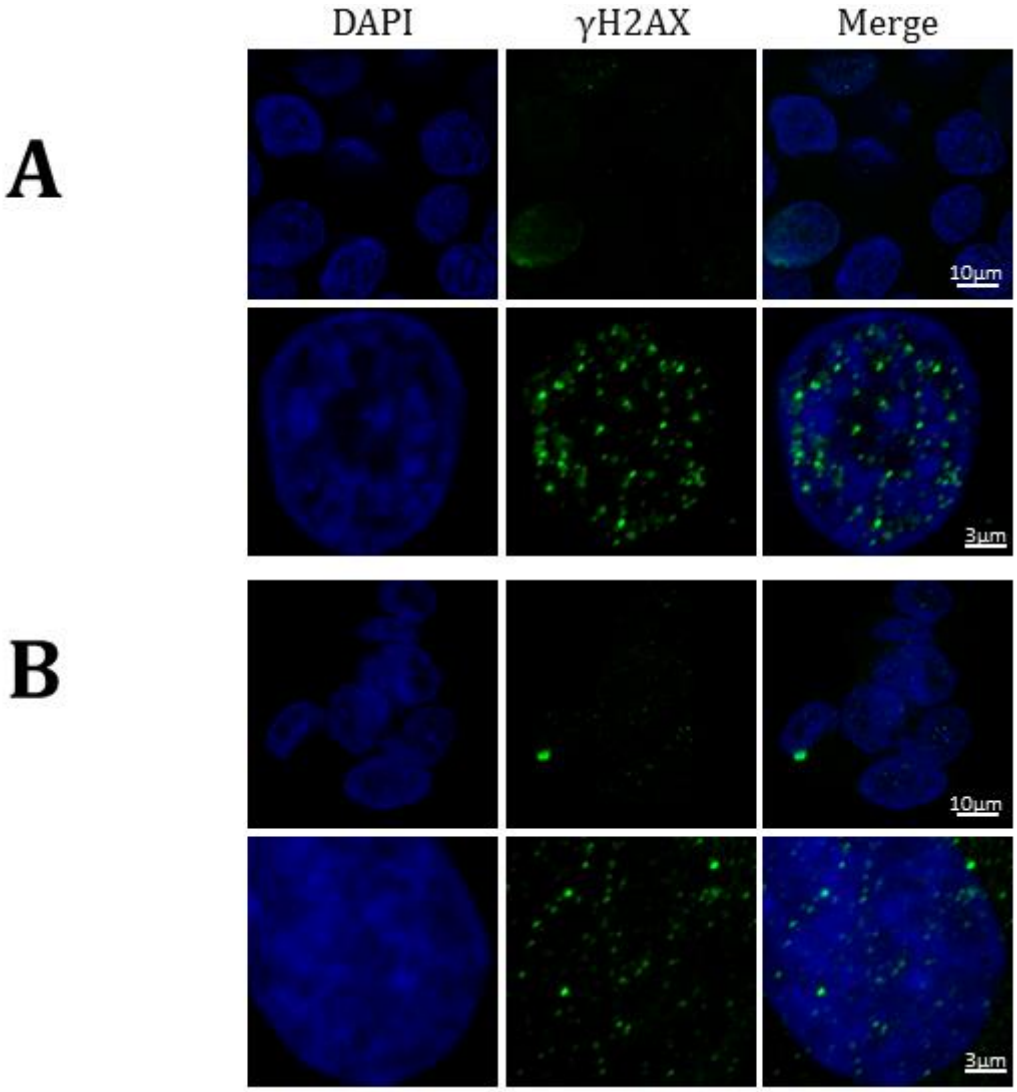
The alteration in methodology coincided with the identification of participants with a different pathology – metastatic melanoma. Participants DSB04 and DSB05 presented with large cutaneous melanoma deposits and were enrolled in a Phase 1 trial of a tumour vaccine. The trial drug was not thought to induce DNA damage, and was administered at least 3 weeks prior to samples being taken for this study.

Participant DSB04 underwent 6 FNA samples over 2 visits. The tumour deposit from which samples were taken was excised soon after the second visit. At least 50 cells were visible on each slide (see Figure 3.5). Confocal microscopy images were subjectively clearer than for epifluorescence and demonstrated less cytoplasmic

staining with Alexa Fluor 488, representing non-specific binding of either anti-mouse secondary antibody, or mouse primary anti-γH2AX antibody. Participant DSB05 also had 6 FNA specimens over two visits, with similar slide appearances to participant DSB04.

Occasional cells from both of these participants were identified with widespread multifocal Alexa Fluor 488 staining. Morphological quality control confirmed these as malignant cells. In some cells these foci were clearly confined to nuclear areas coincident with DAPI staining (see Figure 3.5A) whereas in other images the multifocal area extended beyond the nuclear area.

Figure 3.5 Immunocytochemistry of fine needle aspiration tumour specimens from metastatic melanoma from participant DSB04 showing DNA (DAPI, blue) and γH2AX (green) with merged image. A and B represent cells from different needle passes.

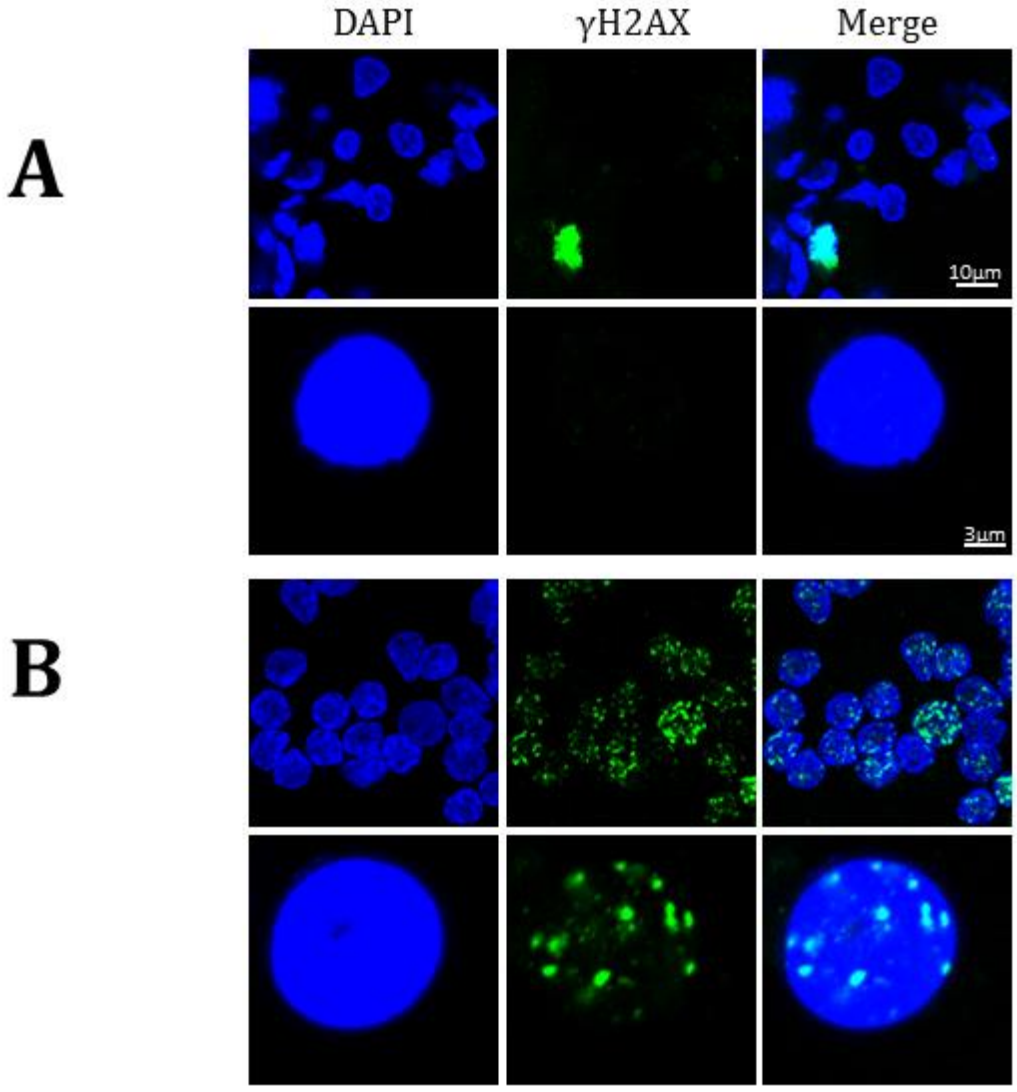


3.3.5. Application of method before and after treatment

For the remainder of the study participant recruitment was restricted to those commencing anticancer therapy to enable FNA samples to be taken before and after the first treatment. Participant DSB07 (participant DSB06 having withdrawn before any samples were taken) commenced a course of radical radiotherapy to cervical node recurrence of a squamous cell carcinoma of the parapharygeal space. FNA samples were taken immediately before and 20 minutes after the first fraction of radiotherapy. The sampled mass lay within the planning target volume

(PTV) for radiotherapy and computed tomography physical simulation indicated a planned absorbed dose of 2 Gy delivered with 6 MV photons.

Figure 3.6 Immunocytochemistry of fine needle aspiration tumour specimens from metastatic squamous cell carcinoma from participant DSB07 before (A) and 20 minutes after irradiation (B) showing DNA (DAPI, blue) and γH2AX (green) with merged image. Bright green staining in a single cell in A (top panel) may represent an apoptotic cell



As demonstrated in Figure 3.6, samples taken after radiotherapy showed a marked increase in intranuclear, Alexa Fluor 488 intense foci when compared with those taken before radiotherapy. Given the clinical context, these were interpreted as γH2AX foci associated with radiation-induced DNA DSBs.

Confocal microscopy images from participant DSB07 were used to optimise image recognition software (TRI2, see methods above and Figure 3.7) to automatically identify and quantify γH2AX foci within nuclear areas defined by the DAPI signal. Figure 3.8 demonstrates the results of this quantification in the three samples before and the three after irradiation.

Figure 3.7 Example of automated image recognition by TRI2 sofware in participant DSB07. A region of interest is detected using the DAPI signal and outlined (red in far right panel); γH2AX foci within this region are detected, outlined (blue in far right panel) and counted

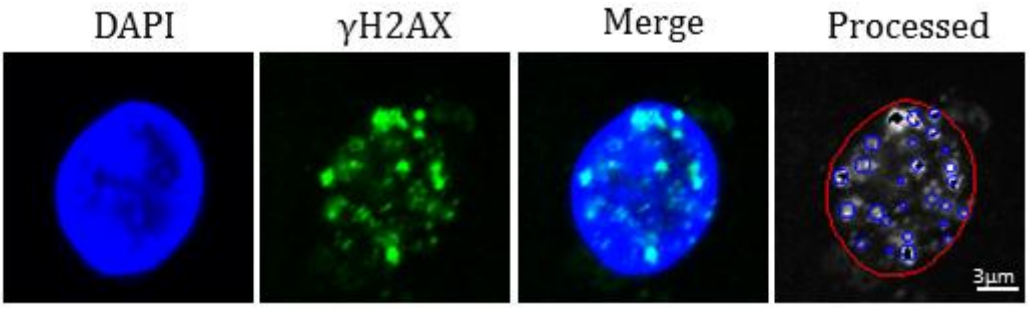
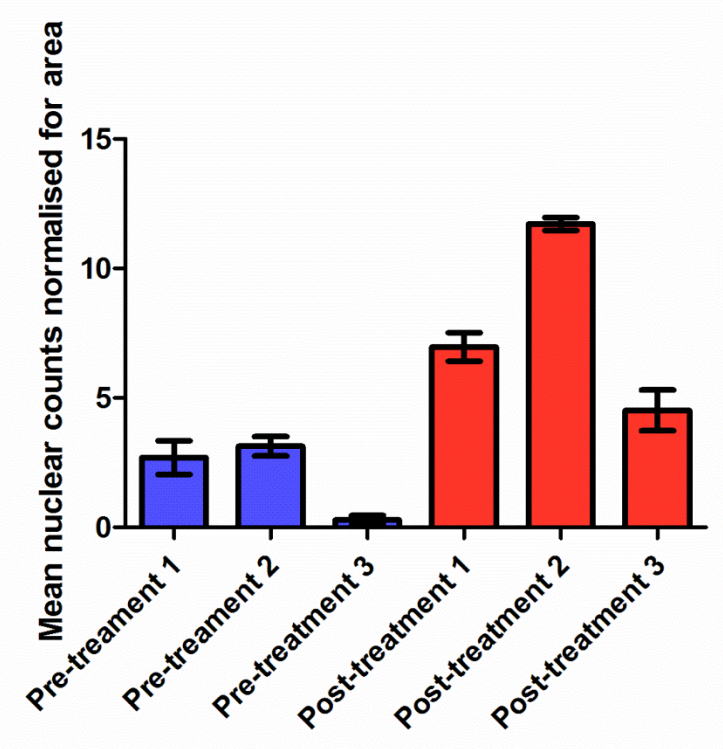


Figure 3.8 Mean foci number normalised for nuclear area (±standard error of mean) calculated by TRI2 image recognition in individual FNAs from participant DSB07 taken before (blue) and 20 minutes after (red) 2 Gy of radiotherapy

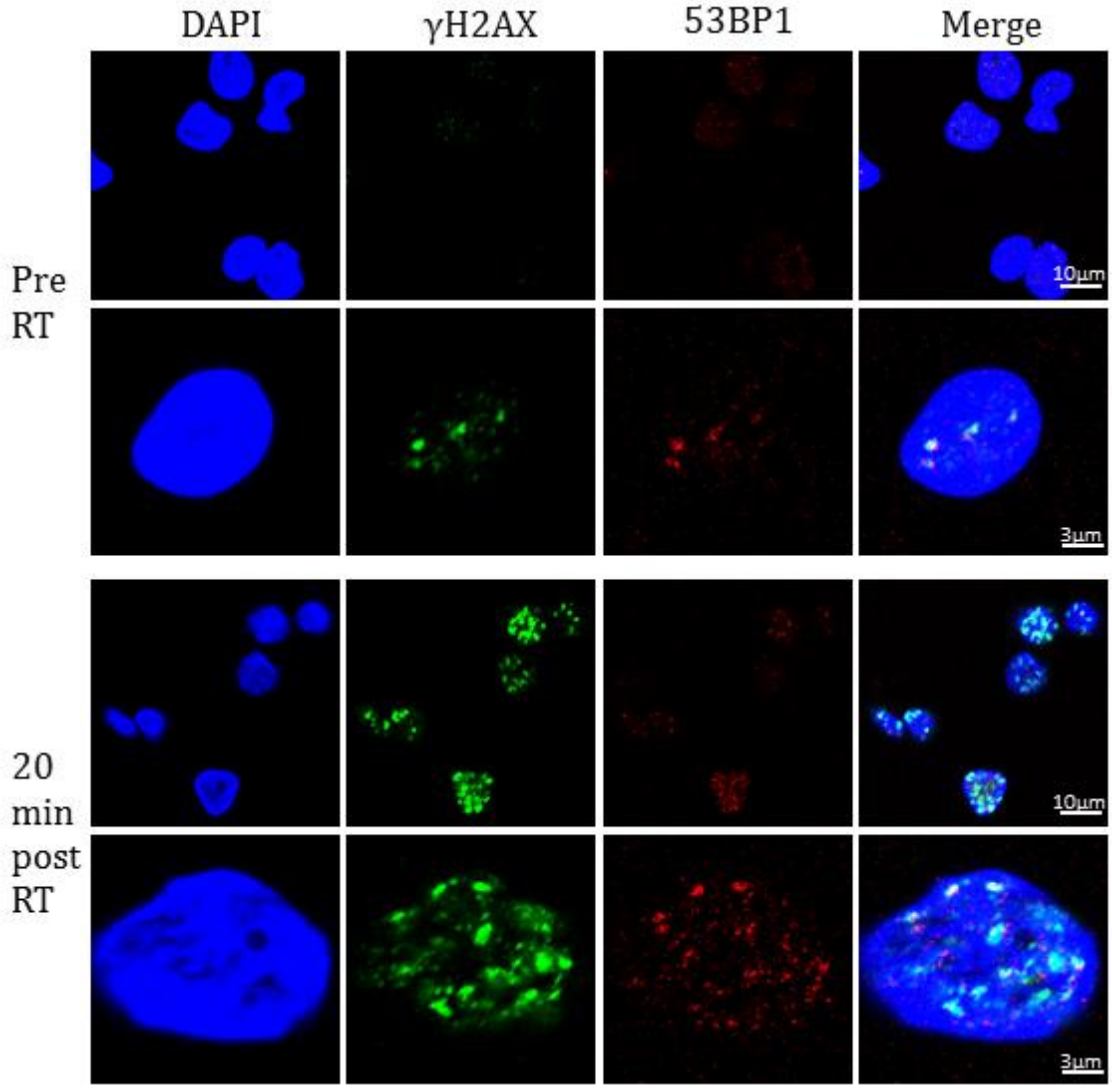


3.3.6. Co-staining for γH2AX and 53BP1

Participant DSB08 had palliative radiotherapy to a metastatic deposit from non small cell lung cancer (NSCLC) in a supraclavicular lymph node. Three FNA samples were taken before and after the first 3Gy fraction of radiotherapy with 6MV photons. Very little material could be aspirated from the very firm tumour deposit, and no malignant cells were visible on slide smear preparations after immunocytochemistry. No further analysis could be performed.

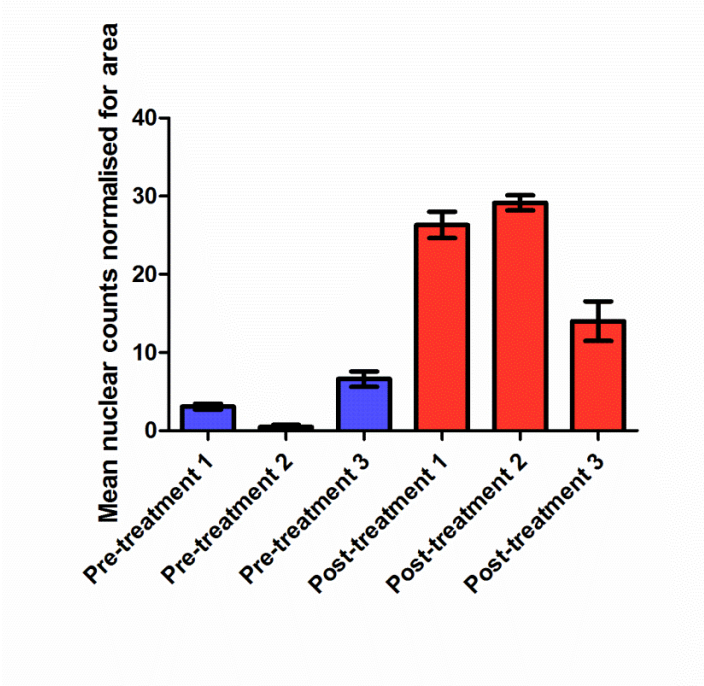
Participant DSB09 had a long history of non-Hodgkins lymphoma and received palliative radiotherapy to a malignant lesion in the posterior triangle of the neck. She consented to 3 FNA samples immediately before and 3 immediately after 3 Gy of radiotherapy treatment. As shown in Figure 3.9 synchronous staining for 53BP1 was introduced (see Section 3.2.6). The number and intensity of γH2AX foci increased with irradiation. 53BP1 foci were seen to largely co-localise with γH2AX foci, both before and after irradiation, but background staining was subjectively greater than for γH2AX, making foci identification difficult. Consistent results for automated foci recognition could not be achieved.

Figure 3.9 Immunocytochemistry of fine needle aspiration tumour specimens of non-Hodgkins lymphoma deposits from participant DSB09 before (Pre RT) and 20 minutes after irradiation (20 min post RT) showing DNA (DAPI, blue), γH2AX (green) and 53BP1 (red) with merged image



Baseline γH2AX foci numbers were lower for participant DSB09 compared to participant DSB07, and post treatment foci more numerous – see Figure 3.10.

Figure 3.10 Mean γH2AX foci normalised for nuclear area (±standard error of mean) calculated by TRI2 image recognition in individual FNAs from non-Hodgkins lymphoma deposits from participant DSB09 taken before (blue) and 20 minutes after (red) 3 Gy of radiotherapy



3.3.7. FNA up to 1 week after radiotherapy

Participant DSB10 had a painful skin metastasis from non-small-cell lung cancer on the right upper arm. This was to be irradiated with 17 Gy divided in two fractions delivered one week apart. Samples were taken immediately before the first, 8.5 Gy, fraction, 20 minutes after this, and one week later, before the second fraction was delivered.

The results (Figure 3.11) showed more foci before treatment than for other samples, and a very large rise in numbers of γH2AX but not 53BP1 foci 20 minutes after treatment, and most surprisingly only slightly fewer γH2AX foci one week later, largely co-localising with 53BP1 staining. Automated foci quantification forall conditions is shown in Figure 3.12.

Figure 3.11 Immunocytochemistry of fine needle aspiration tumour specimens from metastaic non-small cell lung cancer from participant DSB10 before (A) 20 minutes after (B) and 1 week after (C) irradiation (B) for DNA (DAPI, blue), γH2AX (green), 53BP1 (red) and merged image

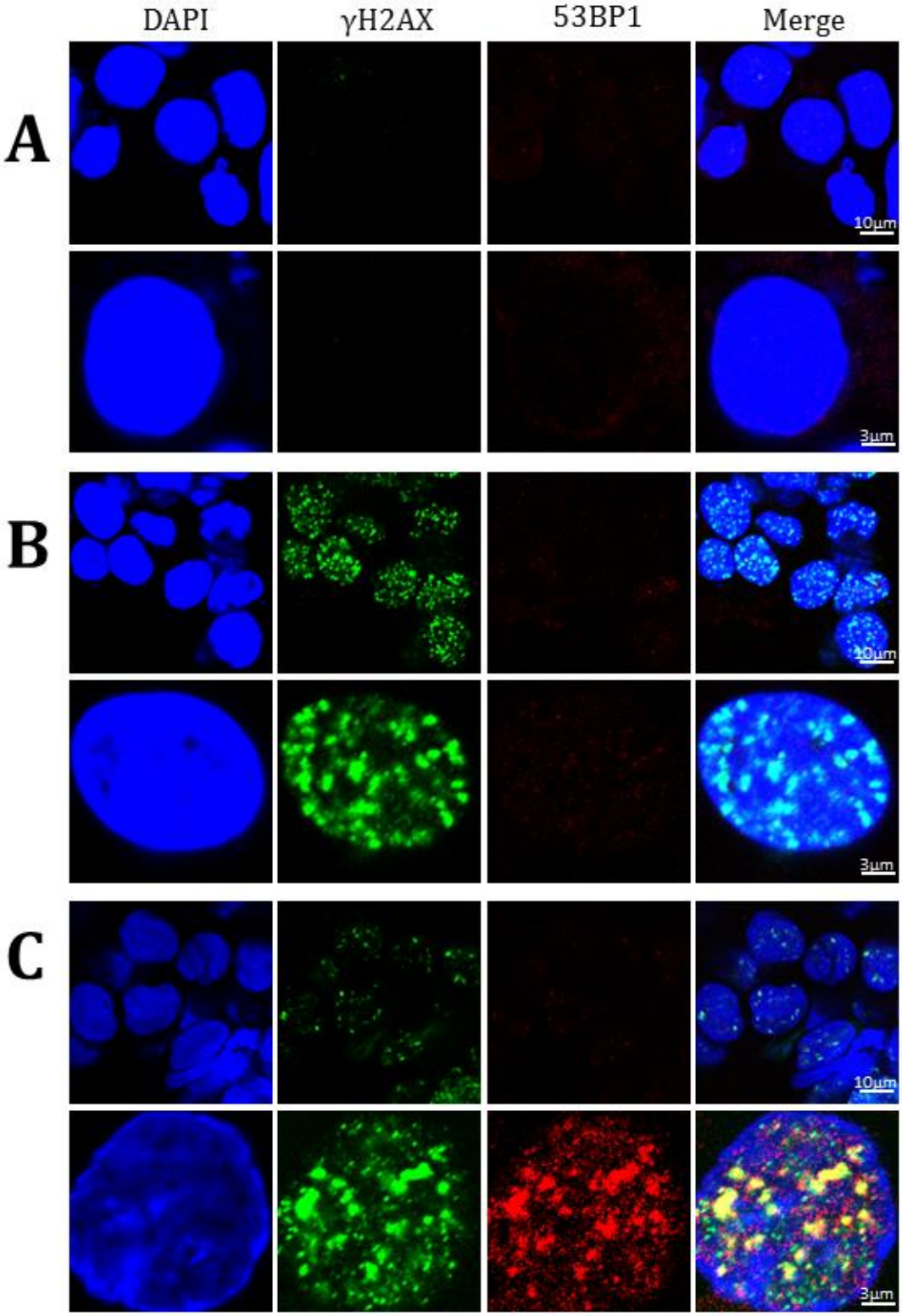
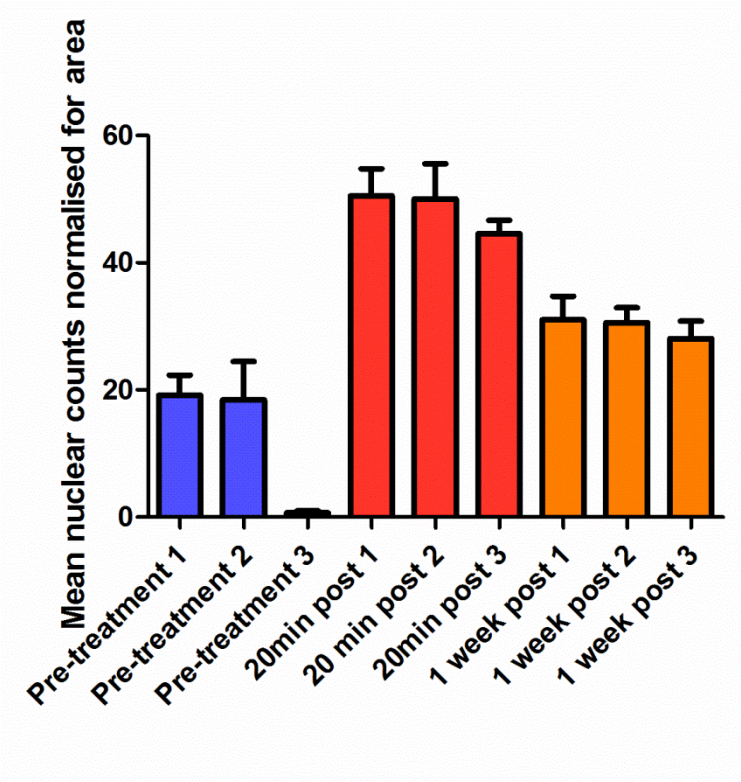


Figure 3.12 Mean γH2AX foci normalised for nuclear area (±standard error of mean) calculated by TRI2 image recognition in individual FNAs from metastatic non-small cell lung cancer from participant DSB10 taken before (blue), 20 minutes after (red) and 1 week after (orange) 8.5 Gy of radiotherapy



3.3.8. Analysis

For patients DSB07, DSB09 and DSB10, similar methods of immunocytochemistry were employed with identical image analysis. The collection of three repeat FNAs allowed an analysis of assay variation to be quantified as the coefficient of variation (CV) in foci number measurement. This was available in a variety of tumour types under a variety of treatment conditions, across which the mean CV was 49% (range 5-91%) – see Table 3.2.

Table 3.2 Coefficient of variation from repeated quantification of γH2AX foci with the optimised immunocytochemistry and image analysis method

Participant number	Condition	CV (%)
DSB 07	Pre-treatment	76%
	20 minutes post 2Gy RT	47%
DSB 09	Pre-treatment	91%
	20 minutes post 3Gy RT	35%
DSB 10	Pre-treatment	82%
	20 minutes post 8.5Gy RT	7%
	1 week post 8.5Gy RT	5%
ALL	**Mean**	**49%**

3.4. Discussion

3.4.1. Development of the FNA Assay

There are no published data or protocols describing the quantification of γH2AX in tumours using fine needle aspiration (FNA). The DSB Biomarkers Pilot Study was conceived to explore this technique. This pilot study was designed to assess the reproducibility of assay signals under a variety of conditions. Data on assay variability would be useful to judge the assay's potential for application to clinical questions, including informing sample size calculations.

The method was intended for application in a phase I clinical trial of a novel radiopharmaceutical, ^{111}Indium-DTPA-EGF.[225] The trial protocol required multiple

administrations of the agent, and a radiodynamic assay that was acceptable to patients for multiple sampling was required. The γH2AX FNA assay was proposed in order to fit these criteria.

The development of a novel clinical assay is limited by the availability of clinical material. The DSB Biomarkers Pilot Study protocol was written to allow up to three synchronous samples to be taken on each of up to three occasions. All patients had a locally advanced or metastatic malignancy for which they were undergoing treatment, and opted to have FNA procedures only when attending the hospital for treatment or clinic appointments. The difficulty encountered in collecting nine FNA specimens from most participants reflects the pressures on this patient population as well as perhaps the poor acceptability of the technique (at least in the context of a clinical study with no direct benefit to the participant's clinical care).

Samples from participants DSB01-DSB03 were used in an attempt to develop a liquid based cytology (LBC) method for the γH2AX immunocytochemical assay. LBC has potential advantages for the standardisation and preservation of cell quality during sample processing.[223] Commercial LBC sample processing platforms developed for cervical cytology are routinely applied to different cytological specimen types including FNA,[226] but lack the flexibility for novel assay development. In particular, cell fixation is restricted under processor guarantee conditions to proprietary solutions the composition of which is not in the public domain. The direct smear method was therefore favoured for further development.

Samples from participant DSB07 were obtained before and after a 2 Gy fraction of radiotherapy. They provided the first indication of the success of the assay in identifying an increase in γH2AX signal in a focal staining pattern. The magnitude of this increase was quantified using automated image recognition. Refinement of the image recognition algorithm does depend on the subjective judgement of the operator, in the same way that manual foci counting is subjective. However the automated method then provides for rapid, standardised foci counting. This approach (as opposed to manual foci counting) has been adopted by other groups seeking to translate the γH2AX foci assay for possible clinical applications.[155, 156, 227]

The performance of the assay is assessed by the reproducibility of assay results. Since each FNA results in a single sample slide, it was not possible to measure true intra-assay variability *i.e.* the parallel assays on the same sample. Some idea of the variation in foci number across the slide is given by the error around each mean foci number plotted. Consecutive FNA samples were used to quantify inter-assay variability, and analysis yielded a coefficient of variation (CV) of 49%. It should be noted that three samples is the minimum for which a CV can be calculated, and the conclusions drawn from this calculation are therefore limited. The variation includes that due to the assay and that due to true biological variation between samples. Biological variation in DSB damage may be significant, relating for example to cell cycle phase or oxygenation.[5]

For comparison, the CV for standardised uptake value in tumour ^{18}FDG-PET scanning is typically 30%,[228] and for a serum PSA immunochemical assay typically 10%.[229] If a two-fold difference in foci numbers were being sought (for example

between less and more responsive areas of a tumour), CV 49% would indicate a 30% chance of observing such a difference because of assay variability where none truly existed.[230]

3.4.2. Comparisons with published data

The immunocytochemical foci assay provides a continuous variable – mean foci number. This contrasts with most immunohistochemical assays which employ a categorical score. Analysis by absolute foci number maintains the assay's sensitivity to detect small differences, but exposes the random error of the measurement.

There are few published data from tumour samples in cancer patients with which to compare these results for γH2AX expression (See Section 1.3.5). The absolute numbers of foci reported for a particular assay depends on the microscopy technique as well as immunocytochemical staining. In this report, confocal microscopy was used to image a plane of 0.5 μm thickness through the nucleus, which had a depth of 5-10 μm when mounted on a slide. There are no comparable methods reported in the literature.

Comparisons of foci number from tissue immunohistochemistry have been made during a course of combined chemotherapy and radiotherapy for cervical squamous cell carcinoma[123, 124] and during Phase I trial treatment with an intrastrand cross-linking agent.[180] In the latter case insufficient data are currently reported to allow any meaningful parallels to be drawn with this report.

Banuelos *et al.* report γH2AX immunohistochemistry in 18 sets of formalin fixed paraffin embedded cervical biopsies before and 24 hours after 1.8-2.0 Gy fractions

of radiotherapy. Foci numbers reported appeared to be lower than in the study presented in this chapter. The proportion of cells with any γH2AX foci was presented, ranging from 8-20% at baseline to 0-62% after treatment. The apparently higher pre-treatment foci numbers in these results could be due to any of the differences in tumour, timing and methodology that exist between the two studies. However it may be that the FNA assay is more sensitive than tissue immunohistochemistry.

There is one report of a cytological γH2AX assay, using circulating tumour cells (CTCs).[178] A threshold in the γH2AX FACS signal was used to categorise cells as positive or negative. The proportion of positive cells increased from 0-7% to 22-64% with chemotherapy treatment, and a mean of only 38 cells were examined. Interassay variability was not measured for clinical CTC data. The extent to which FNA or CTC represents the tumour as a whole is uncertain, although FNA can potentially sample across a whole tumour mass, rather than merely cells near vessels that are able to enter the circulation. Either cytological assay involves a small and probably unrepresentative sample of tumour cells. The relationship of a cytological DNA damage assay to overall tumour response-related clinical outcomes could only be assessed empirically.

More reproducible results may be obtained with the use of a threshold for "positive" cells. However, information about the distribution of foci numbers is lost.

3.4.3. Late residual foci and senescence

Data displaying such variation, from such a diverse group of patients, should be interpreted with caution. The results from participant DSB10 showing extensive γH2AX foci co-localising with 53BP1 one week after radiotherapy are nevertheless intriguing, especially as the significance of so-called late residual foci is debated.[133, 217, 231-233] The tumour had high foci numbers even before treatment, albeit without 53BP1. This patient, or simply the tumour, may have had defective DNA repair, although the persistence of foci in viable cells one week after treatment is striking, and unexplained. A specific study using this FNA immunocytochemistry assay or tissue immunohistochemistry could attempt to replicate these findings in irradiated lesions several days after radiotherapy. The extent of apoptosis and hypoxia may be relevant to γH2AX, although 53BP1 foci are not explained by either of these phenomena. It may be that these represent senescent cells, which are arrested in repair but not able to enter any of the cell death pathways. This hypothesis could be tested using co-staining with β-galactosidase as a marker of senescence.

3.4.4. Conclusion

A "fit-for-purpose" approach is adopted for biomarker validation.[234] The DSB Biomarkers Pilot Study aimed to develop an assay for γH2AX that could be applied in a radiopharmaceutical phase I trial, and on the basis of these results, the assay was included in the protocol for this trial.

This thesis considers the role of γH2AX assays as more general markers of treatment-induced DNA damage. Such application may be limited for this assay due to the variation demonstrated. This may represent tumour heterogeneity or

staining inconsistency or both, and a serious limitation of this study has been its inability to distinguish these factors. Future application should examine intra-assay variability by splitting the FNA sample into several parts to be stained independently.

Chapter 4

Development of a SPECT imaging probe from Fab fragments of anti-γH2AX antibodies

Chapter 4: Development of a SPECT imaging probe from Fab fragments of anti-γH2AX antibodies

4.1. Introduction

4.1.1. Clinical SPECT Imaging

This chapter describes the development of a novel radiopharmaceutical that aims to image γH2AX expression in order to demonstrate and quantify tumour responses to irradiation.

Clinical functional imaging is potentially useful for the evaluation of cancer patients. Depending on the resolution achieved, it can illustrate the state of different parts of a heterogeneous tumour mass, and can provide information about disease sites distributed across the patient at the same time. Clinical imaging modalities are generally non-invasive and can be repeated, providing a longitudinal assessment of disease status. Qualitative and, increasingly, quantitative comparisons can be made between images obtained at various points through the patient pathway.[235]

Single-photon emission computed tomography (SPECT) images the anatomical distribution of a radiopharmaceutical designed to demonstrate a biological state. Radiopharmaceuticals are drugs that incorporate a radioisotope tracer, chosen in this case to emit γ-irradiation in the energy range detectable by the scanner. The utility of a SPECT radiopharmaceutical is determined both by its physical and biological characteristics. Biological targeting depends on the pharmacokinetic properties of the tracer. Three dimensional images are obtained, and a resolution of 1 mm in preclinical small animal imaging and 8-10 mm in clinical imaging can

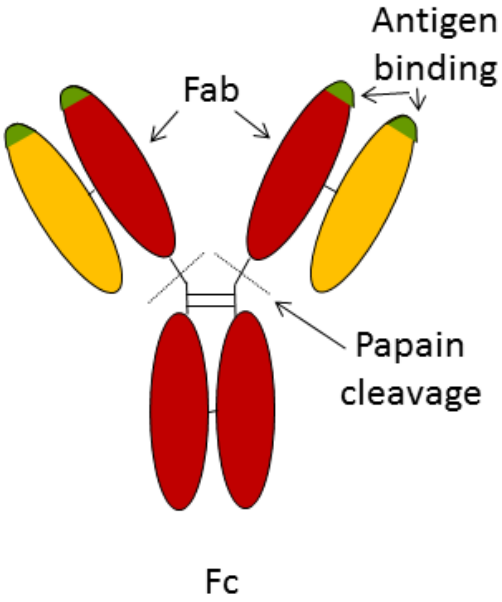
be achieved.[236] This functional information can be complemented by much higher resolution anatomical information using X-ray computed tomography (CT) in a combined modality scanner.

4.1.2. Antibodies for imaging applications

Antibodies provide a potentially attractive basis for biological imaging agents. They can be produced against a wide variety of targets to high specificity and affinity. They are, or can be engineered to be, biocompatible in a variety of immunocompetent hosts, although preclinical development can be conducted in immunodeficient animal models. Whole antibody-based biological imaging agents have been applied clinically,[237, 238] but suffer from poor pharmacokinetic properties for imaging applications including slow clearance, poor tissue penetration and liver and kidney accumulation.[239]

Antibody Fab (fragment antigen binding) fragments, representing one of the two antigen-binding arms of the antibody, can be produced by papain enzyme digestion of whole antibodies, or by genetic engineering hybridoma techniques[240] – see Figure 4.1. They can maintain target specificity using a smaller protein (typically 40-50kDa, compared to 150 kDa for whole antibodies) accelerating blood clearance and improving tissue penetration. In addition liver sequestration may be reduced since this is thought to be mediated in part by the Fc (fragment crystallisable) antibody region that is not present in Fab fragments.[241] The avidity of monovalent Fab fragments is however reduced when compared to bivalent native antibody.

Figure 4.1 Schematic diagram of an antibody molecule, consisting of heavy (red) and light chains (yellow). The site of cleavage by papain is shown, indicating the generation of two antigen binding fragments (Fab) and one crystallisable fragment (Fc) from each antibody molecule.



4.1.3. Intracellular imaging targets

Antibody imaging has been applied largely to extracellular targets since antibodies and their fragments cannot generally pass through cellular and nuclear membranes. However a number of technologies have been developed to deliver pharmaceuticals into the cell and even the nucleus. A cellular delivery mechanism that is readily compatible with *in vivo* imaging is the use of cell-penetrating peptides such as HIV-1 Tat (Human Immunodeficiency Virus Trans-Activator of Transcription).[242] These polycationic or amphipathic peptides mediate the transport of macromolecules across the cell membrane, and may include a sequence of positively-charged residues termed the nuclear localisation sequence (NLS) that improve transition across the nuclear membrane.[243] Other cellular delivery mechanisms include endocytosis mediated by certain cell surface receptors, and hydrophobic micelles that merge with the cell membrane. Nuclear

penetration of antibody-based imaging agents has been facilitated through covalent bonding to Tat peptides.[244, 245] Conjugation can be effected using a carbodiimide to activate carboxyl groups on the antibody in order to react with amine groups on the Tat peptide, a so-called zero-length crosslinking reaction.[246]

^{111}Indium is a readily available radioisotope emitting γ-rays at two energies (171 and 245 keV) that are detectable using SPECT scanners. Metal ions can be attached to proteins via metal-chelators such as diethylenetriaminepentaacetic acid (DTPA) which is available commercially in cyclic and benzyl forms. Cyclic DTPA anhydride binds to primary amines (such as those on lysine amino acid side chains) to form amide bonds.[247, 248] Benzyl DTPA is a potentially more stable chelator[249] and is available as an isothiocyanate derivative which reacts with unprotonated amines at alkaline pH to form a thiourea bond.[246]

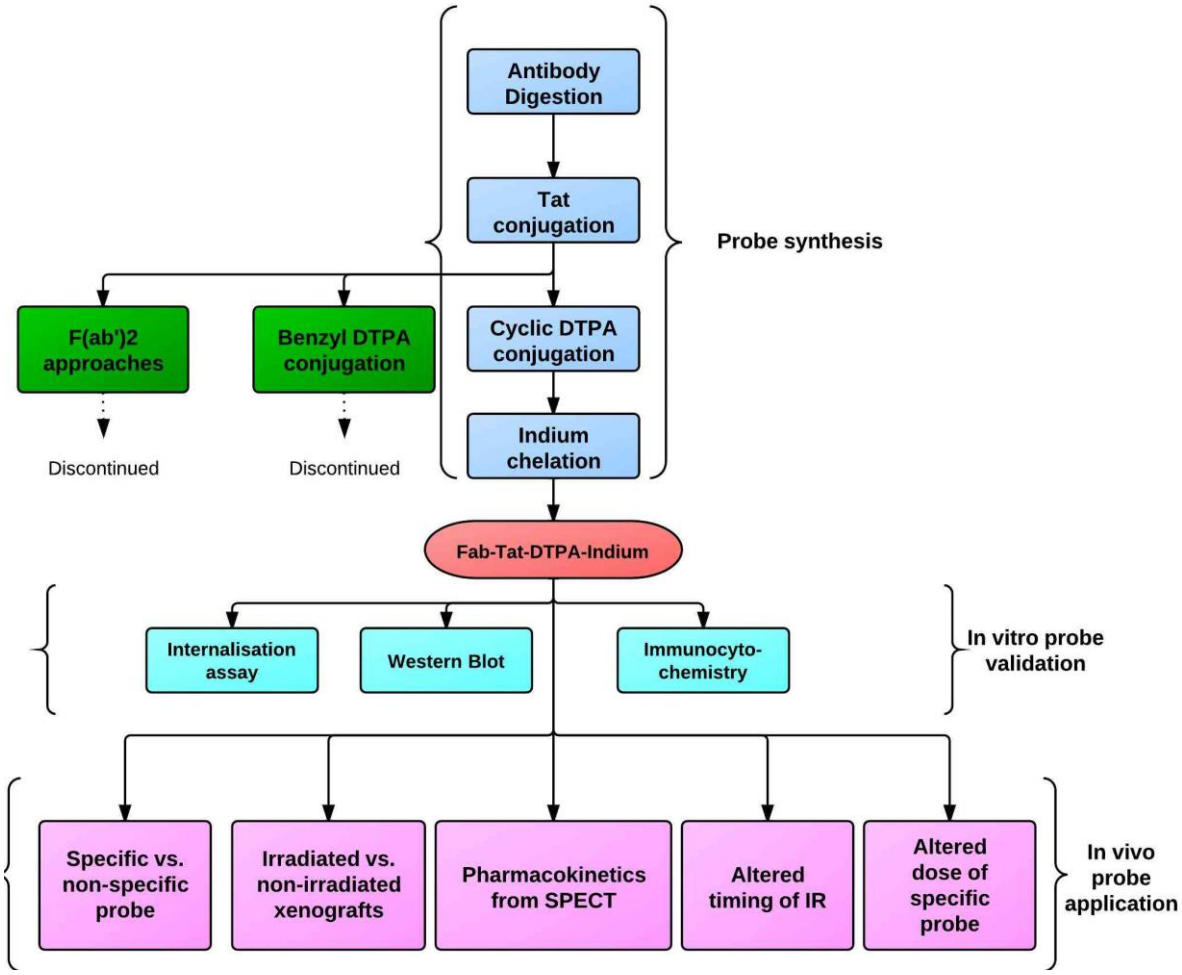
Cornelissen *et al.* developed a SPECT imaging probe using a whole antibody to γH2AX conjugated to Tat, and demonstrated differential uptake in irradiated and unirradiated human breast cancer xenografts in immunocompromised mice.[208] They also reported similar results with tumours treated with bleomycin, a chemotherapeutic agent known to cause DNA double strand breaks. The antibody was however slow to clear from the circulation, so that maximal contrast between the tumour and background signals was obtained at 48 hours after injection of the imaging agent. Liver and kidney background signals were high.

4.1.4. Chapter Outline

As illustrated in Figure 4.2, this chapter reports refinement of antibody-based γH2AX imaging by engineering a novel radiopharmaceutical consisting of Fab

fragments of anti-γH2AX antibody conjugated in turn to Tat cell penetrating peptide and the metal ion chelator DTPA, used for ^{111}In labelling.

Figure 4.2 Chapter 4 outline



The hypotheses tested were that anti-γH2AX Fab-Tat-DTPA would:

1. be internalised into cells by its Tat component;
2. maintain binding of its target, γH2AX;
3. be cleared from the blood more quickly and accumulate less in liver and kidney compared to a whole antibody probe *in vivo*;
4. accumulate in irradiated tumour xenografts to a greater extent than non-irradiated tumours and

5. reduce background SPECT signal through faster blood clearance, allowing in particular early events of normal tissue damage to be imaged.

4.2. Materials and Methods

4.2.1. Generation of antibody Fab fragments

All experiments designed to optimise synthesis of imaging probes were carried out using rabbit IgG (and subsequently its Fab fragments) resulting in a non-specific control Fab probe. The same methods were then replicated using anti-γH2AX antibody.

Antibody Fab fragments were prepared using the Pierce Fab Preparation Kit (Thermo Fisher Scientific, Loughborough, UK) with minor amendments to the manufacturer's protocol. 250 µL of 50% immobilized papain was centrifuged at 5000 x g for 1 minute in a benchtop centrifuge (Heraeus Biofuge Pico, Newport Pagnell, UK), and washed with 250 µL proprietary Fab digestion buffer containing cysteine. All washes with spin columns consisted of addition of buffer followed by centrifugation at 5000 x g (<1 mL column) or 1500 x g (>1 mL column) for 1 minute unless otherwise stated. A Zeba Desalt Spin Column (Thermo Fisher Scientific, Loughborough, UK) was washed three times with 1mL Fab digestion buffer. All steps were optimised with purified rabbit IgG before repetition with specific antibody preparations. Purified rabbit IgG (500 µg; Sigma, Dorset, UK) or rabbit anti-γH2AX antibody (Phosphodetect, Calbiochem, Merck Millipore, Watford, UK) was placed carefully on the salt column, which was centrifuged at 1500 x g for 2 minutes and the throughput was collected as buffer-exchanged IgG/antibody. This was then added to the column containing immobilised papain, and after brief mixing this was placed on a rocker in an incubator at 37°C for 6

hours. At the end of the incubation, the column was placed in a fresh microcentrifuge tube and centrifuged at 5000 x g for 1 minute and the digested antibody mixture collected. The column was washed with 500 µL of 0.1 M 2-N-morpholinoethanesulfonic acid (MES) buffer at pH 6.0. An immobilised Protein A Plus column (Fisher Scientific, Loughborough, UK) was equilibrated to room temperature and washed twice with 500 µL MES. The antibody digestion mixture, consisting of digested antibody Fab fragments, Fc fragments and undigested antibody, was added to the Protein A column and rocked for 10 minutes, to allow Fc fragments and undigested antibody to bind to protein A. Unbound Fab fragments were collected by centrifugation, and the column washed once with MES. The immobilised Protein A Plus column was regenerated by washing 4 times with IgG Elution Buffer (Thermo Fisher Scientific, Loughborough, UK) and 4 times with phosphate buffered saline (PBS, 10 mM phosphate buffer, 2.7 mM potassium chloride and 137 mM sodium chloride, pH 7.4, Sigma Aldrich, Dorset, UK). Individual immobilised Protein A Plus columns were used no more than 10 times.

4.2.2. Measurement of protein concentration

Protein concentration was measured using the bicinchoninic acid method (Pierce BCA Protein Assay Kit, Fisher Scientific, Loughborough, UK) following the manufacturer's instructions, or by spectrophotometry (Nanodrop ND1000 Spectrophotometer, Thermo Fisher Scientific, Delaware, USA) using an extinction coefficient for antibody or antibody fragments of 1.4 absorbance units per mg/mL.

4.2.3. Sodium dodecyl sulphate polyacrylamide gel electrophoresis

Samples of measured protein concentration were diluted in SDS loading buffer

(2% sodium dodecyl sulphate, 10% glycerol, 60 mM Tris pH 6.8) with or without 100 mM dithiothreitol reducing agent. A protein marker (PrecisionPlus, BioRad, UK) was loaded into one well. Up to 50 µg of protein or digest were loaded in each well of NuPAGE 4-12% bis-tris gel (Invitrogen, Paisley, UK) and run with a vertical field at 300V for 1 hour. The gel was stained with Coomassie Brilliant Blue (Sigma, Dorset, UK) for 15 minutes, and excess stain removed with 30% methanol for 30-45 minutes.

4.2.4. Labelling of proteins with ^{123}iodine (Iodogen method)

Cryogenic vials (Nunc Cryotube, Thermo Fisher Scientific, Loughborough, UK) were coated by addition of 75 µg 1,3,4,6-tetrachloro-3alpha,6alpha-diphenylglucoluril (Iodogen, Thermo Fisher Scientific, Loughborough, UK) dissolved in 200 µL chloroform (Sigma, Dorset, UK) which was allowed to evaporate overnight. Sodium ^{123}-iodide was added to the vial (typically 4 MBq). Proteins to be labelled were dissolved at 2 mg/mL (typically 80 µg in 40 µL) in Iodogen buffer (0.1 M sodium phosphate dibasic, pH 8.4) added to the vial and incubated for at least 15 minutes in a shielded chamber at room temperature. Labelling was confirmed by size exclusion chromatography (SEC) with a P2 gel.

4.2.5. Size exclusion chromatography (SEC)

SEC gels were prepared using 150 mm glass Pasteur pipettes (VWR International, Lutterworth, UK) with a small amount of glass wool to block the tapered end. Size exclusion gels Sephadex G25, Sephadex G50 (Sigma, Dorset, UK) and Bio-Gel P2 (BioRad, Hemel Hempstead, UK) were hydrated overnight in PBS and added to Pasteur pipettes to form a gel column 5 mm in diameter and 70 mm long. Samples

were applied to the top of the column, and washed sequentially with 100 μL aliquots of PBS, with simultaneous collection of the run-through fractions.

4.2.6. Carbodiimide peptide coupling of Tat peptide to antibody Fab fragments

Carboxyl groups on Fab fragments were activated to form amine-reactive carbodiimide intermediates by incubation for 15 minutes at room temperature with 1-Ethyl-3-(3-dimethylaminopropyl) carbodiimide (EDC, Thermo Scientific, Loughborough, UK) in 10 to 1000 fold molar excess to Fab in 0.1 M MES solvent pH6.0. The derivative was stabilised with *N*-hydroxysulfosuccinimide (Sulfo-NHS, Thermo Scientific, Loughborough, UK) added concurrently in 2.5 fold molar excess to EDC. After spin column purification and buffer exchange (see above) to PBS pH 7.0, a Tat peptide (amino acid sequence GRKKRRQRRRPQGYGCG, Cambridge Peptides, Cambridge, UK) was added in 1 to 100 fold molar excess and incubated for at least 2 hours at room temperature. The entire reaction mixture was separated on a Sephadex G25 size exclusion column (see above), from which Fab and Fab-Tat species were predicted to elute early (fractions 3-8) and smaller free Tat peptides late (fractions 12-20). The reaction was optimised for tat conjugation using ^{123}I radiolabelled Tat peptide (see above) detected using gamma scintillation counting of eluted fractions (Wizard 2 2480 Gamma Counter, PerkinElmer, Massachusetts, USA) and repeated with unlabelled native Tat detected using spectrophotometry (see above).

4.2.7. Conjugation of p-isothiocyanate benzyl DTPA by thiourea linkage

Proteins to be radiolabelled were buffer exchanged into aqueous 0.1 M sodium bicarbonate buffer (pH 7.0, 8.0, 8.4 or 9.0) or 0.1 M sodium borate (pH 8.0 or 9.0)

at concentrations of 0.2 – 5 mg/mL. p-isothiocyanate benzyl diethylene triamine pentaacetic acid (p-SCN-benzyl-DTPA, Macrocyclics, Dallas, USA) was dissolved in aqueous buffers or dimethyl sulphoxide (DMSO, Sigma, Dorset, UK) at concentrations of 1-5 mg/mL, and added to protein in 1-20 fold molar excess. The isothiocyanate moiety reacts with ε-amino groups on lysine residues or the N-terminal amine, but can be hydrolysed. The mixture was incubated at room temperature or 37°C for 1 – 24 hours during method development. For optimisation of the reaction the entire reaction mixture was buffer exchanged to 0.1 M sodium citrate buffer pH 6.0 and incubated with 0.1-2 MBq ^{111}InCl, then separated on a Sephadex G25 size exclusion chromatography (SEC) column eluted with 100 μL fractions of PBS (see above), from which unlabelled Fab, Fab-Tat, and Fab-Tat-benzyl DTPA species, along with Fab-Tat-benzyl DTPA–^{111}In, were predicted to elute early (fractions 3-8) and smaller free p-SCN-benzyl-DTPA, free ^{111}In and p-SCN-benzyl-DTPA-^{111}In late (fractions 12-20). ^{111}In was detected using gamma scintillation counting (see above). Once this step was optimised, the unlabelled reaction mixture was buffer exchanged and run on the Sephadex SEC column eluted with 0.1 M sodium citrate pH 6.0. Fractions corresponding to the optimal elution in the radiolabelled column were collected and protein concentration measured by spectrophotometry. Fractions containing Fab-Tat-benzyl DTPA were concentrated by centrifugation in a YM30 centrifugal filter unit (Amicon Ultracel 30K, Millipore, Watford, UK).

4.2.8. Conjugation of cyclic DTPA anhydride

Cyclic diethylene triamine pentaacetic acid anhydride (cyclic DTPA anhydride, Sigma, Dorset, UK) contains two anhydride moieties that can react by electrophilic attack linkage with ε-amino groups on lysine residues or the N-terminal amine of

the protein. The reaction was optimised using identical conditions to those described above for p-isothiocyanate-DTPA.

Anti–γH2AX Fab-Tat-DTPA and control probes (Whole anti-γH2AX-Tat-DTPA and Rabbit IgG Fab-Tat-DTPA) were synthesised in parallel and stored in 0.1 M sodium citrate buffer pH 6.0 at -20°C until required.

4.2.9. SEC Quantification and Statistics

Radioactivity in SEC column elution fractions is presented as the proportion of total counts in each fraction to correct for differences in the amount of activity in each assay. Data were compared using Two-Way Analysis of Variance (ANOVA) for drug and elution fraction.

Where two phases of elution are detected (see above) the mean number of (for example) ^{123}Tat molecules incorporated per Fab molecule was calculated using the formula:

$$Mean\ Tat\ per\ Fab = \frac{Counts\ in\ first\ peak\ x\ Molar\ excess\ of\ Tat{:}Fab}{Counts\ in\ second\ peak}$$

4.2.10. Cell culture

The cell lines used for this project were the breast cancer lines MDA-MB-468 and MDA-MB-231/H2N ("H2N" obtained from MDA-MB-231 cells stably transfected with HER2 courtesy of Dr Robert Kerbel, Sunnybrook Cell Research Centre, Toronto, Canada). Cell cultures were grown in plastic tissue culture flasks (Sarstedt, VWR International) in Dulbecco's Modified Eagle's Medium (DMEM; Sigma, Dorset, UK) supplemented with 10% Fetal Bovine Serum (Gibco, Invitrogen, Paisley, UK) and 0.1% penicillin/streptomycin/glutamate mixture (PSG; Sigma, Dorset, UK). Cultures were passaged to new flasks on reaching 75-100%

confluence, generally twice per week. Cultures were not extended beyond 20 weeks or 30 passages.

4.2.11. Immunocytochemistry

H2N cells were grown overnight on coverslips (22 x 22 mm; VWR International, Lutterworth, UK) and processed as for PBMCs - see Section 3.2.3. Anti–γH2AX Fab-Tat-DTPA and controls Whole anti-γH2AX-Tat-DTPA and Rabbit IgG Fab-Tat-DTPA prepared as described above were used in place of the primary antibody at 1:50 dilution, and an Alexa-488 conjugated anti-rabbit IgG heavy and light chain secondary antibody (Catalogue number A11034, Invitrogen, Paisley, UK) was used at 1:500 dilution. For colocalisation experiments, mouse monoclonal anti-γH2AX antibody (Clone JBW301, Millipore, UK) was included in the primary antibody incubation at a dilution of 1:800, and visualised with an Alexa-594-conjugated goat anti-mouse secondary antibody (1:500; catalogue number A11032, Invitrogen, Paisley, UK). Coverslips were mounted and visualised as described in Section 3.2.3.

4.2.12. Internalisation assay

H2N cells were grown overnight in DMEM in 24-well plates (4 x 10^4 cells per well, VWR International, Lutterworth, UK). Plates were irradiated in a ^{137}Cs irradiator at 1 Gy /minute or sham irradiated. Medium was immediately replaced with medium containing probes radiolabelled with ^{123}I by the Iodogen method (see above) at a dilution of 0.5 μg/mL. At each timepoint, free medium was removed and the cells washed twice with PBS (wash fractions were added to the free medium). Membrane stripping buffer (0.1 M glycine pH 2.7 at 4°C) was then added to remove membrane-bound proteins and the plate was refrigerated at 4°C for 6 minutes. Buffer was removed and cells were washed twice with PBS. The

remaining intracellular radioactivity was assessed by lysing cells with 0.1 M Sodium Hydroxide for 20 minutes at room temperature and collecting the lysate with 2 PBS washes. Free, membrane and internalised radioactivity was assessed in collected wash fractions by scintillation counting (see above).

4.2.13. Mice

All animal experiments were carried out in accordance with the Animal (Scientific Procedures) Act 1986 under project licence number 30/2514. Animals were housed in premises licensed by the Home Office.

Nude female mice (Charles River, UK) were used for all *in vivo* xenograft experiments. Mice are bred as a homozygous FOXN1nu/nu strain, lacking a thymus and therefore immunodeficient and able to tolerate xenograft tumours. Mice were obtained from the supplier at 3-5 weeks of age (14-18 g) and inoculated with xenografts within 4 weeks of arrival. Mice were housed in a temperature and light controlled environment.

4.2.14. Establishment of xenografts

H2N cells were harvested from culture (3-5 x 10^6 cells per mouse), washed, resuspended in DMEM (100 µL per xenograft) and placed on ice. Immediately before injection, the cell suspension was mixed with 100 µL of basement membrane (BD Matrigel, BD Biosciences, Bedford, MA, USA) and drawn up into a 0.5 mL B.Braun Omnican insulin syringe. The cell and basement membrane suspension was injected subcutaneously (s.c.) into the left flank of the mouse under brief isofluorane anaesthesia. Mice were observed for the development of s.c. tumours which generally appeared within 1 week and grew until the

experiment. Under the terms of the Home Office project licence, animals were euthanized when tumours grew to more than 12 mm in any dimension.

4.2.15. *In vivo* irradiation and SPECT imaging experiments

Images were acquired following intravenous (i.v.) administration of anti-γH2AX Fab-Tat-DTPA (5 μg or 2 μg), rabbit IgG Fab-Tat-DTPA (5 μg) and whole anti-γH2AX-Tat-DTPA (5μg). Animals (6-12 per group) were irradiated, received imaging probe iv and scanned at selected times up to 24 hours. Under the terms of the Home Office project licence, a maximum of 4 imaging procedures were undertaken in any one animal.

4.2.16. Irradiation of xenografts

Mice were sedated with an intraperitoneal injection of 30 uL of a 1:1:10 mixture of Hypnorm (fentanyl citrate 0.315 mg/mL + fluanisone 10 mg/mL, Vetapharma, Leeds, UK) : Hypnovel (midazolam hydrochloride 5 mg/mL, Roche, Welwyn Garden City, UK): Water (water for injections Ph Eur, BM Browne, Reading, UK). Mice were introduced into a brass tube custom made at the Gray Institute for this purpose. A slit in the tube allowed the left hindlimb and hind flank of the mouse, including the xenograft, to protrude. The brass tube device (which could hold up to 4 mice) was placed into a Gulmay 320 irradiator cabinet. The X-ray tube was energised to 300kV, 10mA, and the time of irradiation adjusted to deliver the planned dose at 0.94 Gy/minute, based on dosimetry measurements performed by Dr Mark Hill of the Gray Institute. Irradiation occurred 1 or 4 hours prior to administration of the imaging radiopharmaceutical.

4.2.17. Preparation of Radiopharmaceutical

Unlabelled probes stored at 1 μg/μL were incubated with 1.0-2.0 MBq/μg ^{111}InCl in hydrochloric acid for at least 45 minutes and diluted in sterile PBS (100 μL for each animal). Labelling efficiency was assessed using Instant Thin Layer Chromatography (ITLC); 1μL of diluted labelled probe was placed 10mm from the bottom edge of a 5 x 100 mm strip of silica chromatography paper (Varian, Crawley, UK) prepared with a pencil mark at 50 mm and a soluble ink mark at the top. The strip was placed in 5 mm depth of 0.1 M Sodium Citrate pH 6.0 solution, until the solution had risen by capillary action to the top of the strip. The strip was then cut at the 50 mm mark, and the bottom (containing the large-molecule less mobile phase) and top (small molecule) halves placed in separate tubes for counting.

4.2.18. Administration of Radiopharmaceutical

Subcutaneous injection syringes (Terumo, Somerset, NJ, USA) were prepared with 2 or 5 μg of radiopharmaceutical in 100 μL PBS. Radioactivity in the syringe was measured in a well counter (Capintec, Ramsay, NJ, USA) before and after injection into the mouse tail vein. Injections were performed by Dr Bart Cornelissen and Dr Veerle Kersemans.

4.2.19. Computed Tomography/ Single Photon Emission Computed Tomography (CT/SPECT), Image Reconstruction and Region of Interest (ROI) Analysis

Mice were anaesthetised using inhaled 2-4% isofluorane in air, and maintained during scanning in a temperature-controlled chamber (air temperature 30-32°C) with continuous respiratory monitoring. A nanoSPECT/CT scanner (Bioscan, Washington DC, USA) was used to obtain a planar "scout" image, followed

immediately by CT images (45 kVp, 15 mA, pitch 1.5) and SPECT (75 seconds per projection; 24 projections). Image sets were reconstructed using Ordered-Subsets Expectation Maximisation (OSEM) by InVivoScope software (Bioscan, Washington DC, USA) and stored as DICOM (Digital Imaging and Communications in Medicine) formatted datasets.

Fused CT and SPECT images were co-registered using Inveon Research Workspace (Siemens, Erlangen, Germany), and six regions of interest defined for each animal - heart, liver, kidney, tumour, and thigh muscles on the irradiated and unirradiated sides (See Figure 4.3 for example). After all volumes were defined, relative SPECT signals were normalised for the injected activity of radioisotope for each animal.

Figure 4.3 Example coronal SPECT-CT reconstruction for definition of regions of interest (ROIs). Left animal in figure: heart=blue, liver=green, tumour=yellow, unirradiated muscle=purple; right animal: heart=blue, liver=yellow, tumour=lilac, kidney=orange, irradiated muscle=purple, unirradiated muscle=grey.



4.2.20. Biodistribution studies

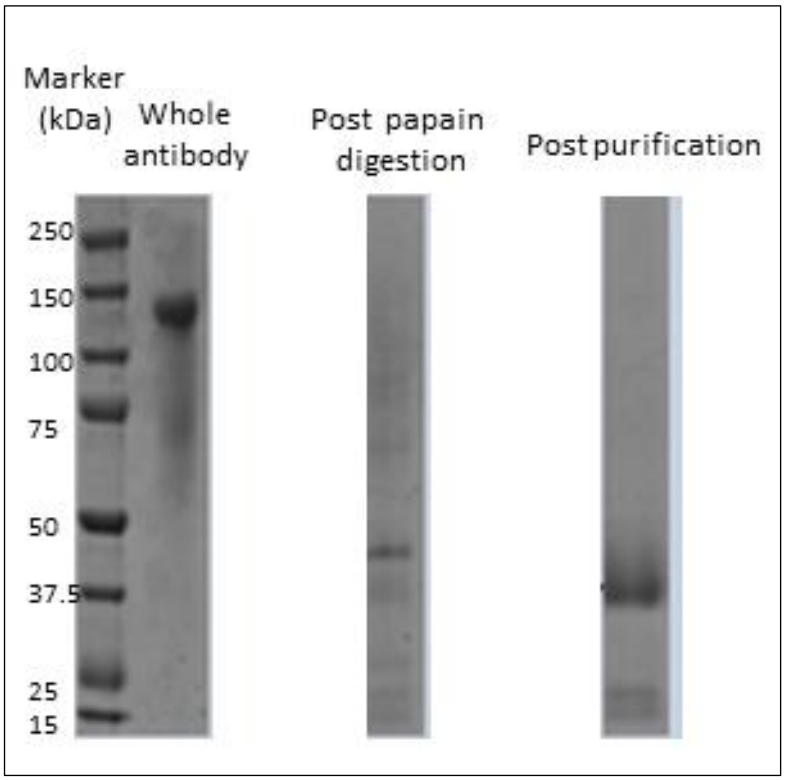
After the final scan, at 22-24 hours after injection of radiopharmaceutical, mice were euthanized and dissected. Blood was collected by cardiac puncture, and the tumour removed. Thigh muscles from the irradiated and unirradiated sides of the animal were dissected, along with the bladder, large intestine, small intestine, spleen, pancreas, stomach, kidney, liver, heart, lungs and skin (from unirradiated foreflank). Organs were washed, weighed and measured for radioactivity in a scintillation counter (see above) before normalisation for injected dose per individual animal. Activity is presented as %injected dose per gram (%ID/g) of tissue.

4.3. Results

4.3.1. Papain digestion of anti-γH2AX antibody

Both rabbit IgG and a rabbit polyclonal anti-γH2AX antibody were digested using papain, and affinity purified using protein A, resulting in a protein band on SDS PAGE corresponding to around 40 kDa in addition to two lighter bands at 10-15 kDa (See Figure 4.4). Successful digestion and collection was achieved using MES buffer for elution, avoiding the need for buffer exchange before Tat conjugation.

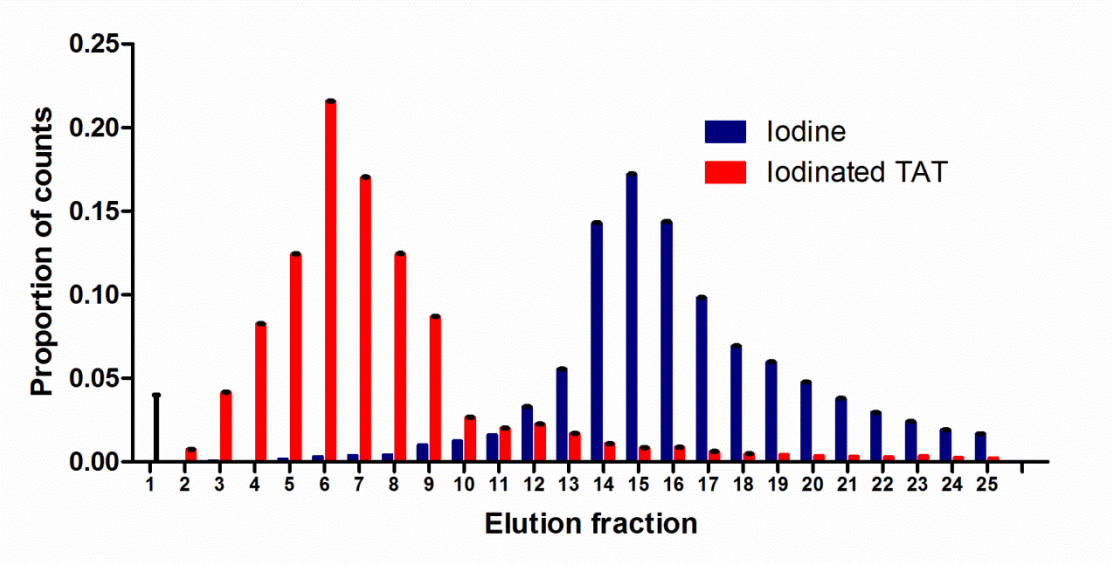
Figure 4.4 SDS PAGE of rabbit antibody before digestion, after papain digestion, and after affinity purification. Gel lanes were not normalised for total protein content.



4.3.2. Conjugation of Tat peptide to Fab fragments using carbodiimide coupling

Optimisation of Tat conjugation was facilitated by radiolabelling of Tat. Figure 4.5 illustrates the generation of a ^{123}I-radiolabelled species eluting with a peak at fraction 6 from a polyacrylamide column, as compared with free ^{123}I eluting with a peak at fraction 16.

Figure 4.5 Polyacrylamide P2 size exclusion radiochromatography demonstrating larger, early eluting iodinated ^{123}I-Tat peptide molecules generated using Iodogen (blue) and smaller, later eluting free ^{123}I control (in red). The mean (± standard error of mean) proportion of radioactivity counts are shown at each elution fraction from 3 independent repeat experiments. ^{123}I-Tat data differ significantly from free ^{123}I data (Two Way ANOVA, p(Interaction)< 0.0001)



Efficient carbodiimide coupling of ^{123}I-Tat to Fab fragments required a 300-fold molar excess of EDC and 750 fold molar excess of sNHS followed by a 10-fold molar excess of Tat (see Table 4.1). These conditions resulted in conjugation of a mean 3.52 moles of Tat per mole of Rabbit IgG Fab (range 3.04 – 4.25, n=4), and this was replicated using specific anti-γH2AX Fab (Figure 4.6). The size of the predominant species in the early-eluting phase was confirmed to be slightly larger than the size of Fab fragments – 40-45kDa in non-reducing conditions, and 20-25kDa after reduction (see Figure 4.7), consistent with conjugation of Tat.

Table 4.1 Optimisation of carbodiimide conjugation of ^{123}I-Tat peptide to antibody Fab fragments. Mean conjugation yield was calculated by size exclusion radiochromatography (see methods). Each line represents a single experiment. Independent repeats of the optimal protocol appear in bold.

Initial Concentration	Molar Excess	Molar Excess	Conjugation Buffer	Molar Excess	Mean Conjugation

of Fab (mg/ml)	EDC:Fab	sNHS:Fab		^{123}I-Tat:Fab	Yield (^{123}I-Tat : Fab)
0.1	100	230	PBS pH 7.0	18	0.25
0.23	20	50	PBS pH 7.0	1	0.07
0.23	20	50	PBS pH 7.0	10	0.16
2.0	20	50	PBS pH 7.0	1	0.03
2.0	20	50	PBS pH 7.0	10	0.35
1.0	125 (ie 2mM)	320	PBS pH 7.0	1	0.03
1.0	125 (ie 2mM)	320	PBS pH 7.0	10	0.08
1.0	125 (ie 2mM)	320	PBS PH 7.5	10	0.08
1.0	125 (ie 2mM)	320	PBS pH 8.0	10	0.02
0.6	300	750	PBS pH 7.0	1	0.15
0.6	300	750	PBS pH 7.0	5	0.90
0.6	**300**	**750**	**PBS pH 7.0**	**10**	**3.07**
0.6	**300**	**750**	**PBS pH 7.0**	**10**	**4.25**
0.6	**300**	**750**	**PBS pH 7.0**	**10**	**3.04**
1.2	300	750	PBS pH 7.0	10	2.81
0.6	**300**	**750**	**PBS pH 7.0**	**10**	**3.73**
0.3 yFab	300	750	PBS pH 7.0	10	3.74

Figure 4.6 Sephadex G25 size exclusion radiochromatography after ^{123}I-Tat conjugation to rabbit IgG and anti-γH2AX Fab fragments showing early elution of ^{123}I consistent with ^{123}I-Tat incorporation into larger Fab molecules, and later elution of smaller unreacted ^{123}I-Tat. The mean (± standard error of mean) proportion of radioactivity counts are shown at each elution fraction from 3 independent repeat experiments. Anti-γH2AX-Fab data do not differ significantly from Rabbit IgG Fab data (Two Way ANOVA, p(Interaction)=0.8390, p(Probe)=0.9531, p(Elution Volume)<0.0001)

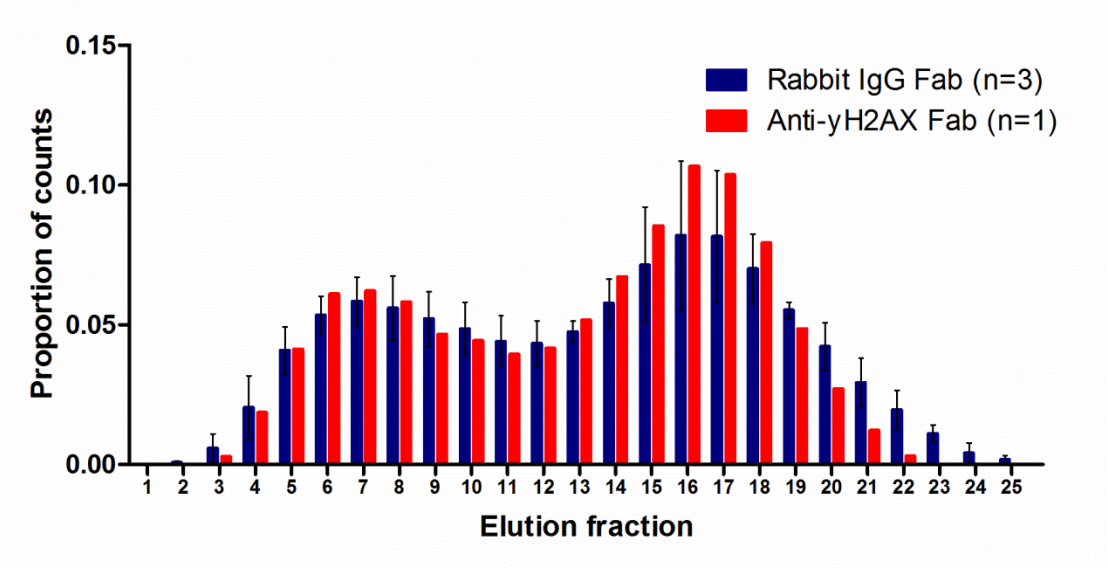
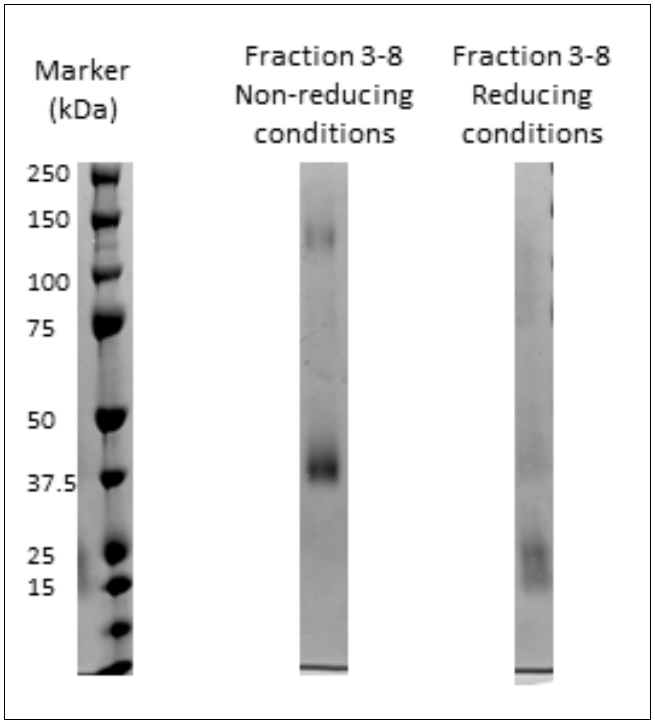


Figure 4.7 SDS PAGE of early-eluting (fraction 3-8) phase from size exclusion chromatography after rabbit IgG Fab conjugation with Tat under non-reducing (NR) and reducing (R) conditions.



4.3.3. Conjugation of DTPA

Despite experimental modification of many reaction parameters, the maximum yield of benzyl DTPA conjugation to Fab or Fab-Tat achievable was 0.64 moles of DTPA per Fab using isothiocyanate-amine crosslinking, and 0.9 moles of DTPA per Fab using carbodiimide coupling with an amine-derivative of benzyl DTPA. (See Table 4.2).

Cyclic anhydride DTPA could however be efficiently coupled resulting in a mean yield of 4.97 moles cyclic DTPA per mole of Fab-Tat (range 4.00-6.38), and tended to be higher when more concentrated reagents were employed. Coupling was efficient for both rabbit IgG Fab-Tat and anti-γH2AX Fab-Tat.

Table 4.2 Optimisation of DTPA conjugation. Mean conjugation yield was calculated using size exclusion radiochromatography data (see methods). Each line represents a single experiment. Independent repeats of the optimal protocol appear in bold. SCN=isothiocyanate, DMSO=dimethylsulphoxide, DTPA= diethylenetriaminepentaacetic acid

Initial substrate	Initial Concentration (mg/mL)	DTPA conjugate	Solute and Concentration of DTPA conjugate (mg/mL)	Molar Excess of DTPA conjugate	Conjugation Buffer	Reaction Time (hours)	Mean conjugation yield (DTPA : initial subtsrate)
Rabbit IgG Fab	1.8	SCN benzyl DTPA	1.0 in DMSO	1	0.1M Sodium bicarb. pH 8.2	1	0.01
Rabbit IgG Fab	1.8	SCN benzyl DTPA	1.0 in DMSO	5	0.1M Sodium bicarb. pH 8.2	1	0.09
Rabbit IgG Fab	1.8	SCN benzyl DTPA	1.0 in DMSO	10	0.1M Sodium bicarb. pH 8.2	1	0.13
Rabbit IgG Fab	1.8	SCN benzyl DTPA	1.0 in DMSO	20	0.1M Sodium bicarb. pH 8.2	1	0.45
Rabbit IgG Fab-Tat	1.7	SCN benzyl DTPA	1.0 in DMSO	10	0.1M Sodium bicarb. pH 8.2	1	0.06
Rabbit IgG Fab-Tat	1.7	SCN benzyl DTPA	1.0 in DMSO	10	0.1M Sodium bicarb. pH 8.2	24	0.06
Rabbit IgG Fab-Tat	1.3	SCN benzyl DTPA	1.0 in DMSO	10	0.1M HEPES pH 8.6	1	0.15
Rabbit IgG Fab-Tat	1.3	SCN benzyl DTPA	1.0 in DMSO	10	0.1M HEPES pH 8.6	24	0.08
Rabbit IgG Fab-Tat	1.3	SCN benzyl DTPA	1.0 in conjugation buffer	2	0.1M Sodium borate pH 9.2	1	0.15 (IgG control 1.6)
Rabbit IgG Fab-Tat	1.3	SCN benzyl DTPA	1.0 in conjugation buffer	10	0.1M Sodium borate pH 9.2	1	0.28 (IgG control 1.8)
Rabbit IgG Fab-Tat	1.3	SCN benzyl DTPA	1.0 in DMSO	10	0.1M Sodium bicarb. pH 8.2	1	0.12 (IgG control 2.1)
Rabbit IgG Fab	5.0	SCN benzyl DTPA	1.0 in DMSO	5	0.1M Sodium borate pH 9.2	1	0.04
Rabbit IgG Fab Tat	5.0	SCN benzyl DTPA	1.0 in DMSO	5	0.1M Sodium borate pH 9.2	1	0.09
Rabbit IgG Fab	5.0	SCN benzyl DTPA	5.0 in DMSO	10	0.1M Sodium bicarb. pH 8.6	1	0.64
Rabbit IgG Fab	5.0	SCN benzyl DTPA	5.0 in DMSO	5	0.1M Sodium bicarb. pH 8.2	1	0.02
Rabbit IgG Fab	5.0	SCN benzyl DTPA	5.0 in DMSO	5	0.1M Sodium carbonate pH 9.0	1	0.03
Rabbit IgG Fab	1.0	SCN benzyl DTPA	1.0 in DMSO	5	0.05M Sodium bicarb. 0.15M Sodium chloride pH 8.5	1	0.01
Rabbit IgG Fab	1.0	SCN benzyl DTPA	1.0 in DMSO	50	0.05M Sodium bicarb. 0.15M Sodium chloride pH 8.5	1	0.13
Rabbit IgG Fab	1.0	SCN benzyl DTPA	1.0 in DMSO	5	0.05M Sodium bicarb. 0.15M Sodium chloride pH 9.5	1	0.02

Table 4.2 (continued)

Initial substrate	Initial Concentration (mg/mL)	DTPA conjugate	Solute and Concentration of DTPA conjugate (mg/mL)	Molar Excess of DTPA conjugate	Conjugation Buffer	Reaction Time (hours)	Mean conjugation yield (DTPA : initial subtsrate)
Rabbit IgG Fab	1.0	SCN benzyl DTPA	1.0 in DMSO	50	0.05M Sodium bicarb. 0.15M Soduim chloride pH 9.5	1	0.05
Anti-γH2AX Fab	0.3	SCN benzyl DTPA	1.0 in conjugation buffer	10	0.1M Sodium bicarb. pH 8.6	1	0.04
Anti-γH2AX Fab-Tat	0.3	SCN benzyl DTPA	1.0 in conjugation buffer	10	0.1M Sodium bicarb. pH 8.6	1	0.17
Rabbit IgG Fab	7.6	SCN benzyl DTPA	1.0 in DMSO	10	PBS pH 7.2	16	0.21 (IgG 0.62)
Rabbit IgG Fab	2.1	SCN benzyl DTPA	1.0 in DMSO	10	0.1M sodium bicarb. pH 8.3	16	0.25 (IgG 4.61)
Rabbit IgG Fab	3.9	SCN benzyl DTPA	1.0 in DMSO	10	0.1M Sodium borate pH 9.2	16	0.25 (IgG 3.94)
Rabbit IgG Fab	2.1	p-amino benzyl DTPA	1.0 in DMSO	10	PBS pH 7.0	2	0.32
Rabbit IgG Fab	2.1	p-amino benzyl DTPA	1.0 in DMSO	50	PBS pH 7.0	2	0.90
Rabbit IgG Fab	0.5	p-amino benzyl DTPA	1.0 in conjugation buffer	10	PBS pH 7.0	2	0.02
Rabbit IgG Fab	0.5	p-amino benzyl DTPA	1.0 in conjugation buffer	10	PBS pH 8.2	2	0.05
Anti-γH2AX Fab	0.3	p-amino benzyl DTPA	1.0 in DMSO	10	PBS pH 7.0	2	0.03
Rabbit IgG Fab-Tat	1.3	Cyclic anhydride DTPA	1.0 in DMSO	10	0.1M Sodium bicarb. pH 8.2	1	1.8
Rabbit IgG Fab	5.0	Cyclic anhydride DTPA	1.0 in DMSO	20	0.1M Sodium bicarb. pH 8.6	1	2.41
Rabbit IgG Fab	**5.0**	Cyclic anhydride DTPA	5.0 in DMSO	**20**	**0.1M Sodium bicarb. pH 8.6**	**1**	**4.00**
Rabbit IgG Fab	**5.0**	Cyclic anhydride DTPA	5.0 in DMSO	**20**	**0.1M Sodium bicarb. pH 8.6**	**1**	**4.38**
Rabbit IgG Fab	**5.0**	Cyclic anhydride DTPA	5.0 in DMSO	**20**	**0.1M Sodium bicarb. pH 8.6**	**1**	**6.52**
Rabbit IgG Fab-Tat	2.0	Cyclic anhydride DTPA	5.0 in DMSO	20	0.1M Sodium bicarb. pH 8.6	1	9.24
Anti – γH2AX Fab Tat	0.2	Cyclic anhydride DTPA	1.0 in DMSO	20	0.1M Sodium bicarb. pH 8.6	1	0.55
Anti – γH2AX Fab-Tat	0.5	Cyclic anhydride DTPA	5.0 in DMSO	20	0.1M Sodium bicarb. pH 8.6	1	4.24

4.3.4. ^{111}Indium radiolabelling of Anti-γH2AX Fab-Tat-DTPA

Radiochemical labelling efficiency of the final product, anti-γH2AX Fab-Tat-DTPA was assessed both with size exclusion chromatography (Figure 4.8) and instant thin layer chromatography (Table 4.3) and compared with the non-specific control product, rabbit IgG Fab-Tat-DTPA. Mean labelling efficiency of anti-γH2AX Fab-Tat-DTPA was 94.1% (n=7) and for rabbit IgG Fab-Tat-DTPA 92.3% (n=2), and specific activity of 1.0-2.0 MBq/μg was achieved for *in vivo* imaging experiments.

Figure 4.8 Sephadex G25 size exclusion radiochromatography of purified rabbit IgG Fab-Tat-DTPA and anti-γH2AX Fab-Tat-DTPA after conjugation with ^{111}Indium. The mean (± standard error of mean) proportion of radioactivity counts is shown at each elution fraction from three independent repeat experiments. Data sets from the two probes do not differ significantly (Two Way ANOVA, p(Interaction)=0.674, p(Probe)=1.000, p(Elution Volume)<0.0001)

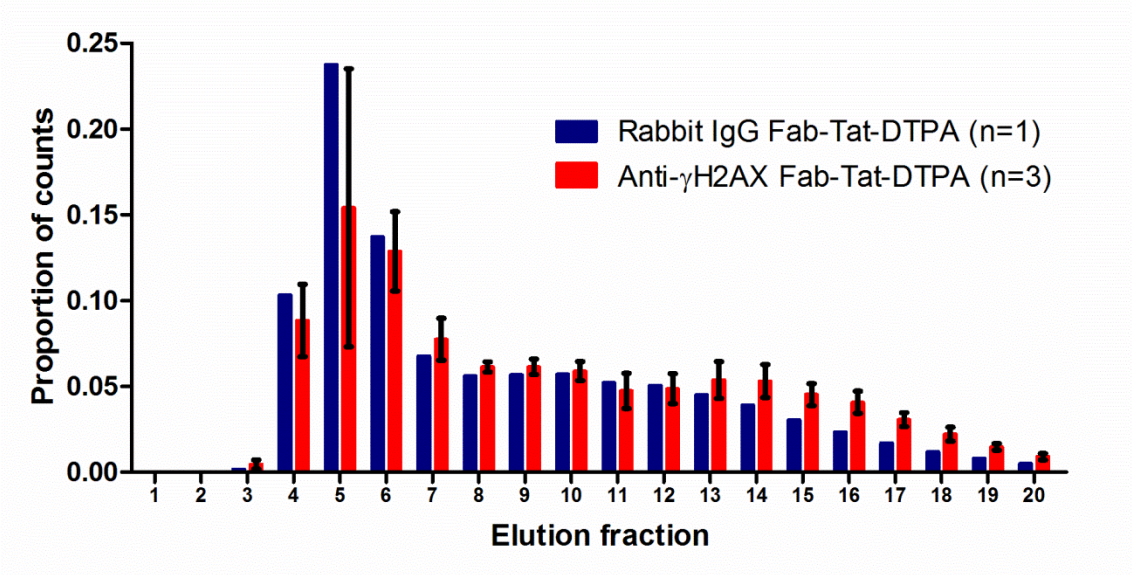


Table 4.3 Instant thin layer chromatography of anti-γH2AX Fab-Tat-DTPA radiolabelled with ^{111}Indium

Experiment	Counts per minute bottom	Counts per minute top	Labelling efficiency (%)
1	1056912	33468	96.9
2	943536	50074	95.0
3	842698	49257	94.5
4	999417	52482	95.0
5	817739	30604	96.7
6	915366	48165	95.0
7	963098	162759	85.5
Mean			**94.1**

4.3.5. Anti-γH2AX Fab-Tat-DTPA binds γH2AX in cells *in vitro*

Immunocytochemistry (see Figure 4.9) confirmed that the anti-γH2AX Fab-Tat-DTPA probe accumulates in intranuclear foci in irradiated but not unirradiated H2N cells. A secondary antibody raised to rabbit heavy and light chains did not accumulate at foci in the absence of the probe.

Figure 4.10 shows immunostaining to demonstrate anti-γH2AX Fab-Tat-DTPA and a mouse monoclonal antibody to γH2AX. Co-localisation is demonstrated, but the foci are not as distinct as in Figure 4.9 and background staining is increased, perhaps because of competition for specific binding sites.

Figure 4.9 Immunocytochemistry demonstrating accumulation of anti-yH2AX Fab-Tat-DTPA, visualised by Alexa Fluor 488 (AF488)-conjugated anti-rabbit heavy and light chain secondary antibody, at foci in irradiated (6Gy) but not unirradiated H2N cells. Lower panel shows control with no primary antibody in irradiated cells.

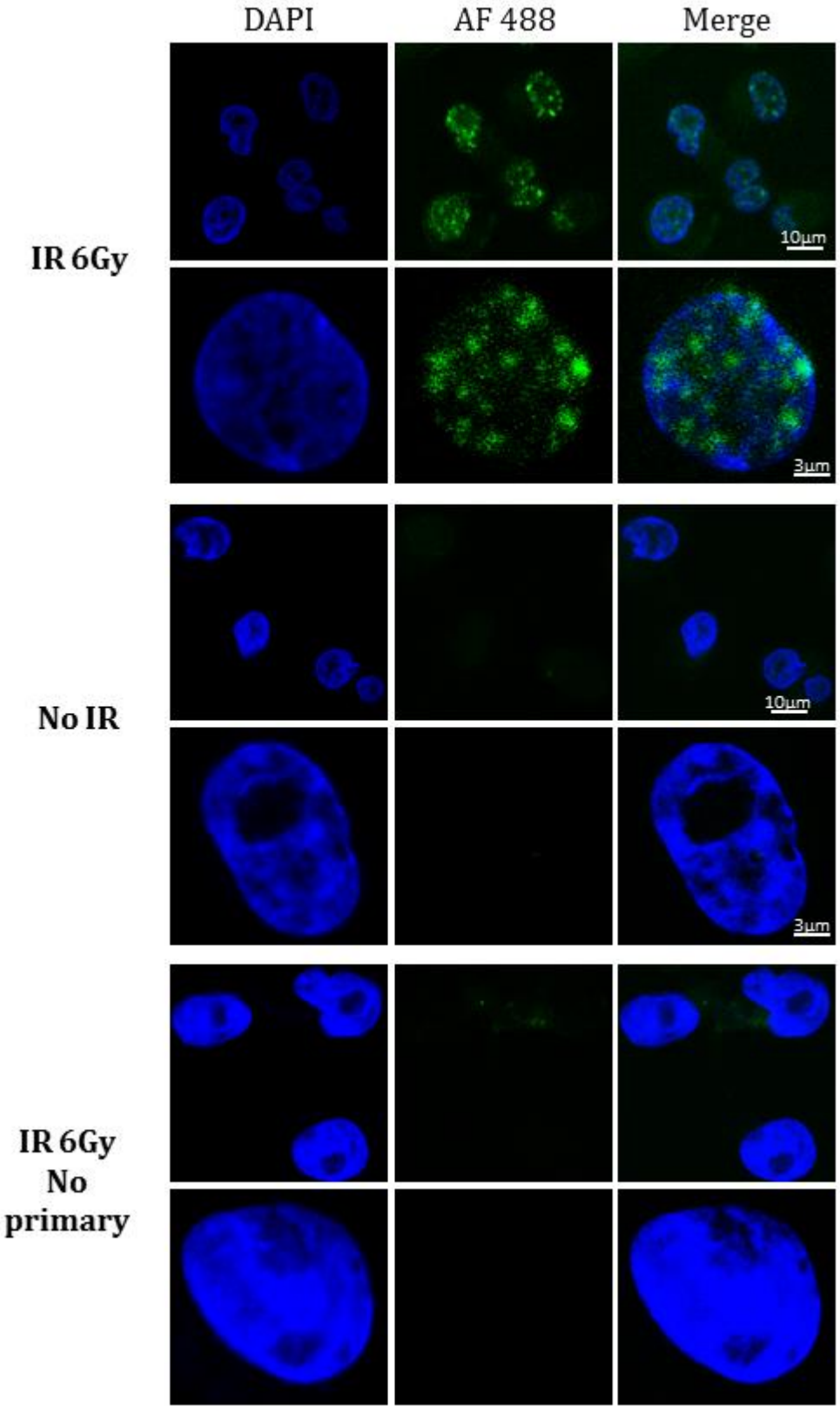
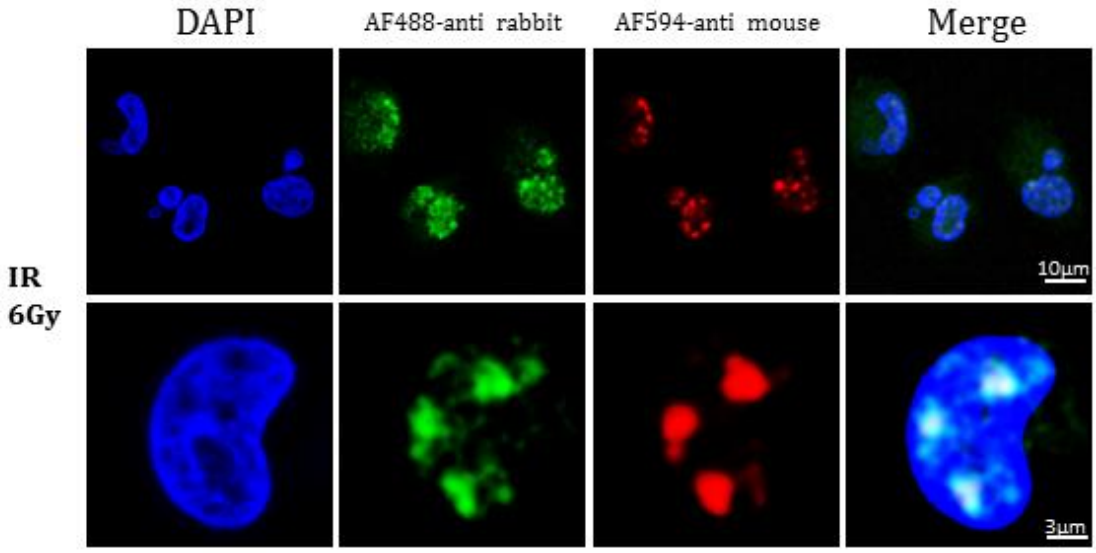


Figure 4.10 Immunocytochemistry demonstrating co-localisation of anti-γH2AX Fab-Tat-DTPA (visualised by AlexaFluor 488 (AF488)-conjugated anti-rabbit heavy and light chain secondary antibody) with a monoclonal mouse anti-γH2AX antibody (visualised by AlexaFluor594 (AF594)-conjugated anti-mouse secondary antibody) at foci 1 hour after irradiation (6Gy) in H2N cells.



4.3.6. Anti-γH2AX Fab-Tat internalises into H2N cells

After 3 hours incubation, 2.5-3.0% of anti-γH2AX Fab-Tat was internalised into H2N cells, and the proportion was, as expected, unaffected by irradiation of cells ($p=0.72$, Student's unpaired t test, two-tailed, see Figure 4.11).

All Tat-containing probes achieved around 3% internalisation compared with around 1% for non-Tat-containing probes. Irradiation of cells made no statistically significant difference to the extent of internalisation at 3 hours in either case (see Figure 4.12).

Figure 4.11 Radioassay demonstrating internalisation of ^{123}I-labelled Tat- and non Tat-conjugated probes into live H2N cells either unirradiated, or irradiated to 6Gy 15 minutes before addition of probe to growth medium. Mean and standard error of mean internal activity are shown from three replicates in each of three independent repeat experiments and data are fitted to a single phase exponential association model.

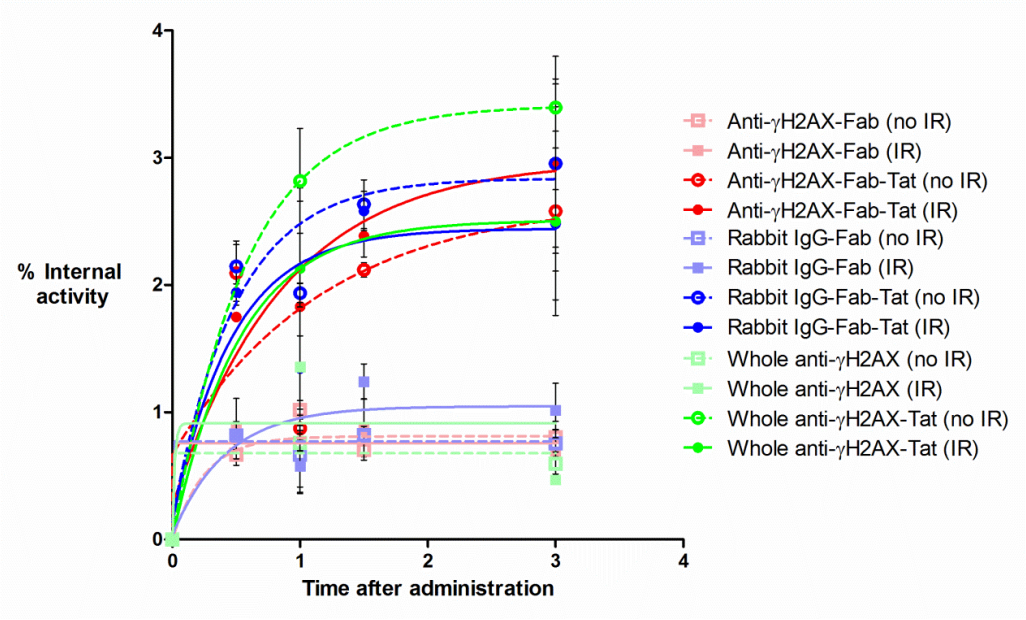
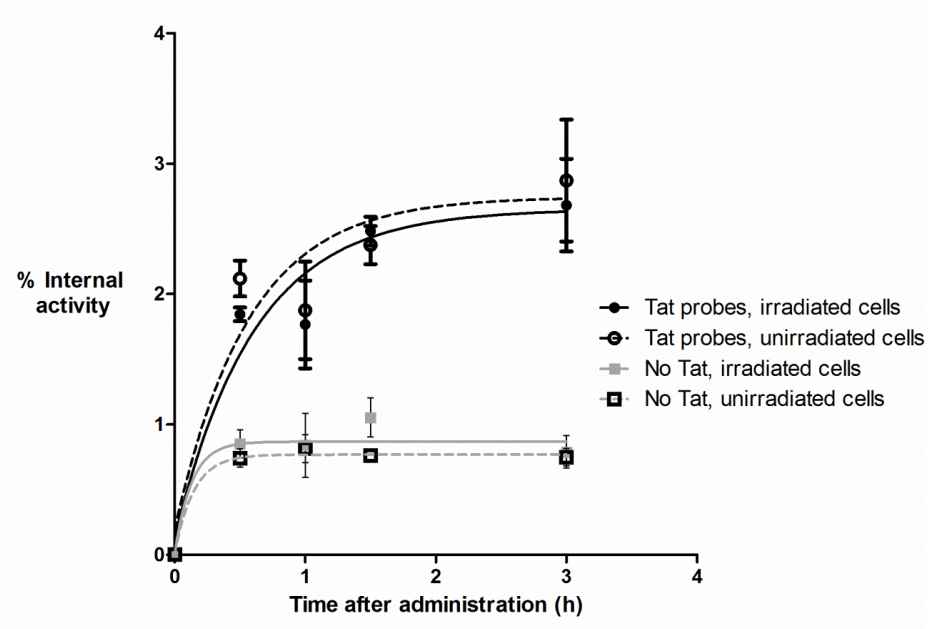


Figure 4.12 Summary data from the same experiments as shown in Figure 4.11 divided by Tat conjugation of probe and irradiation of cells. Internal activity at 3 hours did not differ significantly between assays in irradiated and unirradiated cells (p=0.8587) but did differ between Tat conjugated and non tat conjugated probes (p<0.0001, both by Student's unpaired t test, two tailed)



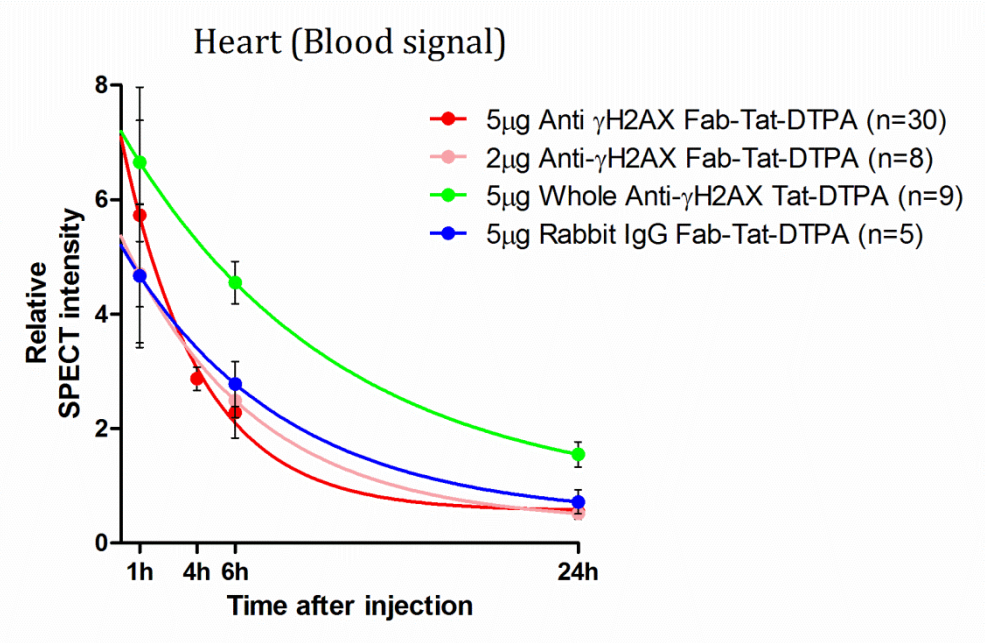
4.3.7. SPECT imaging using Anti-γH2AX Fab-Tat-DTPA and control probes – blood clearance and normal tissues

Maximal γH2AX induction occurs at 30-60 minutes after irradiation in tumour cells *in vitro*[107, 127] and normal tissues *in vivo*[129, 130, 250]. Radiopharmaceutical injection was therefore timed for 1 hour after xenograft irradiation (with the exception of a single experiment in which injection was delayed until 4 hours post irradiation in an attempt to improve the tumour-to-background accumulation ratio(n=4)). Pharmacokinetic and biodistribution data for normal tissues are analysed according to probe identity only (*i.e.* pooled for flank-irradiated and unirradiated animals).

Controls for the *in vivo* experiments included whole anti-γH2AX-Tat-DTPA, and a non-specific rabbit IgG Fab-Tat-DTPA probe of similar size to the experimental probe. The mass amount of administered probe was 5 μg. To investigate the influence of the quantity of injected probe on specific binding, 2 μg was used for one experiment.

The half-life for anti-γH2AX Fab-Tat-DTPA clearance was significantly shorter than for whole anti-γH2AX-Tat-DTPA (2.9 hours (95%CI 2.3-3.8) vs. 7.8 hours (95%CI 2.3-3.8), p= 0.003 by F test from non-linear regression – see Figure 4.13.

Figure 4.13 Blood pharmacokinetics of ^{111}In labelled anti-yH2AX Fab-Tat-DTPA and control SPECT probes calculated by quantification of heart regions of interest on serial SPECT scans. Mean SPECT signal intensity normalised for administered radioactivity ± standard deviation are plotted and fitted to a one phase exponential decay (R^2 0.84-0.95).

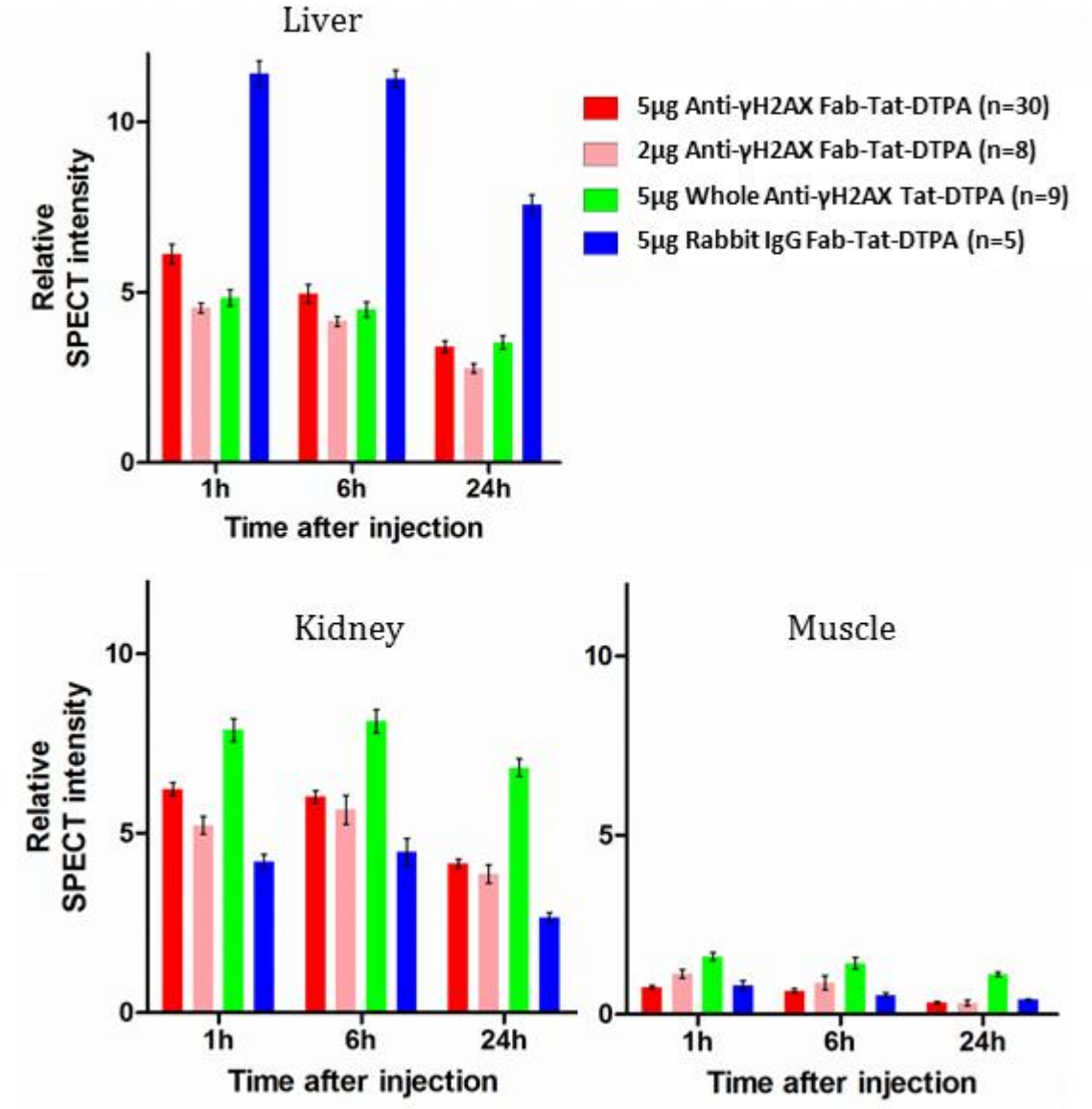


For liver, kidney and unirradiated muscle, SPECT signal for each control condition was compared to that from 5 μg anti-γH2AX Fab-Tat-DTPA using Student's t test at each image time – see Figure 4.14. In the liver, only rabbit IgG Fab-Tat-DTPA showed significantly different uptake, showing much higher binding (p=0.0135). In particular there was no indication that excision of the Fc antibody tail had reduced liver sequestration of the Fab probe compared to whole antibody.

In the kidney, the whole antibody probe had significantly higher (p= 0.0186) and the rabbit IgG Fab significantly lower (p=0.0094) signal than anti-γH2AX Fab-Tat-DTPA. The former result might be expected as larger molecules might accumulate in the kidney. The latter may be a consequence of the massive liver sequestration of rabbit IgG Fab.

Muscle signal was much lower than for other organs, and significantly higher with 5 μg whole anti-γH2AX-Tat-DTPA probe than 5 μg anti-γH2AX Fab-Tat-DTPA ($p=0.0009$). Due to its slower clearance, the whole antibody probe was present in higher quantity at all timepoints. Muscle to blood signal ratio did not differ significantly between the probes ($p=0.109$) despite probable induction of γH2AX within irradiated muscle.

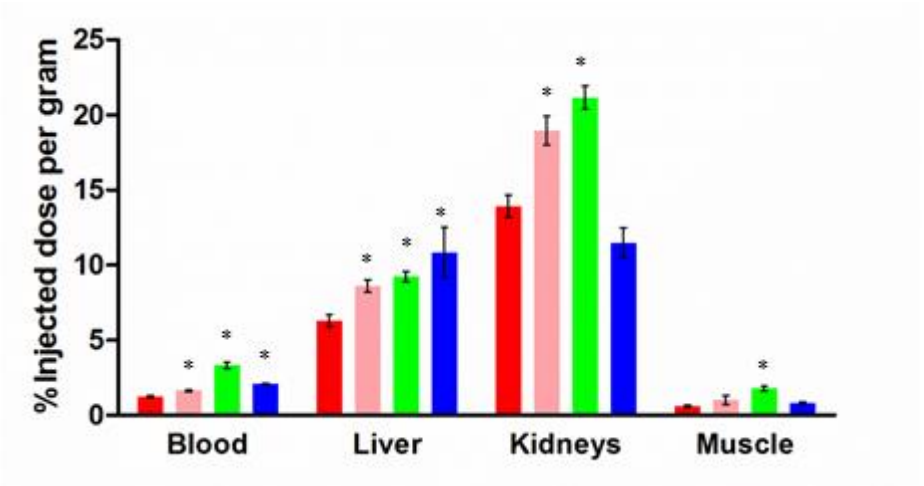
Figure 4.14 Normal tissue pharmacokinetics of anti-γH2AX Fab-Tat-DTPA and control SPECT probes calculated by quantification of regions of interest on serial SPECT scans. Mean SPECT signal intensity normalised for administered radioactivity and standard error of the mean are plotted. For statistical tests see main text.



Direct organ biodistribution data at 24 hours was available from direct excision of tumours and normal tissues at the conclusion of the imaging experiments. For organs where comparison could be made to SPECT data (see Figure 4.15), trends were broadly similar. In the liver, the %ID/g was statistically significantly higher

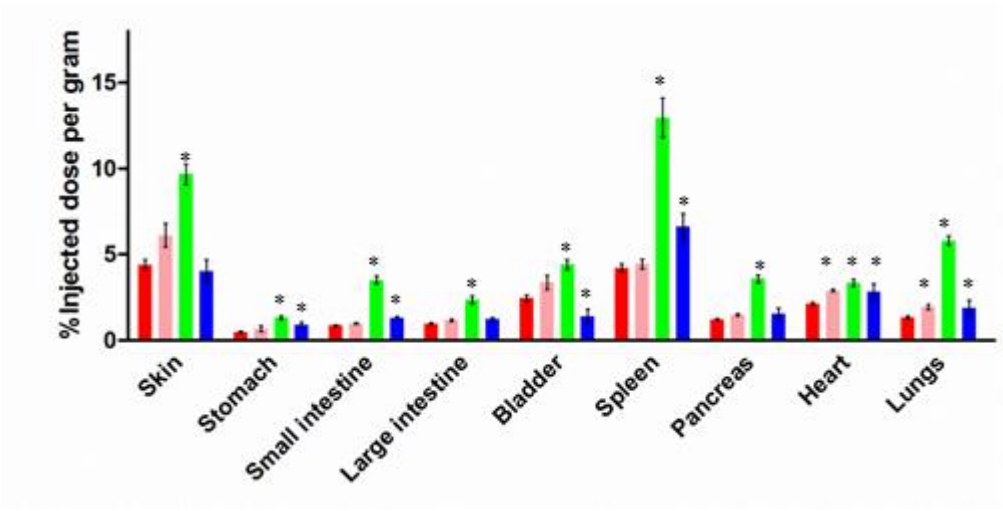
for all conditions when compared to 5 μg anti-γH2AX Fab-Tat-DTPA, but remained highest for rabbit IgG Fab-Tat-DTPA.

Figure 4.15 Biodistribution of imaging probes by dissection at 24 hours post-injection (organs comparable to SPECT signal intensity data). Legend as for Figure 4.13. For each organ, %injected dose per gram ± standard error of the mean are plotted and are compared between control conditions and 5 μg anti-γH2AX Fab-Tat-DTPA by Student's unpaired t test. Statistically significant results ($p<0.05$) are indicated by an asterisk (*).



Data from all harvested organs was available and is presented in Figure 4.16. In keeping with the reduced clearance of whole anti-γH2AX Fab-Tat-DTPA, the remaining organ uptake is highest with this probe at 24 hours after injection in all organs. High spleen activity may partly be explained by the tendency of free indium that dissociates from radiopharmaceuticals *in vivo* to accumulate in the organ.

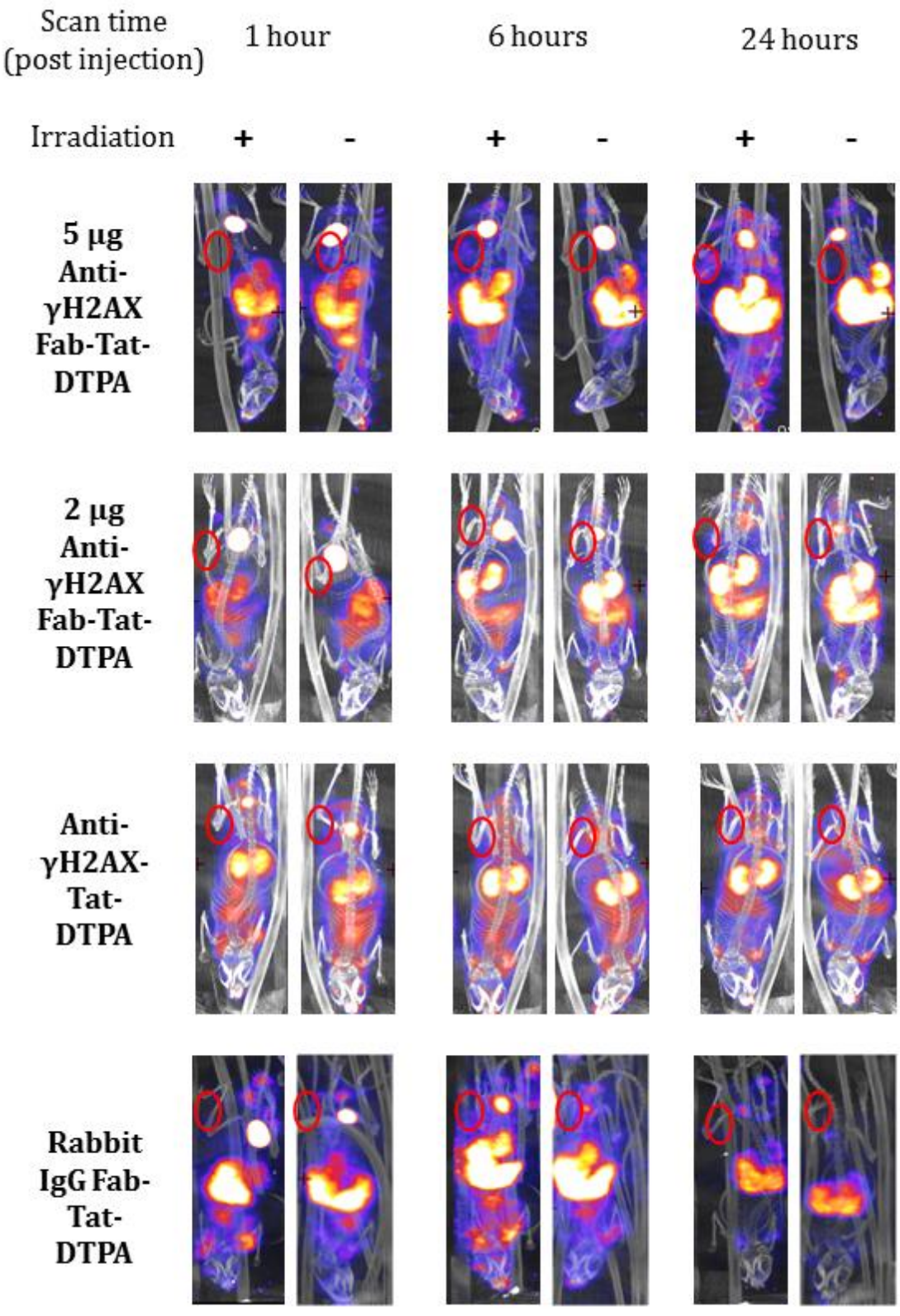
Figure 4.16 Biodistribution of imaging probes by dissection at 24 hours post-injection (for organs not shown in Figure 4.14). Plot and statistics as for Figure 4.14. Legend as for Figure 4.13.



4.3.8. SPECT imaging using anti-γH2AX Fab-Tat-DTPA and control probes – tumour and irradiated muscle

This novel imaging agent was designed to image DNA damage, such as that caused by irradiation, in tumours. The performance of anti-γH2AX Fab-Tat-DTPA as a functional imaging agent was assessed by quantification of SPECT intensity in tumour and regions of interest (illustrated in Figure 4.17, quantification in Figure 4.18), and biodistribution data from dissection at 24 hours post injection (Figure 4.19).

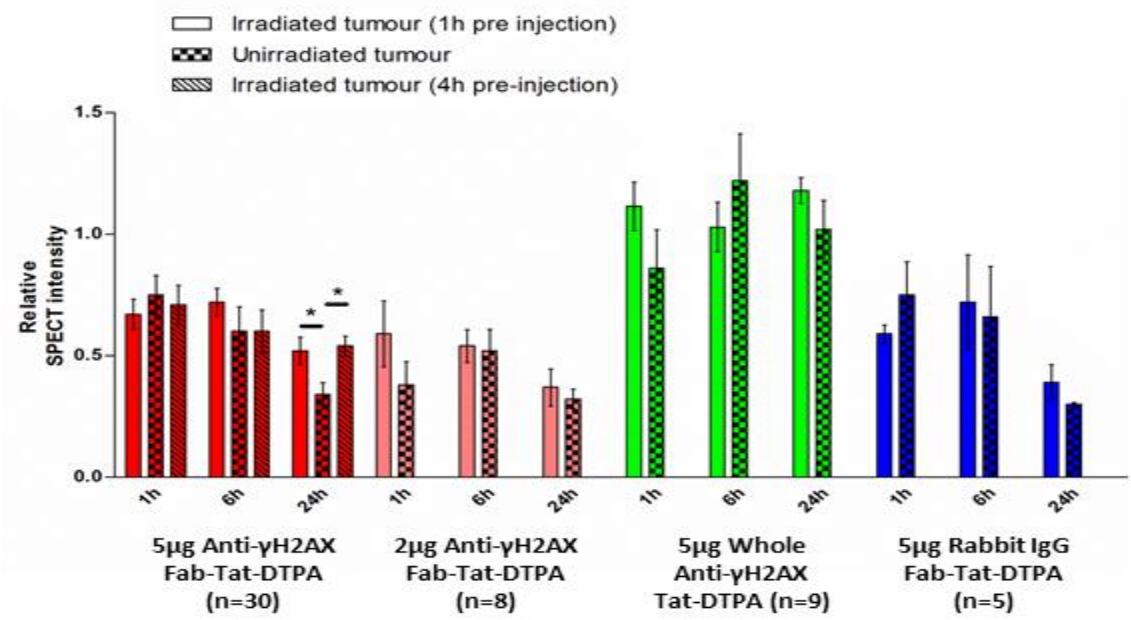
Figure 4.17 Maximal intensity projection SPECT/CT images obtained at 1,6 and 24 hours after tail vein injection anti–γH2AX Fab-Tat-DTPA (5 µg and 2 µg), whole antibody anti-γH2AX-Tat-DTPA (5 µg) and rabbit IgG Fab-Tat-DTPA (5 µg). Tumour regions are highlighted in red. All images at each scan time are normalised to optimise display.



For SPECT quantification, no significant difference was seen between the tumour region of interest signal from 5μg anti-γH2AX Fab-Tat-DTPA in irradiated or unirradiated tumours at 1 or 6 hours post probe injection. Two alternative schedules, involving tumour irradiation 1 or 4 hours before injection, showed similar results. At 24 hours, however, there was a statistically significantly higher signal in irradiated tumours than unirradiated tumours. Mean relative SPECT signal in irradiated tumour regions of interest was 1.5 fold higher for the 1 hour schedule ($p=0.0277$) and 1.6 fold higher for the 4 hour schedule ($p=0.0342$, both by unpaired two-tailed t test).

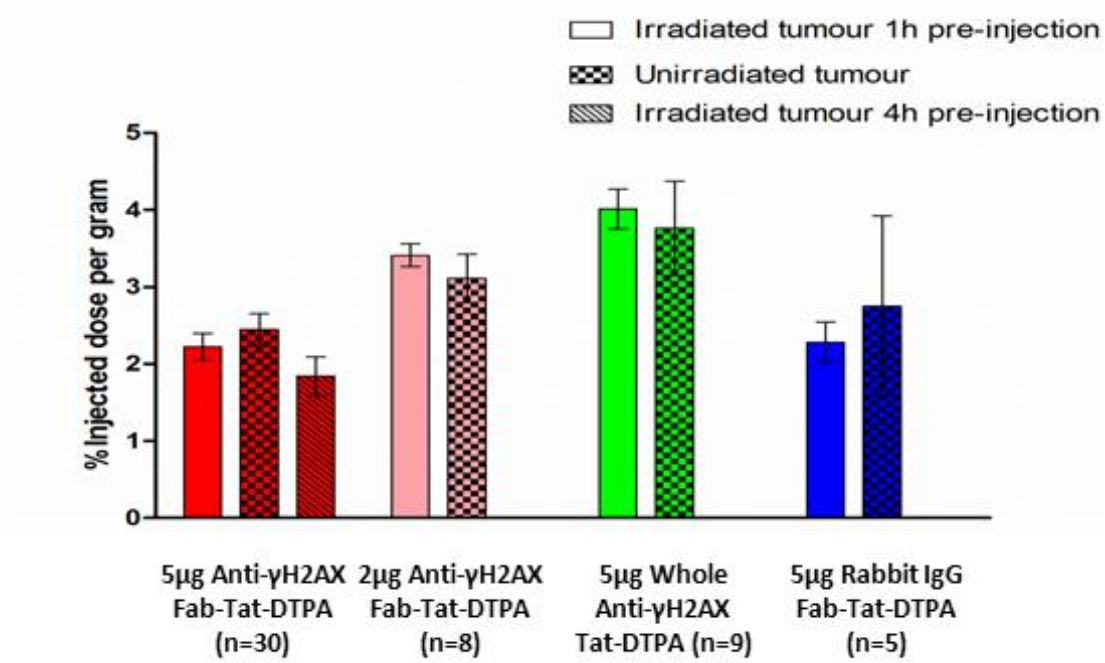
There were no statistically significant differences between probe signals from 2 μg anti-γH2AX Fab-Tat-DTPA, 5μg rabbit IgG Fab-Tat-DTPA or 5μg whole anti-γH2AX-Tat-DTPA in irradiated and unirradiated tumours. (Only a schedule of irradiation 1 hour before probe injection was tested.)

Figure 4.18 Relative SPECT intensity in tumour regions of interest at 1, 6 and 24h post injection in mice either unirradiated, irradiated 1h pre-injection or irradiated 4h pre injection. Mean and standard error of mean relative SPECT signal intensity are plotted. All measurements in irradiated tumours were compared to the reference unirradiated tumour signal for the same drug and timepoint by unpaired two tailed t tests. Statistically significant differences (*i.e.* p<0.05) are indicated with an asterisk(*).



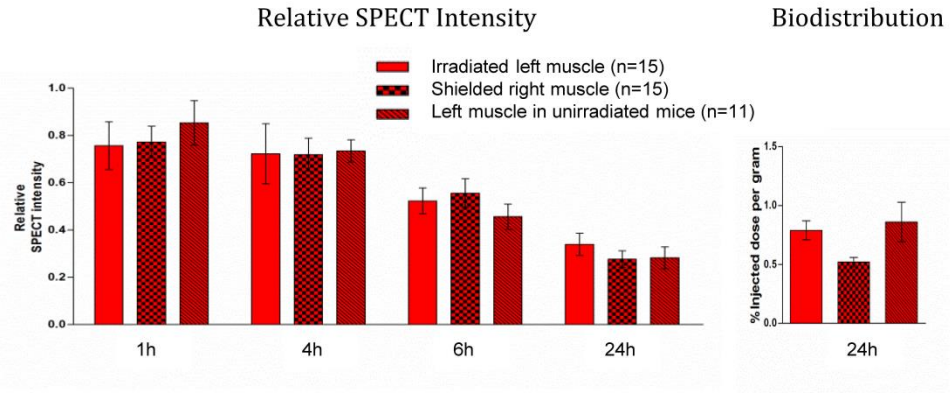
Biodistribution data at 24 hours post-injection did not demonstrate any statistically significant differences between the accumulation of radioactivity in irradiated and unirradiated tumours. In particular, despite dissections occurring directly after the SPECT scans in which signal differences were demonstrated (see above), no statistically different total activity was identified between irradiated and unirradiated tumours in animals injected with the anti-γH2AX Fab-Tat-DTPA probe. This casts doubt on the significance of the small but statistically significant imaging signal difference discussed above.

Figure 4.19 Excised tumour xenograft activity at 24h expressed as %injected dose per gram. Student's unpaired t test was performed by irradiation condition for each imaging probe. No statistically significant ($p<0.05$) differences were shown.



Since only the left, xenograft-containing flank of the mouse was irradiated, hind thigh muscle SPECT signal and probe biodistribution could be compared both with the shielded right hind thigh muscle in these mice, and with left hind thigh in unirradiated control mice. Relative SPECT signal and biodistribution data for 5µg anti-γH2AX Fab-Tat-DTPA only are shown in Figure 4.20. No statistically significant increase in probe retention was demonstrated in irradiated versus unirradiated mice.

Figure 4.20 Relative SPECT intensity in muscle at 1, 4, 6 and 24h post injection and biodistribution at 24h of 5μg anti-γH2AX Fab-Tat-DTPA in mice. Mean and standard error of mean are plotted. Measurements in irradiated left muscles were compared to shielded right muscles by paired two-tailed t test and to left muscles in unirradiated mice by unpaired two-tailed t test at each image time. No statistically significant differences (*i.e.* p<0.05) were shown.



4.4. Discussion

4.4.1. Synthesis of probes

Papain digestion is a quick, cheap method of producing Fab fragments from rabbit antibodies, and is known to produce a major fragment of 35-40kDa in addition to minor fragments[251] as seen in these results. Carbodiimide crosslinking is sensitive to protein concentration as well as the molar excess of EDC and sNHS.[252] The absolute mean conjugation yield depends on the number and accessibility of reactive groups (carboxyl on Tat peptide and amine on Fab fragment) as well as the molar excess of Tat to Fab. In the absence of other published work detailing Fab-Tat conjugation, the absolute yield (mean 3.52 Tat per Fab) is difficult to assess. Before optimisation commenced, a target of 3-4 Tat per Fab was set representing a compromise between high Tat content mediating cellular and nuclear import and the potential for disruption of the antigen-binding site on the Fab molecule. This was the strategy employed in the development of the whole antibody anti-γH2AX-Tat SPECT probe.[208]

The difficulties in conjugating isothiocyanate benzyl DTPA to Fab-Tat and even naked Fab were unexpected. The methods for such conjugation to whole antibodies are well established [247, 253-256] and have been reported successfully with smaller peptides such as recombinant Epidermal Growth Factor. [257] The formation of thiourea bonds depends on the availability of lysine groups on the Fab molecule, just as for the ultimately successful cyclic DTPA anhydride conjugation chemistry. Benzyl-DTPA is a larger molecule than cyclic DTPA and might have been subject to more steric hindrance. It might also have been more subject to hydrolysis. Hydrolysis may also explain the apparent sensitivity of the reaction to absolute concentration.

Target specificity of the probe is an important consideration, especially as the monovalent Fab fragments are expected to bind its antigen target with less avidity than a bivalent whole antibody.[258] Attempts were made to develop a biochemical competitive binding assay. When developed for imaging applications, these are usually intact cell-based assays for binding of probes to extracellular epitopes. It was not possible to develop such as assay successfully for intracellular (indeed intranuclear) γH2AX in fixed cells. In another strategy, irradiated cell lysate was used in an attempt to develop an enzyme-linked immunosorbant assay (ELISA). The lack of availability of purified γH2AX epitope prevented the development of a specific ELISA. Immunocytochemical evidence of antigen-binding was therefore sought, and provided qualitative evidence that probe-target interaction had been preserved.

Imaging of intracellular targets represents an enormous potential expansion in the information available by non-invasive methods. The largest barrier to that

expansion is the physical barrier of the cell membrane. Tat-mediated transport of the imaging probe macromolecule across cell and nuclear membranes is critical to probe function. Cell-penetrating peptides are not specific to cell type, but do mediate transport out of the cell of probe molecules that are not retained by specific probe-target interaction. The proportion of activity internalised *in vitro* using these probes (~3%) is comparable to the 4-5% reported for Tat- and indium-labelled whole antibodies developed for imaging applications.[244] Internalisation *in vivo* has not been assessed in this or previous studies of Tat as a cell penetrating peptide. It would be expected to depend on the pharmacokinetics of probe accumulation and clearance from the target cell microenvironment, parameters that are difficult to assess empirically. Specific retention of probe in irradiated (*i.e.* γH2AX-rich) areas would provide circumstantial evidence of *in vivo* probe internalisation, evidence that can only be assessed by interrogation of *in vivo* SPECT data.

4.4.2. *In vivo* SPECT imaging

The rationale for the development of a Fab-fragment based imaging probe was that compared to a whole antibody probe, it would be cleared more quickly (in order to allow short lived damage such as that in normal tissues to be demonstrated), have reduced liver uptake (due to absence of the Fc tail) and improved tumour penetration.

The Fab-fragment based probes were indeed cleared more quickly from the circulation than a whole antibody probe. Liver uptake, as assessed by SPECT signal over 24 hours was not reduced, however, although in biodistribution studies it was slightly lower with 5 μg of the specific Fab probe (6.3 vs. 9.3%). It is not clear

why 2 μg per animal of the same probe resulted in proportionally greater liver accumulation. The binding mediating liver sequestration may have been stronger than that within the tumour or other organs. A saturable mechanism would have resulted in a higher proportion of the 2 μg being sequestrated than for 5 μg. Of the probes investigated the polyclonal rabbit IgG Fab-Tat-DTPA control accumulated most in the liver, as might be expected since it would bind to a wide range of epitopes. In a comparable study in nude mice over 3 days, a Fab probe showed less than half the accumulation of a whole antibody probe (7.3 vs. 3%).[259] All proteins accumulate in the liver to a greater or lesser degree. For these complex constructs involving Tat peptides as well as DTPA molecules, presence of the Fc tail does not appear to determine liver binding.

Kidney accumulation was higher with the whole antibody than with Fab-based probes and this was expected since whole antibody molecules would be more likely to collect in the glomeruli and tubules.

In calculating normal tissue pharmacokinetics and biodistribution, it has been assumed that hind quarter irradiation does not affect probe behaviour in unirradiated areas. This is likely to be justified since the proportion of SPECT signal uptake in tumour and muscle areas is very small compared to blood background, liver, kidney and most other organs. It should be noted, however, that tumour irradiation *in vivo* has been associated with abscopal effects on γH2AX, particularly in gastrointestinal tissues.[260]

The most important results on which to judge the performance of the probe in regard to this thesis are those relating to the SPECT signal and accumulation in tumours according to conditions of irradiation. Unfortunately the probe does not

perform well. There was a small, if statistically significant, difference between the SPECT signal intensity in irradiated compared to unirradiated tumours at 24 hours post injection. There are a number of limitations to the conclusion that the probe identifies DNA damage in the tumour. The most serious of these is that the result was not confirmed by biodistribution analysis, which was carried out directly after the 24 hour SPECT scan. Tumour regions of interest identified on fused SPECT/CT images may not correlate perfectly with the anatomical tumour entity identified at dissection. Tumour xenografts are heterogeneous, and it may be that areas of the tumour with low signal due to poor perfusion and/or retention of the imaging agent are not identified within the tumour region of interest.

The result at 24 hours was not replicated at earlier times, despite rapid clearance of the anti-γH2AX Fab-Tat-DTPA. It was also not seen with an administered dose of 2 μg of the probe, perhaps because proportionally more of this probe was sequestered in the liver (see above). The whole antibody anti-γH2AX-Tat-DTPA probe showed no difference between irradiated and unirradiated tumours at 24 hours in this set of experiments, despite several previous experiments that consistently showed this difference with the same probe.[261] The results presented in this chapter could be viewed as a failure of the positive control in this experiment, although an investigation of the ability to detect a functional state with a novel imaging probe would often not have an available positive control.[262] The non-specific rabbit IgG Fab-Tat-DTPA probe provides a similar-sized control for non-specific enhanced permeability and retention (EPR) of macromolecules described in tumour xenografts.[263] However it is limited as such a control by its

very marked liver sequestration, which may have altered its distribution elsewhere in the animal.

If it were safe to conclude that SPECT signal from anti-γH2AX Fab-Tat-DTPA is 1.5-1.6 fold higher in tumours irradiated to 10 Gy would this represent a useful tool? Despite a radiation dose well in excess of most clinical doses, the ratio of signal is modest. The most widely used nuclear medicine functional imaging modality in oncology practice is ^{18}Fluorodeoxyglucose-PET (FDG-PET) in which the standardised uptake value (SUV) is a ratio of the signal in an index region to the average signal across the body. A ratio of at least 2.5 has proved a clinically useful benchmark, for example in distinguishing benign from malignant pulmonary nodules.[264] Given the heterogeneity of tumour composition and dose deposition, detection of differences in tumour response that are much more subtle than those in this crude model are likely to be beyond the sensitivity of this method.

Since muscle tissue was necessarily irradiated during xenograft irradiation, some normal tissue imaging data were available. There was no evidence that irradiation-induced damage in muscle DNA could be imaged by the probe. Nuclei make up only a very small proportion of muscle bulk, limiting the potential for a differential signal. In addition, DNA repair-proficient normal cells maintain the γH2AX target for shorter times than is the case for tumours,[119] and the blood background is still high in the first few hours after injection and irradiation.

The other major approach to imaging radiation-induced cell damage has been the quantification of apoptosis using probes based on annexin-V, a 36kDa protein that binds to phosphatidylserine externalised during apoptosis. [265] In a mouse lymphoma model 1.7-2.3 fold higher scintigraphy imaging signals were seen in

tumours treated up to 8Gy compared to unirradiated controls, with up to 2.2 fold higher activity by dissection.[266] These figures compare favourably with the data presented for anti-γH2AX Fab-Tat-DTPA, and importantly the imaging data is reinforced by biodistribution studies. However the radiosensitive lymphoma model may differ from the breast cancer model employed here, and the authors were unable to replicate their results in a sarcoma model. Clinical utility of the annexin-V probes is limited by liver, spleen and kidney uptake.[267]

4.4.3. Conclusion

The goal of imaging the effects of radiation on tumours and normal tissues continues to generate interest. [268, 269] At least in this breast cancer xenograft model in nude mice, the probe has significant liver accumulation despite the lack of an Fc tail; it does not show demonstrate early differences in γH2AX between irradiated and unirradiated muscle tissue despite fast blood clearance; it does not unequivocally show differences in tumour DNA damage after irradiation. Clinical translation of anti-γH2AX Fab-Tat-DTPA would require re-engineering with a human or humanised antibody to ensure compatibility with an immunocompetent patient. Such an investment of time and money is not currently justified by the data presented here.

Chapter 5

Discussion

Chapter 5: Discussion

5.1. γH2AX is a candidate clinical biomarker

Post-translational protein modifications are attractive potential markers of cellular activity. They can be rapid, can result in novel epitopes for immunoassay, and cells can amplify the modification or indeed reverse it through control of modification enzymes.[270] The formation of γH2AX by the phosphorylation of the histone H2AX in response to DNA double strand breaks demonstrates all these attributes, making it an attractive biomarker candidate.[271] This thesis has explored translational assays to apply γH2AX measurements as clinical biomarkers of the response to anti-cancer treatments.

5.2. γH2AX immunohistochemistry in tumour tissue

Tissue immunohistochemistry provides the most direct visualisation of a molecular target of interest, at a microscopic scale and in the context of the microenvironment. The technique is a cornerstone of translational research, particularly when applied to the formalin fixed, paraffin embedded tissue that is a worldwide standard of clinical sample preservation. γH2AX immunohistochemistry in human tumour FFPE tissue has been used in studies published during the period of preparation of this thesis, addressing pre-malignant change in gynaecological cancers[169, 170, 272, 273] and melanoma[168], and prognosis in breast cancer.[274]

This thesis confirms the applicability of γH2AX as a correlate of dose in preclinical tumour models. There is much scope to characterise the γH2AX response in tissues using such models. It would be interesting to examine perturbations of the tissue

microenvironment which are difficult to model in the cytological models of γH2AX induction and repair. Dynamics of the appearance and disappearance of γH2AX continue to be analysed and modelled by immunocytochemistry and normal tissue immunohistochemistry,[130, 275] but a whole-tissue approach in tumours might yield complementary information. This thesis maintained a focus on potentially translatable assays.

The application of γH2AX tissue immunohistochemistry as a clinical biomarker of response to DNA-damaging anticancer therapies is not straightforward. Tumour resection or substantial core biopsy is unusual shortly after the delivery of therapies including ionising radiation and cytotoxic chemotherapy. Tissue collection in such circumstances would be difficult as part of a clinical trial (although it has been achieved on a small scale)[123, 180] and is difficult to envisage as part of routine cancer care. The timing of the DNA damage event in relation to tissue fixation is crucial to the interpretation of the amount of γH2AX demonstrated, for example in archived tissue bank specimens. This timing may be impossible to determine in the case of systemic therapy. Even for ionising radiation, accurate times of radiation delivery and sample fixation may not be recorded.

A clinical situation in which radiotherapy is delivered prior to tissue collection is the use of "short course" (typically 25 Gy in 5 daily fractions) pre-operative irradiation in the week before surgical resection of rectal adenocarcinoma.[276] After work presented below raised questions about the persistence of γH2AX foci in the days after irradiation, a study was initiated to examine archived operative specimens in patients who had received pre-operative radiotherapy. This ongoing

study employs the immunohistochemical methods developed in Chapter 2 of this thesis.

5.3. A novel FNA assay for γH2AX

Repeated biopsies are potentially hazardous and uncomfortable for the patient, hence the interest in developing a minimally invasive assay of γH2AX in tumour cells. Fine needle aspiration (FNA) represents such an opportunity, and the DSB Biomarkers Pilot Study succeeded in developing a γH2AX assay in FNA specimens. The potential applications of the technique in biomarker studies have been recognised,[222] however it is only useful for tumours that are accessible to needles. The study could only be offered to patients with palpable tumours, which probably contributed to the slow rate of recruitment. If clinically useful, an FNA-based assay might be extended to tumours accessible using endoscopic or radiological guidance. The use of automated foci counting introduces standardisation and high throughput, both important considerations in clinical workflow.

While FNA is minimally invasive, it also results in a very small sample, so that random error across a heterogeneous tumour might mask genuine differences in biomarker quantification. The coefficient of variation (CV) across all samples was 49%, and may be due to tumour heterogeneity or to technical imperfection. While differences between pre- and post-irradiation γH2AX foci counts were of the order of 400%, the γH2AX biomarker is likely to be clinically useful only if it can detect much smaller differences in DNA damage in response to treatment. In the immunohistochemistry data in Chapter 2, the assay signal between 1Gy and 2Gy differs by 53%, so that an assay with a CV of 49% would not be able to reliably detect this difference. This CV is however based on a very small number of patients

with diverse tumour types and treatments, and the assay might perform more reliably in a more homogeneous population.

The ability simply to detect whether tumours have been irradiated is unlikely to be clinically useful. The assay might have application as a biomarker of response to systemic treatments that are expected to cause DNA double strand breaks. This might be relevant for chemotherapy drugs (such as topoisomerase inhibitors) and for targeted radiotherapy agents. The assay developed in Chapter 3 is included in the protocol for a Phase 1 trial of ^{111}Indium-DTPA-hEGF, a novel nuclear medicine drug targeting EGFR-overexpressing malignancies.[277] The assay will be used to confirm and potentially to quantify the drug-tumour interaction, which relies on the delivery of very short range Auger electrons to the vicinity of the DNA. The biomarker here measures the fundamental mechanism underlying the drug's effect.

Data from one patient in the DSB Biomarkers Study (DSB10, see Chapter 3) indicated the presence of large numbers of γH2AX foci, co-localised with 53BP1, seven days after irradiation. This is a novel and surprising observation, and invites comparisons with the large numbers of foci seen in tumour xenograft immunohistochemistry experiments in Chapter 2. The clinical data have not been replicated, partly as the patient underwent an unusual radiotherapy fractionation, but do provide at least anecdotal evidence of the phenomenon of late residual foci.[133, 217, 232, 278, 279] In fact it is not clear whether these foci are "residual" after initial induction in the hours after irradiation, or whether they are the result of a second, later wave of γH2AX induction.[209] Tumour xenograft immunohistochemistry also showed more foci at 7 days than at 4 days after

irradiation, reinforcing the argument that future characterisation of the phenomenon may be informative. It may be that these represent senescent cells,[219] a hypothesis that could be tested experimentally both in the xenograft model and in extension of the FNA assay.

5.4. In vivo imaging of γH2AX

An ideal clinical biomarker assay for γH2AX would be non-invasive, quantitative, repeatable, reliable and accurate. A nuclear imaging agent to demonstrate γH2AX using clinically available SPECT or PET modalities could meet these criteria. The principle of whole antibody-based imaging of DNA damage has been established in a preclinical SPECT model,[261] and further refinement of this technique was explored in Chapter 4. Due to the poor pharmacokinetics of whole antibodies for imaging *in vivo*, techniques for antigen binding with smaller molecules such as designed ankyrin repeat proteins (DARPins), single chain variable fragments, affibodies, $F(ab')_2$ and Fab fragments have been investigated for other targets.[280] Readily available enzymes were used to pursue the latter approach for this thesis.

The Fab fragment of the γH2AX antibody was cleared faster than the whole antibody *in vivo*, had lower kidney accumulation and somewhat lower liver accumulation. However, its imaging performance for DNA damage in tumours was limited, probably by the decreased specificity of the univalent construct for the target. This conclusion is limited, however, by the absence of a biochemical competitive inhibition assay for γH2AX. In future development, perhaps with smaller molecules, the maintenance of target specificity, and robust methods to measure that specificity, will be important.

5.5. Taking γH2AX assays into the clinic

Understanding the role of γH2AX is critical to the clinical application of γH2AX assays. The dynamic role it takes in cancer cells in response to therapies that induce DNA double strand breaks means that it could be a quantitative measure of DNA damage. However it is an early member of the DNA repair response, and successful repair will reverse the expected clinical consequence of DNA damage *i.e.* cell death. A reliable assay would first need to be applied to understand more of this dynamic process in real cancers, before hypotheses could be formed about the relationship of γH2AX measurements to clinical outcomes.

The presence of significant numbers of γH2AX foci several days after a DNA damage event have been described in this thesis both in a preclinical xenograft model and in fine needle aspirate samples from a lung cancer patient. These findings (discussed above in Section 5.3) further complicate the interpretation of an assay measurement of γH2AX taken at a particular time. Further investigation of these findings is required, but it may be that γH2AX contributes to the reaction of tumours in the days after therapy, and that γH2AX assays can be used to follow that reaction.

A non-invasive γH2AX imaging technology could theoretically provide useful dynamic information over hours or days during or after treatment with an anticancer therapy.

The reliability (or repeatability) of any clinical assay would first need to be established, and this was the primary objective of the DSB Biomarkers Pilot Study. This study pragmatically recruited patients with all tumour types, but a particular tumour and treatment type might be pursued, for instance in the context of a

clinical trial. Trials of agents that modulate the DNA damage response (such as PARP inhibitors) might expect to use γH2AX as a pharmacodynamic biomarker. As such, it may also relate to clinical response.

For tissue-based assays, practical quality measures such as stability over time, storage and transport conditions are determined. Imaging biomarkers have analogous quality and standardisation parameters to be considered.

A successfully validated assay might be used early in radical radiotherapy courses (such as in cervical and head and neck cancers) as a biomarker of later response, or during neoadjuvant treatment (such as pre-operative rectal cancer treatment) to ensure that the delay in definitive treatment is justified. To the physical isodose plan produced during the planning of external beam radiotherapy, the assay (and an imaging agent in particular) would provide spatial biological feedback about the effectiveness of the physical doses delivered.

Without the tools to measure γH2AX in the clinic, its utility as a biomarker is impossible to gauge. This thesis has explored potential tools, but has not established a clear lead method. It has added to the growing body of evidence that γH2AX is relevant in cancers, encouraging the further development towards the right clinical biomarker technology.

Bibliography

1. Ferlay J SH, Bray F, Forman D, Mathers C and Parkin DM. GLOBOCAN 2008 v1.2. Cancer Incidence and Mortality Worldwide: IARC CancerBase[Internet]. 2010 ed. Lyon, France: International Agency for Research on Cancer; 2010.

2. 2008-2013 Action plan for the global strategy for the prevention and control of noncommunicable diseases. Geneva, Switzerland: World Health Organisation; 2008.

3. Tobias J, Hochhauser D, editors. Cancer and Its Management. 6th ed. London: John Wiley & Sons; 2010.

4. Sobin L, Gospodarowicz M, Wittekind C, editors. TNM classification of malignant tumors. 7th ed. Oxford: Wiley-Blackwell; 2009.

5. van der Kogel A, Joiner M. Basic Clinical Radiobiology: Oxford University Press, USA; 2009.

6. The timely delivery of radical radiotherapy: standards and guidelines for the management of scheduled interruptions London: Royal College of Radiologists; 2008.

7. Bayraktar UD, Chen E, Bayraktar S, Sands LR, Marchetti F, Montero AJ, et al. Does delay of adjuvant chemotherapy impact survival in patients with resected stage II and III colon adenocarcinoma? Cancer. 2011; **117**(11): 2364-70.

8. Coles CE, Burgess L, Tan LT. An audit of delays before and during radical radiotherapy for cervical cancer--effect on tumour cure probability. Clin Oncol (R Coll Radiol). 2003; **15**(2): 47-54.

9. Eisenhauer EA, Therasse P, Bogaerts J, Schwartz LH, Sargent D, Ford R, et al. New response evaluation criteria in solid tumours: Revised RECIST guideline (version 1.1). Eur J Cancer 2009; **45**(2): 228-47.

10. Therasse P, Arbuck SG, Eisenhauer EA, Wanders J, Kaplan RS, Rubinstein L, et al. New guidelines to evaluate the response to treatment in solid tumors. J Natl Cancer Inst. 2000; **92**(3): 205-16.

11. Kernan WN, Viscoli CM, Makuch RW, Brass LM, Horwitz RI. Stratified randomization for clinical trials. J Clin Epidemiol. 1999; **52**(1): 19-26.

12. van den Bent MJ, Afra D, de Witte O, Hassel MB, Schraub S, Hoang-Xuan K, et al. Long-term efficacy of early versus delayed radiotherapy for low-grade astrocytoma and oligodendroglioma in adults: the EORTC 22845 randomised trial. Lancet. 2005; **366**(9490): 985-90.

13. Biomarkers and surrogate endpoints: preferred definitions and conceptual framework. Clin Pharmacol Ther. 2001; **69**(3): 89-95.

14. Connell PP, Hellman S. Advances in radiotherapy and implications for the next century: A historical perspective. Cancer Res. 2009; **69**(2): 383-92.

15. Helleday T, Petermann E, Lundin C, Hodgson B, Sharma RA. DNA repair pathways as targets for cancer therapy. Nat Rev Cancer. 2008; **8**(3): 193-204.

16. Jackson SP, Bartek J. The DNA-damage response in human biology and disease. Nature. 2009; **461**(7267): 1071-8.

17. Hanahan D, Weinberg Robert A. Hallmarks of cancer: The next generation. Cell. 2011; **144**(5): 646-74.

18. Levine AJ, Oren M. The first 30 years of p53: growing ever more complex. Nat Rev Cancer. 2009; **9**(10): 749-58.

19. Núñez MI, McMillan TJ, Valenzuela MT, de Almodóvar JMR, Pedraza V. Relationship between DNA damage, rejoining and cell killing by radiation in mammalian cells. Radiother Oncol. 1996; **39**(2): 155-65.

20. Radford IR. Evidence for a general relationship between the induced level of DNA double-strand breakage and cell-killing after X-irradiation of mammalian cells. Int J Radiat Biol Relat Stud Phys Chem Med. 1986; **49**(4): 611-20.

21. Jeggo PA, Lobrich M. DNA double-strand breaks: their cellular and clinical impact? Oncogene. 2007; **26**(56): 7717-9.

22. Ward JF. The yield of DNA double-strand breaks produced intracellularly by ionizing radiation: a review. Int J Radiat Biol. 1990; **57**(6): 1141-50.

23. Bryant PE. Enzymatic restriction of mammalian cell DNA: Evidence for double-strand breaks as potentially lethal lesions. Int J Radiat Biol. 1985; **48**(1): 55-60.

24. Grądzka I, Iwaneńko T. A non-radioactive, PFGE-based assay for low levels of DNA double-strand breaks in mammalian cells. DNA Repair (Amst). 2005; **4**(10): 1129-39.

25. Ostling O, Johanson KJ. Microelectrophoretic study of radiation-induced DNA damages in individual mammalian cells. Biochem Biophys Res Commun. 1984; **123**(1): 291-8.

26. Olive PL. Impact of the comet assay in radiobiology. Mutat Res. 2009; **681**(1): 13-23.

27. Olive PL, Durand RE, Jackson SM, Le Riche JC, Luo C, Ma R, et al. The comet assay in clinical practice. Acta Oncol. 1999; **38**(7): 839-44.

28. Okada T, Kashino G, Nishiura H, Tano K, Watanabe M. Micronuclei formation induced by X-ray irradiation does not always result from DNA double-strand breaks. J Radiat Res. 2012; **53**(1): 93-100.

29. Polo SE, Jackson SP. Dynamics of DNA damage response proteins at DNA breaks: a focus on protein modifications. Genes Dev. 2011; **25**(5): 409-33.

30. Goodarzi AA, Jeggo PA. Irradiation induced foci (IRIF) as a biomarker for radiosensitivity. Mutat Res. 2012; **736**(1-2): 39-47.

31. Rogakou EP, Pilch DR, Orr AH, Ivanova VS, Bonner WM. DNA double-stranded breaks induce histone H2AX phosphorylation on serine 139. J Biol Chem. 1998; **273**(10): 5858-68.

32. Rogakou EP, Boon C, Redon C, Bonner WM. Megabase chromatin domains involved in DNA double-strand breaks in vivo. J Cell Biol. 1999; **146**(5): 905-16.

33. Fernandez-Capetillo O, Lee A, Nussenzweig M, Nussenzweig A. H2AX: the histone guardian of the genome. DNA Repair (Amst). 2004; **3**(8-9): 959-67.

34. Paull TT, Rogakou EP, Yamazaki V, Kirchgessner CU, Gellert M, Bonner WM. A critical role for histone H2AX in recruitment of repair factors to nuclear foci after DNA damage. Curr Biol. 2000; **10**(15): 886-95.

35. Stiff T, O'Driscoll M, Rief N, Iwabuchi K, Lobrich M, Jeggo PA. ATM and DNA-PK function redundantly to phosphorylate H2AX after exposure to ionizing radiation. Cancer Res. 2004; **64**(7): 2390-6.

36. Kinner A, Wu W, Staudt C, Iliakis G. Gamma-H2AX in recognition and signaling of DNA double-strand breaks in the context of chromatin. Nucleic Acids Res. 2008; **36**(17): 5678-94.

37. Wang H, Wang M, Bocker W, Iliakis G. Complex H2AX phosphorylation patterns by multiple kinases including ATM and DNA-PK in human cells exposed to ionizing radiation and treated with kinase inhibitors. J Cell Physiol. 2005; **202**(2): 492-502.

38. Savic V, Yin B, Maas NL, Bredemeyer AL, Carpenter AC, Helmink BA, et al. Formation of dynamic γ-H2AX domains along broken DNA strands is distinctly regulated by ATM and MDC1 and dependent upon H2AX densities in chromatin. Mol Cell. 2009; **34**(3): 298-310.

39. Burma S, Chen BP, Murphy M, Kurimasa A, Chen DJ. ATM phosphorylates histone H2AX in response to DNA double-strand breaks. J Biol Chem. 2001; **276**(45): 42462-7.

40. Cook PJ, Ju BG, Telese F, Wang X, Glass CK, Rosenfeld MG. Tyrosine dephosphorylation of H2AX modulates apoptosis and survival decisions. Nature. 2009; **458**(7238): 591-6.

41. Iacovoni JS, Caron P, Lassadi I, Nicolas E, Massip L, Trouche D, et al. High-resolution profiling of gammaH2AX around DNA double strand breaks in the mammalian genome. EMBO J. 2010; **29**(8): 1446-57.

42. Seo J, Kim SC, Lee H-S, Kim JK, Shon HJ, Salleh NLM, et al. Genome-wide profiles of H2AX and γ-H2AX differentiate endogenous and exogenous DNA damage hotspots in human cells. Nucl Acids Res. 2012; **40**(13): 5965-74.

43. Jakob B, Splinter J, Conrad S, Voss K-O, Zink D, Durante M, et al. DNA double-strand breaks in heterochromatin elicit fast repair protein recruitment, histone H2AX phosphorylation and relocation to euchromatin. Nucl Acids Res. 2011; **39**(15): 6489-99.

44. Bassing CH, Chua KF, Sekiguchi J, Suh H, Whitlow SR, Fleming JC, et al. Increased ionizing radiation sensitivity and genomic instability in the absence of histone H2AX. Proc Natl Acad Sci U S A. 2002; **99**(12): 8173-8.

45. Celeste A, Difilippantonio S, Difilippantonio MJ, Fernandez-Capetillo O, Pilch DR, Sedelnikova OA, et al. H2AX haploinsufficiency modifies genomic stability and tumor susceptibility. Cell. 2003; **114**(3): 371-83.

46. Yuan J, Adamski R, Chen J. Focus on histone variant H2AX: To be or not to be. FEBS Lett. 2010; **584**(17): 3717-24.

47. Stucki M, Clapperton JA, Mohammad D, Yaffe MB, Smerdon SJ, Jackson SP. MDC1 directly binds phosphorylated histone H2AX to regulate cellular responses to DNA double-strand breaks. Cell. 2005; **123**(7): 1213-26.

48. Goldberg M, Stucki M, Falck J, D'Amours D, Rahman D, Pappin D, et al. MDC1 is required for the intra-S-phase DNA damage checkpoint. Nature. 2003; **421**(6926): 952-6.

49. Lou Z, Minter-Dykhouse K, Wu X, Chen J. MDC1 is coupled to activated CHK2 in mammalian DNA damage response pathways. Nature. 2003; **421**(6926): 957-61.

50. Stewart GS, Wang B, Bignell CR, Taylor AM, Elledge SJ. MDC1 is a mediator of the mammalian DNA damage checkpoint. Nature. 2003; **421**(6926): 961-6.

51. Lukas J, Lukas C, Bartek J. More than just a focus: The chromatin response to DNA damage and its role in genome integrity maintenance. Nat Cell Biol. 2011; **13**(10): 1161-9.

52. Bekker-Jensen S, Mailand N. Assembly and function of DNA double-strand break repair foci in mammalian cells. DNA Repair (Amst). 2010; **9**(12): 1219-28.

53. Wood JL, Singh N, Mer G, Chen J. MCPH1 functions in an H2AX-dependent but MDC1-independent pathway in response to DNA damage. J Biol Chem. 2007; **282**(48): 35416-23.

54. Cha H, Lowe JM, Li H, Lee J-S, Belova GI, Bulavin DV, et al. Wip1 directly dephosphorylates γ-H2AX and attenuates the DNA damage response. Cancer Res. 2010; **70**(10): 4112-22.

55. Moon S-H, Lin L, Zhang X, Nguyen T-A, Darlington Y, Waldman AS, et al. Wild-type p53-induced phosphatase 1 dephosphorylates histone variant H2AX and suppresses DNA double strand break repair. J Biol Chem. **285**(17): 12935-47.

56. Dickey JS, Redon CE, Nakamura AJ, Baird BJ, Sedelnikova OA, Bonner WM. H2AX: functional roles and potential applications. Chromosoma. 2009; **118**(6): 683-92.

57. Sedelnikova OA, Rogakou EP, Panyutin IG, Bonner WM. Quantitative detection of (125)IdU-induced DNA double-strand breaks with γ-H2AX antibody. Radiat Res. 2002; **158**(4): 486-92.

58. Smart DJ, Halicka HD, Schmuck G, Traganos F, Darzynkiewicz Z, Williams GM. Assessment of DNA double-strand breaks and γH2AX induced by the topoisomerase II poisons etoposide and mitoxantrone. Mutat Res. 2008; **641**(1–2): 43-7.

59. Redon C, Nakamura A, Sordet O, Dickey J, Gouliaeva K, Tabb B, et al. Gamma-H2AX detection in peripheral blood lymphocytes, splenocytes, bone marrow, xenografts, and skin. Methods Mol Biol. 2011; **682**: 249-70.

60. Meier A, Fiegler H, Munoz P, Ellis P, Rigler D, Langford C, et al. Spreading of mammalian DNA-damage response factors studied by ChIP-chip at damaged telomeres. EMBO J. 2007; **26**(11): 2707-18.

61. Bewersdorf J, Bennett BT, Knight KL. H2AX chromatin structures and their response to DNA damage revealed by 4Pi microscopy. Proc Natl Acad Sci U S A. 2006; **103**(48): 18137-42.

62. Kim S, Jun DH, Kim HJ, Jeong K-C, Lee C-H. Development of a high-content screening method for chemicals modulating DNA damage response. J Biomol Screen. 2011; **16**(2): 259-65.

63. Higgins GS, Prevo R, Lee YF, Helleday T, Muschel RJ, Taylor S, et al. A small interfering RNA screen of genes involved in DNA repair identifies tumor-specific radiosensitization by POLQ knockdown. Cancer Res. 2010; **70**(7): 2984-93.

64. Johansson P, Muslimovic A, Hultborn R, Fernstrom E, Hammarsten O. In-solution staining and arraying method for the immunofluorescence detection of gammaH2AX foci optimized for clinical applications. Biotechniques. 2011; **51**(3): 185-9.

65. Ivashkevich AN, Martin OA, Smith AJ, Redon CE, Bonner WM, Martin RF, et al. γH2AX foci as a measure of DNA damage: A computational approach to automatic analysis. Mutat Res. 2011; **711**(1–2): 49-60.

66. Barber P, Locke R, Pierce G, Rothkamm K, Vojnovic B. Gamma-H2AX Foci Counting:Image processing and control software for high-content screening. Proc SPIE. 2007; **6441**: 1M-10.

67. Olive PL, Banath JP, Sinnott LT. Phosphorylated histone H2AX in spheroids, tumors, and tissues of mice exposed to etoposide and 3-amino-1,2,4-benzotriazine-1,3-dioxide. Cancer Res. 2004; **64**(15): 5363-9.

68. Tanaka T, Halicka D, Traganos F, Darzynkiewicz Z. Cytometric analysis of DNA damage: phosphorylation of histone H2AX as a marker of DNA double-strand breaks (DSBs). Methods Mol Biol. 2009; **523**: 161-8.

69. Svetlova MP, Solovjeva LV, Tomilin NV. Mechanism of elimination of phosphorylated histone H2AX from chromatin after repair of DNA double-strand breaks. Mutat Res. 2010; **685**(1-2): 54-60.

70. Avondoglio D, Scott T, Kil WJ, Sproull M, Tofilon PJ, Camphausen K. High throughput evaluation of gamma-H2AX. Radiat Oncol. 2009; **4**: 31.

71. Darzynkiewicz Z, Traganos F, Zhao H, Halicka HD, Skommer J, Wlodkowic D. Analysis of individual molecular events of DNA damage response by flow- and image-assisted cytometry. Methods Cell Biol. 2011; **103**: 115-47.

72. Schmid TE, Dollinger G, Beisker W, Hable V, Greubel C, Auer S, et al. Differences in the kinetics of γ-H2AX fluorescence decay after exposure to low and high LET radiation. Int J Radiat Biol. 2010; **86**(8): 682-91.

73. Bouquet F, Muller C, Salles B. The loss of gammaH2AX signal is a marker of DNA double strand breaks repair only at low levels of DNA damage. Cell Cycle. 2006; **5**(10): 1116-22.

74. Olive PL, Banath JP. Kinetics of H2AX phosphorylation after exposure to cisplatin. Cytometry B Clin Cytom. 2009; **76**(2): 79-90.

75. de Feraudy S, Revet I, Bezrookove V, Feeney L, Cleaver J. A minority of foci or pan-nuclear apoptotic staining of {gamma}H2AX in the S phase after UV damage contain DNA double-strand breaks. Proc Natl Acad Sci U S A.

76. Ward IM, Chen J. Histone H2AX Is phosphorylated in an ATR-dependent manner in response to replicational stress. J Biol Chem. 2001; **276**(51): 47759-62.

77. Xu B, Sun Z, Liu Z, Guo H, Liu Q, Jiang H, et al. Replication stress induces micronuclei comprising of aggregated DNA double-strand breaks. PLoS ONE. 2011; **6**(4): e18618.

78. Mukherjee B, Kessinger C, Kobayashi J, Chen BP, Chen DJ, Chatterjee A, et al. DNA-PK phosphorylates histone H2AX during apoptotic DNA fragmentation in mammalian cells. DNA Repair (Amst). 2006; **5**(5): 575-90.

79. Kurose A, Tanaka T, Huang X, Halicka HD, Traganos F, Dai W, et al. Assessment of ATM phosphorylation on Ser-1981 induced by DNA topoisomerase I and II inhibitors in relation to Ser-139-histone H2AX phosphorylation, cell cycle phase, and apoptosis. Cytometry A. 2005; **68A**(1): 1-9.

80. Zykova TA, Zhu F, Lu C, Higgins L, Tatsumi Y, Abe Y, et al. Lymphokine-activated killer T-cell-originated protein kinase phosphorylation of histone H2AX prevents arsenite-induced apoptosis in RPMI7951 melanoma cells. Clin Cancer Res. 2006; **12**(23): 6884-93.

81. Lu C, Zhu F, Cho Y-Y, Tang F, Zykova T, Ma W-y, et al. Cell apoptosis: Requirement of H2AX in DNA ladder formation, but not for the activation of caspase-3. Mol Cell. 2006; **23**(1): 121-32.

82. Tanaka T, Halicka HD, Huang X, Traganos F, Darzynkiewicz Z. Constitutive histone H2AX phosphorylation and ATM activation, the reporters of DNA damage by endogenous oxidants. Cell Cycle. 2006; **5**(17): 1940-5.

83. Tanaka T, Huang X, Halicka HD, Zhao H, Traganos F, Albino AP, et al. Cytometry of ATM activation and histone H2AX phosphorylation to estimate extent of DNA damage induced by exogenous agents. Cytometry A. 2007; **71**(9): 648-61.

84. Artus C, Boujrad H, Bouharrour A, Brunelle M-N, Hoos S, Yuste VJ, et al. AIF promotes chromatinolysis and caspase-independent programmed necrosis by interacting with histone H2AX. EMBO J. 2010; **29**(9): 1585-99.

85. Hammond EM, Denko NC, Dorie MJ, Abraham RT, Giaccia AJ. Hypoxia Links ATR and p53 through Replication Arrest. Mol Cell Biol. 2002; **22**(6): 1834-43.

86. Hammond EM, Dorie MJ, Giaccia AJ. ATR/ATM targets are phosphorylated by ATR in response to hypoxia and ATM in response to reoxygenation. J Biol Chem. 2003; **278**(14): 12207-13.

87. Kumareswaran R, Ludkovski O, Meng A, Sykes J, Pintilie M, Bristow RG. Chronic hypoxia compromises repair of DNA double-strand breaks to drive genetic instability. J Cell Sci. 2012; **125**(1): 189-99.

88. Harding S, Coackley C, Bristow R. ATM-dependent phosphorylation of 53BP1 in response to genomic stress in oxic and hypoxic cells. Radiother Oncol. 2011; **99**(3): 307-12.

89. Olcina M, Lecane PS, Hammond EM. Targeting hypoxic cells through the DNA damage response. Clin Cancer Res. 2010; **16**(23): 5624-9.

90. Blanco-Rodríguez J. γH2AX marks the main events of the spermatogenic process. Microsc Res Tech. 2009; **72**(11): 823-32.

91. Mahadevaiah SK, Turner JM, Baudat F, Rogakou EP, de Boer P, Blanco-Rodriguez J, et al. Recombinational DNA double-strand breaks in mice precede synapsis. Nat Genet. 2001; **27**(3): 271-6.

92. Bartkova J, Horejsi Z, Koed K, Kramer A, Tort F, Zieger K, et al. DNA damage response as a candidate anti-cancer barrier in early human tumorigenesis. Nature. 2005; **434**(7035): 864-70.

93. Gorgoulis VG, Vassiliou L-VF, Karakaidos P, Zacharatos P, Kotsinas A, Liloglou T, et al. Activation of the DNA damage checkpoint and genomic instability in human precancerous lesions. Nature. 2005; **434**(7035): 907-13.

94. Nuciforo PG, Luise C, Capra M, Pelosi G, d'Adda di Fagagna F. Complex engagement of DNA damage response pathways in human cancer and in lung tumor progression. Carcinogenesis. 2007; **28**(10): 2082-8.

95. Warters RL, Adamson PJ, Pond CD, Leachman SA. Melanoma cells express elevated levels of phosphorylated histone H2AX foci. J Investig Dermatol. 2005; **124**(4): 807-17.

96. Lantuejoul S, Raynaud C, Salameire D, Gazzeri S, Moro-Sibilot D, Soria J-C, et al. Telomere maintenance and DNA damage responses during lung carcinogenesis. Clinical Cancer Research. 2010; **16**(11): 2979-88.

97. Raynaud CM, Hernandez J, Llorca FP, Nuciforo P, Mathieu MC, Commo F, et al. DNA damage repair and telomere length in normal breast, preneoplastic lesions, and invasive cancer. Am J Clin Oncol. 2010; **33**(4): 341-5.

98. Baure J, Izadi A, Suarez V, Giedzinski E, Cleaver JE, Fike JR, et al. Histone H2AX phosphorylation in response to changes in chromatin structure induced by altered osmolarity. Mutagenesis. 2009; **24**(2): 161-7.

99. Terry SY, Vallis KA. Relationship between chromatin structure and sensitivity to molecularly targeted auger electron radiation therapy. Int J Radiat Oncol Biol Phys. 2012; **83**(4): 1298-305.

100. Pospelova TV, Demidenko ZN, Bukreeva EI, Pospelov VA, Gudkov AV. Pseudo-DNA damage response in senescent cells. Cell Cycle. 2009; **8**(24): 4112-8.

101. Daniel R, Ramcharan J, Rogakou E, Taganov KD, Greger JG, Bonner W, et al. Histone H2AX Is Phosphorylated at Sites of Retroviral DNA Integration but Is Dispensable for Postintegration Repair. J Biol Chem. 2004; **279**(44): 45810-4.

102. Zhu F, Zykova TA, Peng C, Zhang J, Cho Y-Y, Zheng D, et al. Phosphorylation of H2AX at Ser139 and a new phosphorylation site Ser16 by RSK2 decreases H2AX ubiquitination and inhibits cell transformation. Cancer Res. 2011; **71**(2): 393-403.

103. Mutsaers CA, Wishart TM, Lamont DJ, Riessland M, Schreml J, Comley LH, et al. Reversible molecular pathology of skeletal muscle in spinal muscular atrophy. Hum Mol Genet. 2011; **20**(22): 4334-44.

104. Redon CE, Nakamura AJ, Martin OA, Parekh PR, Weyemi US, Bonner WM. Recent developments in the use of gamma-H2AX as a quantitative DNA double-strand break biomarker. Aging (Albany NY). 2011.

105. Mah L-J, El-Osta A, Karagiannis TC. γH2AX as a molecular marker of aging and disease. Epigenetics. 2010; **5**(2): 129-36.

106. Löbrich M, Shibata A, Beucher A, Fisher A, Ensminger M, Goodarzi AA, et al. γH2AX foci analysis for monitoring DNA double-strand break repair: Strengths, limitations and optimization. Cell Cycle. 2010; **9**(4): 662-9.

107. Banath JP, MacPhail SH, Olive PL. Radiation sensitivity, H2AX phosphorylation, and kinetics of repair of DNA Strand Breaks in Irradiated Cervical Cancer Cell Lines. Cancer Res. 2004; **64**(19): 7144-9.

108. Martin NT, Nahas SA, Tunuguntla R, Fike F, Gatti RA. Assessing 'radiosensitivity' with kinetic profiles of γ-H2AX, 53BP1 and BRCA1 foci. Radiother Oncol. 2011; **101**(1): 35-8.

109. Klokov D, MacPhail SM, Banáth JP, Byrne JP, Olive PL. Phosphorylated histone H2AX in relation to cell survival in tumor cells and xenografts exposed to single and fractionated doses of X-rays. Radiother Oncol. 2006; **80**(2): 223-9.

110. Mirzayans R, Severin D, Murray D. Relationship between DNA double-strand break rejoining and cell survival after exposure to ionizing radiation in human fibroblast strains with differing ATM/p53 status: Implications for evaluation of clinical radiosensitivity. Int J Radiat Oncol Biol Phys. 2006; **66**(5): 1498-505.

111. Mahrhofer H, Bürger S, Oppitz U, Flentje M, Djuzenova CS. Radiation induced DNA damage and damage repair in human tumor and fibroblast cell lines assessed by histone H2AX phosphorylation. Int J Radiat Oncol Biol Phys. 2006; **64**(2): 573-80.

112. Olive PL. In regard to Mahrhofer et al.: Radiation induced DNA damage and damage repair in human tumor and fibroblast cell lines assessed by histone H2AX phosphorylation (Int J Radiat Oncol Biol Phys 2006;64:573–580). Int J Radiat Oncol Biol Phys. 2006; **65**(3): 956.

113. Taneja N, Davis M, Choy JS, Beckett MA, Singh R, Kron SJ, et al. Histone H2AX phosphorylation as a predictor of radiosensitivity and target for radiotherapy. J Biol Chem. 2004; **279**(3): 2273-80.

114. Fuhrman CB, Kilgore J, LaCoursiere YD, Lee CM, Milash BA, Soisson AP, et al. Radiosensitization of cervical cancer cells via double-strand DNA break repair inhibition. Gynecol Oncol. 2008; **110**(1): 93-8.

115. Rothkamm K, Lobrich M. Evidence for a lack of DNA double-strand break repair in human cells exposed to very low x-ray doses. Proc Natl Acad Sci U S A. 2003; **100**(9): 5057-62.

116. Vasireddy RS, Sprung CN, Cempaka NL, Chao M, McKay MJ. H2AX phosphorylation screen of cells from radiosensitive cancer patients reveals a novel DNA double-strand break repair cellular phenotype. Br J Cancer. 2010; **102**(10): 1511-8.

117. Horn S, Barnard S, Rothkamm K. Gamma-H2AX-based dose estimation for whole and partial body radiation exposure. PLoS ONE. 2011; **6**(9): e25113.

118. Bhogal N, Jalali F, Bristow RG. Microscopic imaging of DNA repair foci in irradiated normal tissues. Int J Radiat Biol. 2009; **85**(9): 732-46.

119. Rübe CE, Dong X, Kühne M, Fricke A, Kaestner L, Lipp P, et al. DNA double-strand break rejoining in complex normal tissues. Int J Radiat Oncol Biol Phys. 2008; **72**(4): 1180-7.

120. Kinders RJ, Hollingshead M, Lawrence S, Ji J, Tabb B, Bonner WM, et al. Development of a validated immunofluorescence assay for gammaH2AX as a pharmacodynamic marker of topoisomerase I inhibitor activity. Clin Cancer Res. 2010.

121. Kummar S, Chen A, Ji J, Zhang Y, Reid JM, Ames M, et al. Phase I study of PARP inhibitor ABT-888 in combination with topotecan in adults with refractory solid tumors and lymphomas. Cancer Res. 2011; **71**(17): 5626-34.

122. Kummar S, Jiuping J, Morgan RJ, Lenz HJ, Puhalla SL, Belani CP, et al. A phase I study of veliparib in combination with metronomic cyclophosphamide in adults with refractory solid tumors and lymphomas. Clin Cancer Res. 2012; **18**(6): 1726-34.

123. Banuelos CA, Banath JP, Kim JY, Aquino-Parsons C, Olive PL. gammaH2AX expression in tumors exposed to cisplatin and fractionated irradiation. Clin Cancer Res. 2009; **15**(10): 3344-53.

124. Olive PL, Banuelos CA, Durand RE, Kim J-Y, Aquino-Parsons C. Endogenous and radiation-induced expression of γH2AX in biopsies from patients treated for carcinoma of the uterine cervix. Radiother Oncol. 2010; **94**(1): 82-9.

125. Cleaver JE. gammaH2AX: biomarker of damage or functional participant in DNA repair "All that glitters is not gold!". Photochem Photobiol. 2011; **87**(6): 1230-9.

126. Mladenov E, Iliakis G. Induction and repair of DNA double strand breaks: The increasing spectrum of non-homologous end joining pathways. Mutat Res. 2011; **711**(1–2): 61-72.

127. Galleani J, Miranda C, Pierotti MA, Greco A. H2AX phosphorylation and kinetics of radiation-induced DNA double strand break repair in human primary thyrocytes. Thyroid. 2009; **19**(3): 257-64.

128. Kühne M, Riballo E, Rief N, Rothkamm K, Jeggo PA, Löbrich M. A double-strand break repair defect in ATM-deficient cells contributes to radiosensitivity. Cancer Res. 2004; **64**(2): 500-8.

129. Koike M, Sugasawa J, Yasuda M, Koike A. Tissue-specific DNA-PK-dependent H2AX phosphorylation and γ-H2AX elimination after X-irradiation in vivo. Biochem Biophys Res Commun. 2008; **376**(1): 52-5.

130. Rübe CE, Fricke A, Wendorf J, Stützel A, Kühne M, Ong MF, et al. Accumulation of DNA double-strand breaks in normal tissues after fractionated irradiation. Int J Radiat Oncol Biol Phys. 2010; **76**(4): 1206-13.

131. Koike M, Mashino M, Sugasawa J, Koike A. Dynamic change of histone H2AX phosphorylation independent of ATM and DNA-PK in mouse skin in situ. Biochem Biophys Res Commun. 2007; **363**(4): 1009-12.

132. Reitsema T, Klokov D, Banath JP, Olive PL. DNA-PK is responsible for enhanced phosphorylation of histone H2AX under hypertonic conditions. DNA Repair (Amst). 2005; **4**(10): 1172-81.

133. Bhogal N, Kaspler P, Jalali F, Hyrien O, Chen R, Hill RP, et al. Late residual γ-H2AX foci in murine skin are dose responsive and predict radiosensitivity in vivo. Radiat Res. 2010; **173**(1): 1-9.

134. Chua ML, Somaiah N, A'Hern R, Davies S, Gothard L, Yarnold J, et al. Residual DNA and chromosomal damage in ex vivo irradiated blood lymphocytes correlated with late normal tissue response to breast radiotherapy. Radiother Oncol. 2011; **99**(3): 362-6.

135. Podhorecka M, Skladanowski A, Bozko P. H2AX phosphorylation: Its role in DNA damage response and cancer therapy. J Nucleic Acids. 2010; **2010**.

136. Bonner WM, Redon CE, Dickey JS, Nakamura AJ, Sedelnikova OA, Solier S, et al. GammaH2AX and cancer. Nat Rev Cancer. 2008; **8**(12): 957-67.

137. Redon CE, Nakamura AJ, Zhang YW, Ji JJ, Bonner WM, Kinders RJ, et al. Histone gammaH2AX and poly(ADP-ribose) as clinical pharmacodynamic biomarkers. Clin Cancer Res. 2010; **16**(18): 4532-42.

138. Ivashkevich A, Redon CE, Nakamura AJ, Martin RF, Martin OA. Use of the γ-H2AX assay to monitor DNA damage and repair in translational cancer research. Cancer Lett. 2011; (http://www.cancerletters.info/article/S0304-3835(11)00772-5/pdf.).

139. Ward TH, Cummings J, Dean E, Greystoke A, Hou JM, Backen A, et al. Biomarkers of apoptosis. Br J Cancer. 2008; **99**(6): 841-6.

140. Bartek J, Mistrik M, Bartkova J. Thresholds of replication stress signaling in cancer development and treatment. Nat Struct Mol Biol. 2012; **19**(1): 5-7.

141. Takahashi A, Ohnishi T. Does γH2AX foci formation depend on the presence of DNA double strand breaks? Cancer Lett. 2005; **229**(2): 171-9.

142. Glazer PM, Le QT, Bristow R, Helleday T, Pelroy R, Bernhard EJ. New translational possibilities for microenvironmental modulation of radiosensitivity. Radiat Res. 2011; **176**(3): 412-4.

143. Löbrich M, Rief N, Kühne M, Heckmann M, Fleckenstein J, Rübe C, et al. In vivo formation and repair of DNA double-strand breaks after computed tomography examinations. Proc Natl Acad Sci U S A. 2005; **102**(25): 8984-9.

144. Rothkamm K, Balroop S, Shekhdar J, Fernie P, Goh V. Leukocyte DNA damage after multi-detector row CT: a quantitative biomarker of low-level radiation exposure. Radiology. 2007; **242**(1): 244-51.

145. Ismail IH, Wadhra TI, Hammarsten O. An optimized method for detecting gamma-H2AX in blood cells reveals a significant interindividual variation in the gamma-H2AX response among humans. Nucl Acids Res. 2007; **35**(5): e36.

146. Sak A, Grehl S, Erichsen P, Engelhard M, Grannass A, Levegrun S, et al. γ-H2AX foci formation in peripheral blood lymphocytes of tumor patients after local radiotherapy to

different sites of the body: dependence on the dose-distribution, irradiated site and time from start of treatment. Int J Radiat Biol. 2007; **83**(10): 639-52.

147. Beels L, Bacher K, De Wolf D, Werbrouck J, Thierens H. gamma-H2AX foci as a biomarker for patient X-ray exposure in pediatric cardiac catheterization: are we underestimating radiation risks? Circulation. 2009; **120**(19): 1903-9.

148. Lassmann M, Hanscheid H, Gassen D, Biko J, Meineke V, Reiners C, et al. In vivo formation of gamma-H2AX and 53BP1 DNA repair foci in blood cells after radioiodine therapy of differentiated thyroid cancer. J Nucl Med. 2010; **51**(8): 1318-25.

149. Lindholm C, Acheva A, Koivistoinen A, Perala M, Heinavaara S, Jahns J, et al. Search for clastogenic factors in the plasma of locally irradiated individuals. Radiat Res. 2011; **177**(3): 298-306.

150. Zwicker F, Swartman B, Sterzing F, Major G, Weber KJ, Huber PE, et al. Biological in-vivo measurement of dose distribution in patients' lymphocytes by gamma-H2AX immunofluorescence staining: 3D conformal- vs. step-and-shoot IMRT of the prostate gland. Radiat Oncol. 2011; **6**: 62.

151. Belyaev IY. Radiation-induced DNA repair foci: Spatio-temporal aspects of formation, application for assessment of radiosensitivity and biological dosimetry. Mutat Res 2010; **704**(1-3): 132-41.

152. Sak A, Grehl S, Engelhard M, Wierlemann A, Kaelberlah HP, Erichsen P, et al. Long-term in vivo effects of cisplatin on γ-H2AX foci signaling in peripheral lymphocytes of tumor patients after irradiation. Clin Cancer Res. 2009; **15**(8): 2927-34.

153. Bourton EC, Plowman PN, Smith D, Arlett CF, Parris CN. Prolonged expression of the gamma-H2AX DNA repair biomarker correlates with excess acute and chronic toxicity from radiotherapy treatment. Int J Cancer. 2011; **129**(12): 2928-34.

154. Fleckenstein J, Kuhne M, Seegmuller K, Derschang S, Melchior P, Graber S, et al. The impact of individual in vivo repair of DNA double-strand breaks on oral mucositis in adjuvant radiotherapy of head-and-neck cancer. Int J Radiat Oncol Biol Phys. 2010.

155. Qvarnstrom OF, Simonsson M, Johansson KA, Nyman J, Turesson I. DNA double strand break quantification in skin biopsies. Radiother Oncol. 2004; **72**(3): 311-7.

156. Simonsson M, Qvarnstrom F, Nyman J, Johansson KA, Garmo H, Turesson I. Low-dose hypersensitive gammaH2AX response and infrequent apoptosis in epidermis from radiotherapy patients. Radiother Oncol. 2008; **88**(3): 388-97.

157. Chua MLK, Somaiah N, Bourne S, Daley F, A'Hern R, Nuta O, et al. Inter-individual and inter-cell type variation in residual DNA damage after in vivo irradiation of human skin. Radiat Oncol. 2011; **99**(2): 225-30.

158. Olive PL, Banath JP, Keyes M. Residual gammaH2AX after irradiation of human lymphocytes and monocytes in vitro and its relation to late effects after prostate brachytherapy. Radiother Oncol. 2008; **86**(3): 336-46.

159. Porcedda P, Turinetto V, Brusco A, Cavalieri S, Lantelme E, Orlando L, et al. A rapid flow cytometry test based on histone H2AX phosphorylation for the sensitive and specific diagnosis of ataxia telangiectasia. Cytometry A. 2008; **73**(6): 508-16.

160. Fong PC, Boss DS, Yap TA, Tutt A, Wu P, Mergui-Roelvink M, et al. Inhibition of poly(ADP-ribose) polymerase in tumors from BRCA mutation carriers. N Engl J Med. 2009; **361**(2): 123-34.

161. Werbrouck J, De Ruyck K, Beels L, Vral A, Van Eijkeren M, De Neve W, et al. Prediction of late normal tissue complications in RT treated gynaecological cancer patients: potential of the gamma-H2AX foci assay and association with chromosomal radiosensitivity. Oncol Rep. 2010; **23**(2): 571-8.

162. González JE, Roch-Lefèvre SH, Mandina T, García O, Roy L. Induction of γ-H2AX foci in human exfoliated buccal cells after in vitro exposure to ionising radiation. Int J Radiat Biol. 2010; **86**(9): 752-9.

163. Negrini S, Gorgoulis VG, Halazonetis TD. Genomic instability--an evolving hallmark of cancer. Nat Rev Mol Cell Biol. 2010; **11**(3): 220-8.

164. Kasparek TR, Humphrey TC. DNA double-strand break repair pathways, chromosomal rearrangements and cancer. Semin Cell Dev Biol. 2011; **22**(8): 886-97.

165. McClelland SE, Burrell RA, Swanton C. Chromosomal instability: A composite phenotype that influences sensitivity to chemotherapy. Cell Cycle. 2009; **8**(20): 3262-6.

166. Bertagnolli MM, Redston M, Compton CC, Niedzwiecki D, Mayer RJ, Goldberg RM, et al. Microsatellite instability and loss of heterozygosity at chromosomal location 18q: prospective evaluation of biomarkers for stages II and III colon cancer—A study of CALGB 9581 and 89803. J Clin Oncol. 2011; **29**(23): 3153-62.

167. Wasco MJ, Pu RT. Comparison of PAX-2, RCC antigen, and antiphosphorylated H2AX antibody (γ-H2AX) in diagnosing metastatic renal cell carcinoma by fine-needle aspiration. Diagn Cytopathol. 2008; **36**(8): 568-73.

168. Wasco MJ, Pu RT, Yu L, Su L, Ma L. Expression of gamma-H2AX in melanocytic lesions. Hum Pathol. 2008; **39**(11): 1614-20.

169. Brunner AH, Hinterholzer S, Riss P, Heinze G, Weiss K, Brustmann H. Expression of gamma-H2AX in endometrial carcinomas: An immunohistochemical study with p53. Gynecol Oncol. 2010.

170. Brustmann H, Hinterholzer S, Brunner A. Expression of phosphorylated histone H2AX (γH2AX) in normal and neoplastic squamous epithelia of the uterine cervix: An immunohistochemical study with epidermal growth factor receptor. Int J Gynecol Pathol. 2010.

171. Cheung WL, Albadine R, Chan T, Sharma R, Netto GJ. Phosphorylated H2AX in noninvasive low grade urothelial carcinoma of the bladder: correlation with tumor recurrence. J Urol. 2009; **181**(3): 1387-92.

172. Martin OA, Bonner WM. Gamma-H2AX in cancer cells: A potential biomarker for cancer diagnostics, prediction and recurrence. Cell Cycle. 2006; **5**(24): 2909-13.

173. Karp JE, Flatten K, Feldman EJ, Greer JM, Loegering DA, Ricklis RM, et al. Active oral regimen for elderly adults with newly diagnosed acute myelogenous leukemia: a preclinical and phase 1 trial of the farnesyltransferase inhibitor tipifarnib (R115777, Zarnestra) combined with etoposide. Blood. 2009; **113**(20): 4841-52.

174. Karp JE, Ricklis RM, Balakrishnan K, Briel J, Greer J, Gore SD, et al. A phase 1 clinical-laboratory study of clofarabine followed by cyclophosphamide for adults with refractory acute leukemias. Blood. 2007; **110**(6): 1762-9.

175. Mah LJ, El-Osta A, Karagiannis TC. gammaH2AX: a sensitive molecular marker of DNA damage and repair. Leukemia. 2010; **24**(4): 679-86.

176. Halicka HD, Ozkaynak F, Levendoglu-Tugal O, Sandoval C, Seiter K, Kajstura M, et al. DNA damage response as a biomarker in treatment of leukemias. Cell Cycle. 2009; **8**(11): 1720-4.

177. Zhe X, Cher ML, Bonfil RD. Circulating tumor cells: finding the needle in the haystack. Am J Cancer Res. 2011; **1**(6): 740-51.

178. Wang LH, Pfister TD, Parchment RE, Kummar S, Rubinstein L, Evrard YA, et al. Monitoring drug-induced gammaH2AX as a pharmacodynamic biomarker in individual circulating tumor cells. Clin Cancer Res. 2010; **16**(3): 1073-84.

179. Abe H, Kawahara A, Sugita Y, Yamaguchi T, Terasaki M, Kage M. Follow-up evaluation of radiation-induced DNA damage in CSF disseminated high-grade glioma using phospho-histone H2AX antibody. Diagn Cytopathol. 2011.

180. Hochhauser D, Meyer T, Spanswick VJ, Wu J, Clingen PH, Loadman P, et al. Phase I study of sequence-selective minor groove DNA binding agent SJG-136 in patients with advanced solid tumors. Clin Cancer Res. 2009; **15**(6): 2140-7.

181. Asakawa H, Koizumi H, Koike A, Takahashi M, Wu W, Iwase H, et al. Prediction of breast cancer sensitivity to neoadjuvant chemotherapy based on status of DNA damage repair proteins. Breast Cancer Res. 2010; **12**(2): R17.

182. Bentzen SM, Parliament M, Deasy JO, Dicker A, Curran WJ, Williams JP, et al. Biomarkers and surrogate endpoints for normal-tissue effects of radiation therapy: the importance of dose–volume effects. Int J Radiat Oncol Biol Phys. 2010; **76**(3, Supplement): S145-S50.

183. Duffy SW, Treasure FP. Potential surrogate endpoints in cancer research – some considerations and examples. Pharm Stat. 2011; **10**(1): 34-9.

184. Poste G, Carbone DP, Parkinson DR, Verweij J, Hewitt SM, Jessup JM. Leveling the playing field: Bringing development of biomarkers and molecular diagnostics up to the standards for drug development. Clin Cancer Res. 2012; **18**(6): 1515-23.

185. CRUK. Prognostic/Predictive Biomarker Roadmap: Cancer Research UK; 2007.

186. Hegi ME, Diserens A-C, Gorlia T, Hamou M-F, de Tribolet N, Weller M, et al. MGMT Gene Silencing and Benefit from Temozolomide in Glioblastoma. N Engl J Med. 2005; **352**(10): 997-1003.

187. Stupp R, Hegi ME, Mason WP, van den Bent MJ, Taphoorn MJ, Janzer RC, et al. Effects of radiotherapy with concomitant and adjuvant temozolomide versus radiotherapy alone on survival in glioblastoma in a randomised phase III study: 5-year analysis of the EORTC-NCIC trial. Lancet Oncol. 2009; **10**(5): 459-66.

188. Medicine Io. Evaluation of Biomarkers and Surrogate Endpoints in Chronic Disease: The National Academies Press; 2010.

189. CRUK. Biomarkers and Imaging Discovery and Development Committee. 2010 [cited 2012 13 March]; Available from: http://science.cancerresearchuk.org/funding/funding-committees/biomarkers-imaging-committee

190. Hulley S, Cummings S, Browner W, Grady D, Newman T. Designing Clinical Research. 3 ed. Philadephia, USA: Lippincott Willimans and Wilkins; 2007.

191. Hewitt SM, Badve SS, True LD. Impact of preanalytic factors on the design and application of integral biomarkers for directing patient therapy. Clin Cancer Res. 2012; **18**(6): 1524-30.

192. Buyse M. Use of meta-analysis for the validation of surrogate endpoints and biomarkers in cancer trials. Cancer J. 2009; **15**(5): 421-5.

193. Cour JLl, Brok J, Gøtzsche PC. Inconsistent reporting of surrogate outcomes in randomised clinical trials: cohort study. BMJ. 2010; **341**.

194. Baker S, Kramer B. A perfect correlate does not a surrogate make. BMC Med Res Methodol. 2003; **3**(1): 16.

195. Aronson JK. An agenda for UK clinical pharmacology Research priorities in biomarkers and surrogate endpoints. Brit J Clin Pharm. 2012: no-no.

196. Bai J, Bell R, Buckman S, Burckart G, Eichler H-G, Fang K, et al. Translational Biomarkers: from Preclinical to Clinical a Report of 2009 AAPS/ACCP Biomarker Workshop. AAPS J. 2011; **13**(2): 274-83.

197. Huang Y, Gilbert PB. Comparing biomarkers as principal surrogate endpoints. Biometrics. 2011; **67**(4): 1442-51.

198. Olson RA, Brastianos PK, Palma DA. Prognostic and predictive value of epigenetic silencing of MGMT in patients with high grade gliomas: a systematic review and meta-analysis. J Neurooncol. 2011; **105**(2): 325-35.

199. Weller M, Stupp R, Reifenberger G, Brandes AA, van den Bent MJ, Wick W, et al. MGMT promoter methylation in malignant gliomas: ready for personalized medicine? Nat Rev Neurol. 2010; **6**(1): 39-51.

200. Williams PM, Lively TG, Jessup JM, Conley BA. Bridging the gap: Moving predictive and prognostic assays from research to clinical use. Clin Cancer Res. 2012; **18**(6): 1531-9.

201. Economos C, Morrissey C, Vessella RL. Circulating tumor cells as a marker of response: implications for determining treatment efficacy and evaluating new agents. Curr Opin Urol. 2012.

202. Cortez MA, Bueso-Ramos C, Ferdin J, Lopez-Berestein G, Sood AK, Calin GA. MicroRNAs in body fluids - the mix of hormones and biomarkers. Nat Rev Clin Oncol. 2011; **8**(8): 467-77.

203. Alix-Panabières C, Schwarzenbach H, Pantel K. Circulating tumor cells and circulating tumor DNA. Annu Rev Med. 2012; **63**(1): 199-215.

204. Wahl RL, Jacene H, Kasamon Y, Lodge MA. From RECIST to PERCIST: Evolving considerations for PET response criteria in solid tumors. J Nucl Med. 2009; **50**(Suppl 1): 122S-50S.

205. Jeraj R, Cao Y, Ten Haken RK, Hahn C, Marks L. Imaging for assessment of radiation-induced normal tissue effects. Int J Radiat Oncol Biol Phys. 2010; **76**(3 Suppl): S140-4.

206. Verheij M. Clinical biomarkers and imaging for radiotherapy-induced cell death. Cancer Metastasis Rev. 2008; **27**(3): 471-80.

207. Haimovitz-Friedman A, Yang TI, Thin TH, Verheij M. Imaging radiotherapy-induced apoptosis. Radiat Res. 2012; **177**(4): 467-82.

208. Cornelissen B, Kersemans V, Darbar S, Thompson J, Shah K, Sleeth K, et al. Imaging DNA damage in vivo using gammaH2AX-targeted immunoconjugates. Cancer Res. 2011; **71**(13): 4539-49.

209. Li W, Li F, Huang Q, Shen J, Wolf F, He Y, et al. Quantitative, noninvasive imaging of radiation-induced DNA double-strand breaks in vivo. Cancer Res. 2011; **71**(12): 4130-7.

210. Lord CJ, Ashworth A. The DNA damage response and cancer therapy. Nature. 2012; **481**(7381): 287-94.

211. Nakamura A, Sedelnikova OA, Redon C, Pilch DR, Sinogeeva NI, Shroff R, et al. Techniques for gamma-H2AX Detection. Methods in Enzymology: Academic Press; 2006. p. 236-50.

212. Mandell JW. Immunohistochemical assessment of protein phosphorylation state: the dream and the reality. Histochem Cell Biol. 2008; **130**(3): 465-71.

213. Gonzalez JE, Lee M, Barquinero JF, Valente M, Roch-Lefevre S, Garcia O. Quantitative image analysis of gamma-H2AX foci induced by ionizing radiation applying open source programs. Anal Quant Cytol Histol. 2012; **34**(2): 66-71.

214. Cai Z, Vallis KA, Reilly RM. Computational analysis of the number, area and density of gamma-H2AX foci in breast cancer cells exposed to (111)In-DTPA-hEGF or gamma-rays using Image-J software. Int J Radiat Biol. 2009; **85**(3): 262-71.

215. Jucha A, Wegierek-Ciuk A, Koza Z, Lisowska H, Wojcik A, Wojewodzka M, et al. FociCounter: a freely available PC programme for quantitative and qualitative analysis of gamma-H2AX foci. Mutat Res. 2010; **696**(1): 16-20.

216. Olive PL, Banath JP. Phosphorylation of histone H2AX as a measure of radiosensitivity. Int J Radiat Oncol Biol Phys. 2004; **58**(2): 331-5.

217. Olive PL. Retention of gammaH2AX foci as an indication of lethal DNA damage. Radiother Oncol. 2011; **101**(1): 18-23.

218. Coates PJ, Appleyard MV, Murray K, Ackland C, Gardner J, Brown DC, et al. Differential contextual responses of normal human breast epithelium to ionizing radiation in a mouse xenograft model. Cancer Res. 2010; **70**(23): 9808-15.

219. Suzuki M, Suzuki K, Kodama S, Yamashita S, Watanabe M. Persistent amplification of DNA damage signal involved in replicative senescence of normal human diploid fibroblasts. Oxid Med Cell Longev. 2012; **2012**: 310534.

220. Fokas E, Yoshimura M, Prevo R, Higgins G, Hackl W, Maira SM, et al. NVP-BEZ235 and NVP-BGT226, dual phosphatidylinositol 3-kinase/mammalian target of rapamycin inhibitors, enhance tumor and endothelial cell radiosensitivity. Radiat Oncol. 2012; **7**: 48.

221. Clark DP. Seize the opportunity. Cancer Cytopathol. 2009; **117**(5): 289-97.

222. Krishnamurthy S. Applications of molecular techniques to fine-needle aspiration biopsy. Cancer Cytopathol. 2007; **111**(2): 106-22.

223. TA69 - Guidance on the use of liquid-based cytology for cervical screening. London: National Institute for Health and Clinical Excellence

2003.

224. Fadda G, Rossi ED. Liquid-based cytology in fine-needle aspiration biopsies of the thyroid gland. Acta Cytol. 2011; **55**(5): 389-400.

225. Cai Z, Chen Z, Bailey KE, Scollard DA, Reilly RM, Vallis KA. Relationship between induction of phosphorylated H2AX and survival in breast cancer cells exposed to 111In-DTPA-hEGF. J Nucl Med. 2008; **49**(8): 1353-61.

226. Thinprep T2000 Manual. Marlborough, USA: Hologic Inc.; 2002.

227. Vasireddy RS, Tang MM, Mah LJ, Georgiadis GT, El-Osta A, Karagiannis TC. Evaluation of the spatial distribution of gammaH2AX following ionizing radiation. J Vis Exp. 2010; (42).

228. Claeys J, Mertens K, D'Asseler Y, Goethals I. Normoglycemic plasma glucose levels affect F-18 FDG uptake in the brain. Ann Nucl Med. 2010; **24**(6): 501-5.

229. Yan Y. Intraindividual variation of prostate specific antigen measurement and implications for early detection of prostate carcinoma. Cancer. 2001; **92**(4): 776-80.

230. Reed GF, Lynn F, Meade BD. Use of coefficient of variation in assessing variability of quantitative assays. Clin Diagn Lab Immunol. 2002; **9**(6): 1235-9.

231. Banath JP, Klokov D, MacPhail SH, Banuelos CA, Olive PL. Residual gammaH2AX foci as an indication of lethal DNA lesions. BMC Cancer. 2010; **10**: 4.

232. Markova E, Torudd J, Belyaev I. Long time persistence of residual 53BP1/gamma-H2AX foci in human lymphocytes in relationship to apoptosis, chromatin condensation and biological dosimetry. Int J Radiat Biol. 2011; **87**(7): 736-45.

233. Ahmed EA, Agay D, Schrock G, Drouet M, Meineke V, Scherthan H. Persistent DNA damage after high dose in vivo gamma exposure of minipig skin. PLoS ONE. 2012; **7**(6): e39521.

234. Cummings J, Raynaud F, Jones L, Sugar R, Dive C. Fit-for-purpose biomarker method validation for application in clinical trials of anticancer drugs. Br J Cancer. 2010; **103**(9): 1313-7.

235. Histed SN, Lindenberg ML, Mena E, Turkbey B, Choyke PL, Kurdziel KA. Review of functional/anatomical imaging in oncology. Nucl Med Commun. 2012; **33**(4): 349-61.

236. Zanzonico P. Principles of nuclear medicine imaging: Planar, SPECT, PET, multi-modality, and autoradiography systems. Radiat Res. 2012; **177**(4): 349-64.

237. Bohdiewicz PJ, Scott GC, Juni JE, Fink-Bennett D, Wilner F, Nagle C, et al. Indium-111 OncoScint CR/OV and F-18 FDG in colorectal and ovarian carcinoma recurrences. Early observations. Clin Nucl Med. 1995; **20**(3): 230-6.

238. Hong H, Sun J, Cai W. Radionuclide-based cancer imaging targeting the carcinoembryonic antigen. Biomark Insights. 2008; **3**: 435-51.

239. Haberkorn U, Markert A, Eisenhut M, Mier W, Altmann A. Development of molecular techniques for imaging and treatment of tumors. Q J Nucl Med Mol Imaging. 2011; **55**(6): 655-70.

240. Zhao Y, Gutshall L, Jiang H, Baker A, Beil E, Obmolova G, et al. Two routes for production and purification of Fab fragments in biopharmaceutical discovery research: Papain digestion of mAb and transient expression in mammalian cells. Prot Expr Purif. 2009; **67**(2): 182-9.

241. Datta-Mannan A, Witcher DR, Tang Y, Watkins J, Wroblewski VJ. Monoclonal antibody clearance. Impact of modulating the interaction of IgG with the neonatal Fc receptor. J Biol Chem. 2007; **282**(3): 1709-17.

242. Fawell S, Seery J, Daikh Y, Moore C, Chen LL, Pepinsky B, et al. Tat-mediated delivery of heterologous proteins into cells. Proc Natl Acad Sci U S A. 1994; **91**(2): 664-8.

243. Marfori M, Mynott A, Ellis JJ, Mehdi AM, Saunders NFW, Curmi PM, et al. Molecular basis for specificity of nuclear import and prediction of nuclear localization. Biochimica et Biophysica Acta (BBA) - Molecular Cell Research. 2011; **1813**(9): 1562-77.

244. Cornelissen B, Hu M, McLarty K, Costantini D, Reilly RM. Cellular penetration and nuclear importation properties of 111In-labeled and 123I-labeled HIV-1 tat peptide immunoconjugates in BT-474 human breast cancer cells. Nucl Med Biol. 2007; **34**(1): 37-46.

245. Cornelissen B, McLarty K, Kersemans V, Scollard DA, Reilly RM. Properties of [111In]-labeled HIV-1 tat peptide radioimmunoconjugates in tumor-bearing mice following intravenous or intratumoral injection. Nucl Med Biol. 2008; **35**(1): 101-10.

246. Hermanson G. Bioconjugate Techniques. 2nd ed. Oxford: Elsevier; 2008.

247. Hnatowich DJ, Childs RL, Lanteigne D, Najafi A. The preparation of DTPA-coupled antibodies radiolabeled with metallic radionuclides: An improved method. J Immunol Meth. 1983; **65**(1-2): 147-57.

248. Paik CH, Ebbert MA, Murphy PR, Lassman CR, Reba RC, Eckelman WC, et al. Factors influencing DTPA conjugation with antibodies by cyclic DTPA anhydride. J Nucl Med. 1983; **24**(12): 1158-63.

249. Mirzadeh S, Brechbiel MW, Atcher RW, Gansow OA. Radiometal labeling of immunoproteins: covalent linkage of 2-(4-isothiocyanatobenzyl)diethylenetriaminepentaacetic acid ligands to immunoglobulin. Bioconj Chem. 1990; **1**(1): 59-65.

250. Rübe CE, Grudzenski S, Kühne M, Dong X, Rief N, Löbrich M, et al. DNA double-strand break repair of blood lymphocytes and normal tissues analysed in a preclinical mouse model: Implications for radiosensitivity testing. Clin Cancer Res. 2008; **14**(20): 6546-55.

251. Schlamowitz M, Kaplan M, Shaw AR, Tsay DD. Preparation and characterization of rabbit IgG fractions. J Immunol. 1975; **114**(5): 1590-8.

252. Motta-Hennessy C, Eccles SA, Dean C, Coghlan G. Preparation 67-Ga-labelled human IgG and its Fab fragments using desferoxamine as chelating agent. Eur J Nucl Med Mol Imaging. 1985; **11**(6): 240-5.

253. Hnatowich DJ. Antibody radiolabeling, problems and promises. Int J Rad Appl Instrum B. 1990; **17**(1): 49-55.

254. Pham DT, Kaspersen FM, Bos ES. Electrophoretic method for the quantitative determination of a benzyl-DTPA ligand in DTPA monoclonal antibody conjugates. Bioconj Chem. 1995; **6**(3): 313-5.

255. Reilly R, Lee N, Houle S, Law J, Marks A. In vitro stability of EDTA and DTPA immunoconjugates of monoclonal antibody 2G3 labeled with indium-111. Int J Rad Appl Instrum A. 1992; **43**(8): 961-7.

256. Tolmachev V, Nilsson FY, Widstrom C, Andersson K, Rosik D, Gedda L, et al. 111In-benzyl-DTPA-ZHER2:342, an affibody-based conjugate for in vivo imaging of HER2 expression in malignant tumors. J Nucl Med. 2006; **47**(5): 846-53.

257. Sundberg AL, Orlova A, Bruskin A, Gedda L, Carlsson J, Blomquist E, et al. [111)In-Bz-DTPA-hEGF: Preparation and in vitro characterization of a potential anti-glioblastoma targeting agent. Cancer Biother Radiopharm. 2003; **18**(4): 643-54.

258. Rudnick SI, Adams GP. Affinity and avidity in antibody-based tumor targeting. Cancer Biother Radiopharm. 2009; **24**(2): 155-61.

259. Andrew SM, Perkins AC, Pimm MV, Baldwin RW. A comparison of iodine and indium labelled anti CEA intact antibody, F(ab)2 and Fab fragments by imaging tumour xenografts. Eur J Nucl Med. 1988; **13**(11): 598-604.

260. Martin OA, Redon CE, Nakamura AJ, Dickey JS, Georgakilas AG, Bonner WM. Systemic DNA damage related to cancer. Cancer Research. 2011; **71**(10): 3437-41.

261. Cornelissen B, Kersemans V, Darbar S, Thompson J, Shah K, Sleeth K, et al. Imaging DNA damage in vivo using {gamma}H2AX-targeted immunoconjugates. Cancer Res. 2011; **71**(13): 4539-49.

262. Haimovitz-Friedman A, Yang T-IJ, Thin TH, Verheij M. Imaging radiotherapy-induced apoptosis. Radiat Res. 2012; **177**(4): 467-82.

263. Iyer AK, Khaled G, Fang J, Maeda H. Exploiting the enhanced permeability and retention effect for tumor targeting. Drug Discov Today. 2006; **11**(17-18): 812-8.

264. Khalaf M, Abdel-Nabi H, Baker J, Shao Y, Lamonica D, Gona J. Relation between nodule size and 18F-FDG-PET SUV for malignant and benign pulmonary nodules. J Hematol Oncol. 2008; **1**: 13.

265. Blankenberg FG, Katsikis PD, Tait JF, Davis RE, Naumovski L, Ohtsuki K, et al. In vivo detection and imaging of phosphatidylserine expression during programmed cell death. Proceedings of the National Academy of Sciences. 1998; **95**(11): 6349-54.

266. Guo M-f, Zhao Y, Tian R, Li L, Guo L, Xu F, et al. In vivo99mTc-HYNIC-annexin V imaging of early tumor apoptosis in mice after single dose irradiation. J Exp Clin Cancer Res. 2009; **28**(1): 136.

267. Haas RLM, de Jong D, Valdés Olmos RA, Hoefnagel CA, van Den Heuvel I, Zerp SF, et al. In vivo imaging of radiation-induced apoptosis in follicular lymphoma patients. Int J Radiat Oncol Biol Phys. 2004; **59**(3): 782-7.

268. Jakob B, Durante M. Radiation dose detection by imaging response in biological targets. Radiat Res. 2012; **177**(4): 524-32.

269. Robbins ME, Brunso-Bechtold JK, Peiffer AM, Tsien CI, Bailey JE, Marks LB. Imaging radiation-induced normal tissue injury. Radiat Res. 2012; **177**(4): 449-66.

270. Redon CE, Weyemi U, Parekh PR, Huang D, Burrell AS, Bonner WM. gamma-H2AX and other histone post-translational modifications in the clinic. Biochim Biophys Acta. 2012; **1819**: 743-56.

271. Shah K, Cornelissen B, Kiltie AE, Vallis KA. Can γH2AX be used to personalise cancer treatment? Curr Mol Med. 2012.

272. Brunner AH, Hinterholzer S, Riss P, Heinze G, Weiss K, Brustmann H. Expression of γ-H2AX in endometrial carcinomas: An immunohistochemical study with p53. Gynecologic Oncology. 2011; **121**(1): 206-11.

273. Brustmann H, Hinterholzer S, Brunner A. Immunohistochemical expression of survivin and gamma-H2AX in vulvar intraepithelial neoplasia and low-stage squamous cell carcinoma. Int J Gynecol Pathol. 2011; **30**(6): 583-90.

274. Nagelkerke A, van Kuijk SJA, Sweep FCGJ, Nagtegaal ID, Hoogerbrugge N, Martens JWM, et al. Constitutive expression of γ-H2AX has prognostic relevance in triple negative breast cancer. Radiother Oncol. 2011; **101**(1): 39-45.

275. Firsanov D, Vasilishina A, Kropotov A, Mikhailov V. Dynamics of γH2AX formation and elimination in mammalian cells after X-irradiation. Biochimie. (0).

276. Sebag-Montefiore D, Stephens RJ, Steele R, Monson J, Grieve R, Khanna S, et al. Preoperative radiotherapy versus selective postoperative chemoradiotherapy in patients with rectal cancer (MRC CR07 and NCIC-CTG C016): a multicentre, randomised trial. The Lancet. 2009; **373**(9666): 811-20.

277. Vallis KA, Shah K. A Phase I dose accumulation trial of [111Indium]-DTPA-hEGF given sequentially by an intravenous infusion in patients with metastatic EGFR-positive cancers. University of Oxford; 2011.

278. Andratschke N, Blau T, Schill S, Nieder C. Late residual γ-H2AX foci in murine spinal cord might facilitate development of response-modifying strategies: a research hypothesis. Anticancer Res. 2011; **31**(2): 561-4.

279. Menegakis A, Eicheler W, Yaromina A, Thames HD, Krause M, Baumann M. Residual DNA double strand breaks in perfused but not in unperfused areas determine different radiosensitivity of tumours. Radiother Oncol. 2011; **100**(1): 137-44.

280. Romer T, Leonhardt H, Rothbauer U. Engineering antibodies and proteins for molecular in vivo imaging. Curr Opin Biotechnol. 2011; **22**(6): 882-7.

281. Banath JP, Olive PL. Expression of Phosphorylated Histone H2AX as a Surrogate of Cell Killing by Drugs That Create DNA Double-Strand Breaks. Cancer Res. 2003; **63**(15): 4347-50.

282. Schultz LB, Chehab NH, Malikzay A, Halazonetis TD. p53 binding protein 1 (53BP1) is an early participant in the cellular response to DNA double-strand breaks. J Cell Biol. 2000; **151**(7): 1381-90.

283. Joubert A, Zimmerman KM, Bencokova Z, Gastaldo J, Chavaudra N, Favaudon V, et al. DNA double-strand break repair defects in syndromes associated with acute radiation response: at least two different assays to predict intrinsic radiosensitivity? Int J Radiat Biol. 2008; **84**(2): 107-25.

284. Kotsopoulos J, Chen Z, Vallis KA, Poll A, Ainsworth P, Narod SA. DNA repair capacity as a possible biomarker of breast cancer risk in female BRCA1 mutation carriers. Br J Cancer. 2007; **96**(1): 118-25.

285. Cai Z, Chen Z, Bailey KE, Scollard DA, Reilly RM, Vallis KA. Relationship between induction of phosphorylated H2AX and survival in breast cancer cells exposed to 111In-DTPA-hEGF. J Nucl Med. 2008; **49**(8): 1353-61.

286. DECLARATION OF HELSINKI Ethical Principles for Medical Research Involving Human Subjects. World Medical Association. Oct 2008.

287. *Guideline for Good Clinical Practice E6(R1)* International Commission on Harmonisation. June 1996.

288. Research Governance Framework for Health and Social Care 2nd Edition. Department of Health. 2005.

Appendix: DSB Biomarkers Pilot Study Protocol

Oxford Biomedical Research Centre

UNIVERSITY OF OXFORD

Oxford Radcliffe Hospitals NHS Trust

DSB Biomarkers Pilot Study

Study Protocol

24 July 2009 Version 3.6

Sponsor/ Berkshire REC number: 09/H0505/106

Chief Investigator	Dr Ketan Shah Gray Institute for Radiation Oncology and Biology University of Oxford Old Road Campus Research Building Off Roosevelt Drive Headington Oxford OX3 7DQ
Sponsor	University of Oxford University Offices Wellington Square Oxford OX1 2JD United Kingdom

GRAY INSTITUTE FOR RADIATION ONCOLOGY & BIOLOGY

CANCER RESEARCH UK

MRC Radiation Oncology and Biology

NHS National Institute for Health Research

DSB Biomarkers Pilot Study - Protocol

Participating Investigators and Centres

Participating Centre	Oxford Radcliffe Hospitals NHS Trust
Participating Address	John Radcliffe Hospital Headley Way Headington Oxford. OX3 9DU Churchill Hospital Old Road Headington Oxford OX3 7LJ
Chief Investigator	Dr Ketan Shah Gray Institute for Radiation Oncology & Biology University of Oxford Old Road Campus Research Building Off Roosevelt Drive Headington Oxford. OX3 7DQ ketan.shah@rob.ox.ac.uk
Educational Supervisor & Co-Investigator	Dr Katherine Vallis CRUK Senior Group Leader Gray Institute for Radiation Oncology & Biology katherine.vallis@rob.ox.ac.uk
Co-investigators	Dr Amanda Salisbury Consultant Clinical Oncologist Oxford Radcliffe Hospitals NHS Trust Dr Colin Clelland Consultant Pathologist Oxford Radcliffe Hospitals NHS Trust

Table of Contents

1. Introduction
2. Rationale
3. Study Objectives
4. Study Design
5. Participant Selection
    a. Inclusion Criteria
    b. Exclusion Criteria
6. Study Procedure
7. Data Analysis
8. Duration of Study Participation
9. Risks and Inconvenience of Study Participation
10. Benefits of Study Participation
11. Study Administration
    a. Regulatory and Ethical Considerations
        i. Ethical conduct and approval
        ii. NHS Research Governance
        iii. Protocol amendments
        iv. Informed Consent
    b. Quality Assurance
    c. Patient Data and Confidentiality
    d. Study Funding
    e. Indemnity
    f. Publication Policy
12. References

Abbreviations

DNA	Deoxyribose Nucleic Acid
DSB	Double Strand Break
DTPA	DiethyleneTriaminePentaAcetic acid
FNA	Fine Needle Aspirate
GCP	Good Clinical Practice
hEGF	human Epidermal Growth Factor
(γ)H2AX	(phosphorylated) Histone 2AX
ICH	International Commission on Harmonisation
NHS	National Health Service
ORH	Oxford Radcliffe Hospitals
PBMC	Peripheral Blood Mononuclear Cell
REC	Research Ethics Committee
R&D	Research and Development
(TP)53BP1	(Tumour suppressor) p53 Binding Protein 1

1. Introduction

The number of methods used to attack cancer cells is increasing all the time. The effect of these efforts on the cells can be difficult to gauge however, and usually relies on clinical and radiological assessments over time. More immediate markers of the damage to cells could help both in the development of new drugs, and in judging the sensitivity of normal cells and cancer cells to existing treatments.

Development of such "biomarkers", i.e. characteristics that are objectively measured as an indicator of biologic processes is recognized as an important technique to assist the progress of cancer therapeutic research.[13]

Fine needle aspiration is a very widely used clinical technique used to obtain cells from tissues and tumours. It is quick, simple, requires little specialist equipment. It does involve temporary discomfort for the patient, but it is a minimally invasive method of obtaining a direct sample of cells.

This is a pilot study to judge the feasibility and utility of assays of tumour fine needle aspirate (FNA) samples for known markers of DNA damage such as phosphorylated histone 2AX (γH2AX) and tumour suppressor protein p53 Binding Protein 1 (53BP1).

If the assays prove reliable, data from this pilot study will be used to plan their incorporation into future studies of agents thought to cause DNA double strand breaks. This would include this research group's forthcoming phase 1 study of the novel radiopharmaceutical 111-indium-DTPA-hEGF.

2. Rationale

The most commonly used treatments for cancer kill cells by damaging DNA. There are many correlates of DNA damage used in preclinical studies to demonstrate that the intended damage is indeed occurring. A recently characterized example is the accumulation of phosphorylated histone 2AX (γH2AX),[136] which has been shown in vitro to occur as foci at sites of DNA double strand breaks (DSBs).[31] The foci can be detected using immunofluorescence, either visualized with immunohistochemistry and confocal microscopy or with fluorescence automated cell sorting (FACS) analysis. Several protocols for such staining have been published.[211]

A large literature attests to the utility of the technique in elucidating the effects of cytotoxic agents and radiation in cell culture.[36] The kinetics of double strand break formation and repair, and the association of these variables with the chemosensitivity[281] and radiosensitivity of cell lines has been studied.[107] The technique is now starting to be developed for fresh human tissue samples such as biopsies of irradiated skin during external beam radiotherapy for prostate cancer [156] and more recently tumour biopsies during external beam radiotherapy for cervical cancer[123] and novel targeted systemic agents.[180] As the range of application in clinical samples becomes broader, more confidence can be placed on the interpretation of γH2AX foci in clinical settings.

DSB Biomarkers Pilot Study - Protocol

It may be possible to characterise other markers of DNA double strand breaks such as 53BP1 [282] identified by simultaneous immunocytochemistry in human tumour samples. Similar methods have proven useful in cell culture experiments. [211] Given the diverse nature of the cellular responses to DSBs, it is reasonable to expect that multiple markers may best predict radio- and chemosensitivity. [283]

Cellular material is required to look for γH2AX and other markers. For tumours lying close to the skin, fine needle aspiration can provide a quick and reliable method of obtaining cells. The procedure involves the insertion of a fine-bore hypodermic needle into the tumour, whose position is established on clinical or radiological grounds. Insertion of the needle does involve discomfort for the patient, for around 10 seconds with each pass of the needle. The number of passes required varies with the individual characteristics of the patient and tumour, and with the amount of cellular material required. Complications from the procedure are rare, the most common being bruising.

The current pilot study aims to investigate the extension of immunocytochemistry for DSB biomarkers to clinical fine needle aspirate (FNA) samples from tumours in participants. The variability of measurements between separate synchronous samples, and between samples taken on different occasions from the same tumour will be quantified. In participants undergoing chemotherapy and radiotherapy, a sample will be taken where possible immediately after the first treatment.

Peripheral blood mononuclear cells (PBMCs) will also be collected. These cells will provide a control for expected baseline DSB biomarker staining within a subject, and the cells can also be irradiated in the laboratory to show the effect on the biomarkers. A protocol for such staining has been reported.[284]

Consent will be taken to take samples on up to three separate occasions. This pilot study aims to establish the reliability of the biomarker. Repeat measurements are required to establish the range, variability and robustness of the measurements.

In suitable patients subsequent samples may be taken after radiotherapy or chemotherapy treatment, where it would be expected that DNA damage including double strand breaks would be shown. There would be particular interest in repeating samples after radiotherapy, where the timing of the DNA damage event is known.

The current published data on the measurement of these markers in small numbers of human tumour samples [57, 123, 136, 156, 180, 284] describe a variety of methods in different clinical settings. The data are not sufficient to predict the expected statistical characteristics of measurements in these FNA samples. The primary objective of this study is therefore to establish a reliable assay method, providing initial data on which to base decisions about further application of the method to tackling clinical research questions.

Cancer Research UK's (CRUK) Biomarkers and Imaging Discovery and Development (BIDD) Committee has produced a Biomarker Roadmap as a framework for developing such tests. [185] Although not adopted by CRUK, this pilot study corresponds to BIDD Assay Development Stage 1. Data from this initial study will inform decisions about use of the markers in future studies.

Specifically in relation to the novel radiopharmaceutical 111-indium-DTPA-hEGF, immunocytochemistry for γH2AX has helped to confirm the mechanism and effect of the compound in vitro.[285] This group intends to take the agent into a phase 1 human trial during 2010, and if the current study shows that DSB Biomarkers can be detected in human FNA samples, the technique can be applied in the phase 1 trial to confirm the cellular effect of 111-indium-DTPA-hEGF in trial subjects.

3. Study Objectives

Primary Objective:

To establish a reliable method for the detection of DNA double strand breaks (DSBs) by immunocytochemistry in human tumour cells obtained by fine needle aspiration.

Secondary Objectives

1. To measure the variability in quantitative measurement of DSB biomarkers between synchronous tumour samples.
2. To measure the robustness in quantitative measurement of DSB biomarkers from the same tumour at different times.
3. To use peripheral blood mononuclear cells from participants in the study as a control for baseline DSB markers and the response to irradiation ex-vivo.
4. To provide preliminary evidence that DSB biomarkers increase after treatment of the tumour.

4. Study Design

This is a single centre non randomized study. The aim will be to recruit fifteen participants.

5. Participant Selection

Participants with a biopsy-confirmed cancer diagnosis and a palpable lesion suspicious for malignancy suitable for fine needle aspiration will be identified by the direct healthcare team and approached for their consent to enter the study.

a. Inclusion Criteria:

1. Age 18 years or over.
2. Capacity to consent to inclusion in the study.
3. Previous histologically confirmed diagnosis of malignancy.
4. Palpable lesion suspicious for recurrence or residual disease.
5. Signed informed consent.

b. Exclusion Criterion:

On anticoagulant medication or known clotting disorder

6. Study Procedure

Potential subjects will be identified by the multidisciplinary team directing clinical care. Suitable patients attending outpatient clinics will be approached by a member of the health care team, who will provide a written information sheet. They will be given contact details for the research team, and also asked for their consent for a researcher to contact them. Some patients may be referred for fine needle aspiration (FNA) for clinical reasons. They will have at least one day to consider the information before their FNA appointment.

On the day of the FNA appointment, the study coordinator will obtain written evidence of informed consent. The procedure for withdrawing consent at any time during the procedure will be emphasized.

During the procedure, if clinical referral has been made, material required for direct clinical care purposes will be obtained first to the satisfaction of the cytopathologist. The participant's permission will then be sought to continue taking material for research purposes. A maximum of three further needle passes will be attempted, and cells placed in suspension.

For procedures where no material is required for direct clinical care, a maximum of three needle passes will be performed.

After the FNA procedure 10ml of peripheral blood will be taken from participants using aseptic venepuncture technique into a heparin tube.

Consent will be taken to take further samples two separate occasions at least 24 hours after the initial FNA, and usually timed to coincide with a visit to the hospital for a clinical appointment. In most cases there would not be any clinical reason to take further samples. The FNA procedure will be the same as for the initial visit, with a maximum of three needle passes, plus 10ml peripheral blood venepuncture.

In participants due to start radiotherapy or chemotherapy treatment, the second and/or third set of samples may be timed immediately after the first fraction of radiotherapy or first cycle of chemotherapy.

Tumour cells and peripheral lymphocytes will be processed for immunocytochemical analysis directed at identifying DSB markers including foci of γH2AX and 53BP1. Cell processing will take place at the Pathology Department of John Radcliffe Hospital, the Oxford Cancer Centre facilities at the Churchill Hospital and the facilities of the Gray Institute for Radiation Oncology and Biology. The assay method will be based upon this group's method for γH2AX immunocytochemistry of cultured cells, modified as required for these fresh FNA samples and simultaneous detection of other markers such as 53BP1. Fluorescently labelled secondary antibodies will be employed, and foci visualised with fluorescent microscopy. The foci will be counted manually or using computer image processing software.

7. Sample Size & Data Analysis

Data will be analysed both as direct counts of foci per cell, and the proportion of cells with numbers of foci above a threshold. Descriptive statistics will be produced, including for continuous counts arithmetic mean, range and standard deviation, and for threshold-based categories frequency distribution. Groups will be compared using models including Student's t test (two groups, for example pre and post irradiation of PBMCs) and analysis of variance (ANOVA) models (more than two groups, for example where three sets of samples are taken over time).

Since the range, variability and robustness of measurements of DSB marker foci in fine needle aspiration samples is not known in advance of the study, it is not possible to perform a formal hypothesis-led sample size calculation for validation of reliability of the assay. The sample size for this pilot study has therefore been selected to establish descriptive statistics of the assay results.

For comparison, the closest data on which to base a sample size calculation to test the hypothesis that DSB biomarker foci increase with treatment comes from a study using cell suspensions from biopsies to measure γH2AX foci per 50 cells before and after a targeted DNA-damaging agent in two patients.[180] Assuming similar statistical characteristics in this study, in order to test the hypothesis using a two tailed paired t test at significance level 0.05 would require 10 paired samples to give a 90% power to detect a difference of 10 foci per 50 cells. [Graphpad Statmate version 2.0, Graphpad Software Inc, La Jolla, USA]

8. Duration of Study Participation

Participation in the study will last from documentation of informed consent until the last peripheral blood sample is taken (or the subject withdraws his or her consent).

9. Risks and Inconvenience of Study Participation

Talking about the study and performing the FNA procedure takes time – around 30 minutes on the first occasion, and around 20 minutes on the second and third visits. Visits will typically be timed when participants are coming to the hospital for direct care. However, if they agree to a procedure at another time, this will involve the cost and inconvenience of travelling to the hospital for an extra visit. Travel expenses will be repaid.

The study will require up to three FNA procedures than would not be required for purely clinical reasons, each with a maximum of three passes of the needle. This will entail the discomfort of the procedure and the risk of complications such as bruising.

Where FNA is required on clinical grounds, the study would involve a longer initial procedure than would otherwise be required. The material needed for clinical diagnosis may also be re-examined, but only if there is no detriment to the participant's clinical care as judged by the cytopathologist.

Three 10ml peripheral blood samples for research purposes will be taken - one after each FNA procedure. This involves discomfort for the participant.

10. Benefits of Study Participation

Participants will derive no direct benefit from participation in the study. It is explained in the participant information leaflet that we aim to use the knowledge and experience gained from the study to develop tests to guide cancer treatments, offering benefit to cancer patients in the future.

11. Study Administration

a. Regulatory and Ethical Considerations

The investigators believe that the risks and inconvenience to study participants should be minimised, but are justified by the importance of the objectives of the study. The University of Oxford as sponsor and the Chief Investigator will ensure that this study will be conducted in accordance with the principles of the World Medical Association Declaration of Helsinki[286] and International Commission on Harmonisation Good Clinical Practice (GCP[287]) guidelines along with all applicable policies of the Oxford Radcliffe Hospitals (ORH)NHS Trust and the University of Oxford.

i. Ethical conduct and approval

The principles of the study have undergone peer review by the Oxford Early Phase and Translational Research Trial Steering Committee. The protocol, participant information leaflet, consent form and letter to the General Practitioner have reviewed by the University of Oxford as sponsor and have been given a favourable opinion by the independent Berkshire Research Ethics Committee (REC).

ii. NHS Research Governance

The study will be conducted with regard to the Research Governance Framework for Health and Social Care.[288] The investigators will apply to the ORH Trust Research and Development department for approval to conduct the study in accordance with local policy. Trust approval will be confirmed in writing before recruitment of participants commences.

iii. Protocol amendments

Amendments to the protocol or other documents that have been approved by the REC may only be made with the written approval of the Chief Investigator and the sponsor. Substantial amendments will be submitted to the REC for approval, and minor amendments will be notified to REC according to published guidance.

iv. Informed Consent

An investigator will discuss informed consent to enter the study with the participant. All participants will have received written information on the study at least 24 hours in advance. The discussion will include an explanation of the aims of the study, its methods, and the potential risks and inconvenience to which those entering the study will be exposed. Consent will be documented on a specific written consent form. Applicable GCP guidelines will be followed, including training for investigators in obtaining informed consent.

b. Quality Assurance

Responsible members of the University of Oxford or the Oxford Radcliffe Hospitals NHS Trust may be given access to data for monitoring and/or audit of the study to ensure compliance with regulations and the NHS Research Governance Framework.

c. Security, Patient Data and Confidentiality

The data collected from participants will include name, date of birth, address, telephone number, hospital identifier number, consultant, diagnosis, previous treatment, proposed future treatment etc

Access to the department is limited to staff or authorised visitors and managed by 24 hour electronic security system Laboratories are designed and managed to the Advisory Committee on Dangerous Pathogens (ACDP) standards for Containment level 2.

All data will be held securely - paper data will be physically secure, and electronic data encrypted. Data will be held for 15 years at least.

d. Study Funding

The funding will be underwritten from Dr Vallis' group core funding including the Oxford Biomedical Research Centre Cancer Theme and a programme grant from Cancer Research UK. The Gray Institute receives core funding from the Cancer Research UK and the Medical Research Council. In addition, funding in the form of a Small Project Grant from the Royal College of Radiologists will be applied for. Dr Shah's salary is funded from the Oxford Biomedical Research Centre.

e. Indemnity

The Chief Investigator holds a contract with the University of Oxford. Compensation for harm arising from an accidental injury and occurring as a consequence of subjects' participation in the study will be covered by the University of Oxford.

f. Publication Policy

The results of the trial are intended for submission to a peer-reviewed biomedical journal and inclusion in a D Phil thesis by the Chief Investigator Dr Ketan Shah.

Once the results are published (or a decision not to publish has been made), a lay summary of results will be produced and will be made available to study participants and other interested parties.

12. References

1. Biomarkers and surrogate endpoints: preferred definitions and conceptual framework. Clin Pharmacol Ther, 2001. 69(3): p. 89-95.
2. Bonner, W.M., et al., GammaH2AX and cancer. Nat Rev Cancer, 2008. 8(12): p. 957-67.
3. Rogakou, E.P., et al., DNA double-stranded breaks induce histone H2AX phosphorylation on serine 139. J Biol Chem, 1998. 273(10): p. 5858-68.
4. Nakamura, A., et al., Techniques for gamma-H2AX Detection, in Methods in Enzymology. 2006, Academic Press. p. 236-250.
5. Kinner, A., et al., Gamma-H2AX in recognition and signaling of DNA double-strand breaks in the context of chromatin. Nucleic Acids Res, 2008. 36(17): p. 5678-94.
6. Banath, J.P. and P.L. Olive, Expression of Phosphorylated Histone H2AX as a Surrogate of Cell Killing by Drugs That Create DNA Double-Strand Breaks. Cancer Res, 2003. 63(15): p. 4347-4350.
7. Banath, J.P., S.H. MacPhail, and P.L. Olive, Radiation Sensitivity, H2AX Phosphorylation, and Kinetics of Repair of DNA Strand Breaks in Irradiated Cervical Cancer Cell Lines. Cancer Res, 2004. 64(19): p. 7144-7149.
8. Simonsson, M., et al., Low-dose hypersensitive gammaH2AX response and infrequent apoptosis in epidermis from radiotherapy patients. Radiother Oncol, 2008. 88(3): p. 388-97.
9. Banuelos, C.A., et al., gammaH2AX expression in tumors exposed to cisplatin and fractionated irradiation. Clin Cancer Res, 2009. 15(10): p. 3344-53.
10. Hochhauser, D., et al., Phase I study of sequence-selective minor groove DNA binding agent SJG-136 in patients with advanced solid tumors. Clin Cancer Res, 2009. 15(6): p. 2140-7.
11. Schultz, L.B., et al., p53 binding protein 1 (53BP1) is an early participant in the cellular response to DNA double-strand breaks. J Cell Biol, 2000. 151(7): p. 1381-90.
12. Joubert, A., et al., DNA double-strand break repair defects in syndromes associated with acute radiation response: at least two different assays to predict intrinsic radiosensitivity? Int J Radiat Biol, 2008. 84(2): p. 107-25.
13. Kotsopoulos, J., et al., DNA repair capacity as a possible biomarker of breast cancer risk in female BRCA1 mutation carriers. Br J Cancer, 2007. 96(1): p. 118-25.
14. Sedelnikova, O.A., et al., Quantitative detection of (125)IdU-induced DNA double-strand breaks with gamma-H2AX antibody. Radiat Res, 2002. 158(4): p. 486-92.
15. Prognostic/Predictive Biomarker Roadmap. 2007; Available from: http://science.cancerresearchuk.org/reps/pdfs/bidd_prognostic_roadmap.pdf?version=1.
16. Cai, Z., et al., Relationship between induction of phosphorylated H2AX and survival in breast cancer cells exposed to 111In-DTPA-hEGF. J Nucl Med, 2008. 49(8): p. 1353-61.
17. DECLARATION OF HELSINKI Ethical Principles for Medical Research Involving Human Subjects. World Medical Association, Oct 2008.

18. Guideline for Good Clinical Practice E6(R1) International Commission on Harmonisation, June 1996.
19. Research Governance Framework for Health and Social Care 2nd Edition. Department of Health, 2005.